UNIVERSIDADE FEDERAL DE SÃO CARLOS
CENTRO DE CIÊNCIAS EXATAS E DE TECNOLOGIA
DEPARTAMENTO DE QUÍMICA
PROGRAMA DE PÓS-GRADUAÇÃO EM QUÍMICA

“Nanocompósitos ternários baseados em nanocristais de celulose, materiais condutores e fibras eletrofiadas aplicados em sensores para detecção de metais pesados em água”

Kelcilene Bruna Ricardo Teodoro*

Tese apresentada como parte dos requisitos para obtenção do título de DOUTORA EM CIÊNCIAS, área de concentração: QUÍMICA

Orientador(a): Dr. Daniel Souza Corrêa

*** Bolsista - FAPESP**

São Carlos / SP
2019

FEDERAL UNIVERSITY OF SAO CARLOS
CENTER OF EXACT SCIENCES AND TECHNOLOGY
CHEMISTRY DEPARTMENT
GRADUATE PROGRAM IN CHEMISTRY

"Ternary nanocomposites based on cellulose nanocrystals, conductive materials and electrospun fibers applied in sensors for detection of heavy metals in water"

Kelcilene Bruna Ricardo Teodoro*

Thesis presented as part of the requirements to obtain PhD degree in SCIENCES, concentration area: CHEMISTRY.

Advisor: Dr. Daniel Souza Corrêa

*** Scholarship - FAPESP**

São Carlos / SP
2019

UNIVERSIDADE FEDERAL DE SÃO CARLOS

Centro de Ciências Exatas e de Tecnologia
Programa de Pós-Graduação em Química

Folha de Aprovação

Assinaturas dos membros da comissão examinadora que avaliou e aprovou a Defesa de Tese de Doutorado da candidata Kelcilene Bruna Ricardo Teodoro, realizada em 28/03/2019:

Prof. Dr. Daniel Souza Corrêa
EMBRAPA

Profa. Dra. Cristiane Sanchez Farinas
EMBRAPA

Prof. Dr. José Mario de Aquino
UFSCar

Profa. Dra. Sonia Regina Biaggio Rocha
UFSCar

Profa. Dra. Maria Alice Martins
EMBRAPA

Aos meus pais,

Tereza e Vander (*in memoriam*), por me conceder as dádivas da vida e da prática do bem. Dedico meus esforços e sucessos a vocês! Todo fruto que eu colher sempre será vosso também!

AGRADECIMENTOS

Agradeço a Deus, por me conduzir em mais esta trajetória, por presentear-me com pessoas sensatas que me aconselharam, mãos macias que me afagaram e ombros largos que me acolheram. Por me possibilitar oferecer flores, mesmo quando espinhos feriram meus pés.

Ao Programa de Pós-Graduação em Química da UFSCar, pela oportunidade e contribuição em minha formação profissional, além de todo auxílio e cooperação dos funcionários.

Á Embrapa Instrumentação, pela infraestrutura e oportunidades de crescimento que não se cessam.

Ao Dr. Daniel por tornar-me uma cientista, com sua orientação, ensinamentos, suporte, amizade e confiança, dedicando-se pacientemente à minha formação profissional.

Á minha família, por toda atenção, proteção e carinho.

Á minha mãe Tereza que, sendo meu porto seguro, foi essencial para que eu pudesse resistir às tempestades.

Ao meu pai Vander (*in memoriam*), que me fez forte, ensinou a levantar e continuar, quantas vezes fosse necessário. E a importância de cumprir com minha palavra e minhas obrigações!

Às minhas irmãs, Karina e Kátia que jamais deixaram que eu perdesse minha essência. Ao meu esposo Marcelo, que de todo seu amor sempre foi atento, compreensivo, prestativo e carinhoso. Aos meus pequeninos Henrique, Stephanie e Ícaro, por amaciar minha vida adulta com a generosidade e gentileza de seus puros corações. Ao meu cunhado Guilherme, por compartilhar das piadas que apenas os nerds entendem.

Aos meus amigos que, sempre que estive ansiosa, me trouxeram mais uma taça de vinho (cerveja, gim, sorvete ou chocolate)!

Aos meus companheiros de trabalho (Fernanda, Rafa Sanfelice, Makoto, Murilo, Vanessa, Idelma e Wania), com a colaboração de vocês eu pude ir muito mais além!

Aos meus amigos e companheiros de sala, pelos momentos de descontração e, sobretudo, pelas boas ideias, bons conselhos e disposição a ajudar no que pudessem. Além de todos os lanchinhos compartilhados!

Aos técnicos dos laboratórios (Adriana, Joana, Silviane, Alice, Viviane, Mattêo, Paulinho), pela cooperação e treinamentos, sempre com paciência e amizade.

À Coordenação de Aperfeiçoamento de Pessoal de Nível Superior - Brasil (CAPES) - Código de Financiamento 001 por todo auxílio concedido à pesquisa.

À Fundação de Amparo à Pesquisa do Estado de São Paulo (FAPESP) pelo suporte financeiro no país (2014/21184-5) e no exterior (2016/21899-0) pelo suporte financeiro e oportunidades concedidas.

A todos que contribuíram para minha formação e realização deste trabalho.

A vocês, o meu MUITO OBRIGADA!!!

LIST OF FIGURES

LIST OF TABLES

RESUMO

NANOCOMPÓSITOS TERNÁRIOS BASEADOS EM NANOCRISTAIS DE CELULOSE, MATERIAIS CONDUTORES E FIBRAS ELETROFIADAS APLICADOS EM SENSORES PARA DETECÇÃO DE METAIS PESADOS EM ÁGUA. O monitoramento de recursos hídricos destinados para fins de consumo é de grande importância para manutenção da qualidade de vida da população e dos ecossistemas. A contaminação destes recursos com metais pesados, geralmente relacionada com o descarte impróprio de resíduos industriais, é um problema recorrente no Brasil e no mundo. O emprego de estratégias advindas da nanociência e nanotecnologia podem auxiliar no desenvolvimento de dispositivos sensores capazes de fornecer um rápido e confiável diagnóstico da qualidade de água. Neste sentido, a presente tese relata o desenvolvimento de sensores químicos nanoestruturados com nanocompósitos ternários constituídos de fibras eletrofiadas de poliamida 6 (PA6), nanocristais de celulose (CNC) e materiais condutores, como nanopartículas de prata (AgNP) e óxido de grafeno reduzido (rGO). Os estudos revelaram a possibilidade de utilizar os CNC como reagente verde na estabilização, redução e dispersão das espécies condutoras. Sendo assim, os CNC foram adicionados às sínteses de AgNP e rGO, e os híbridos resultantes foram caracterizados quanto à morfologia utilizando técnicas de microscopia eletrônica MEV, MEV-FEG e MET, e composição química utilizando técnicas como espectroscopia de absorção UV-Vis e FTIR, difração de raios-X (DRX), e análise termogravimétrica (TG). Posteriormente, os materiais híbridos de CNC/AgNP e CNC/rGO foram combinados às fibras eletrofiadas de PA6. As diferentes estratégias para combinação destes materiais foram avaliadas e os nanocompósitos resultantes caracterizados quanto à morfologia por microscopias eletrônicas de varredura e de transmissão (MEV, MEV-FEG e TEM), composição por espectroscopia FTIR, interação entre os componentes por calorimetria exploratória diferencial (DSC) e habilidade de transferência de carga por espectroscopia de impedância eletroquímica (EIS) e voltametria cíclica (CV). Estes nanocompósitos foram aplicados na fabricação de plataformas sensoras, as quais, fazendo uso das técnicas elétricas e eletroquímicas, foram capazes de detectar metais pesados em baixas concentrações. As plataformas sensoras resultantes das distintas combinações de CNC, AgNP e PA6 foram arranjadas compondo uma língua eletrônica impedimétrica. Os dados de capacitância foram tratados fazendo uso de análise estatística multivariada, por meio da qual verificou-se a eficiente classificação de soluções contendo água contaminada por chumbo(II), cádmio(II), cobre(II) e níquel(II) e água pura. O mesmo arranjo sensorial possibilitou distinguir água pura de soluções contendo chumbo em concentrações tão baixas quanto 10 nmol. L^{-1}. A plataforma sensora constituída de CNC, rGO e PA6 foi aplicada na detecção eletroquímica de mercúrio. Aplicando-se a técnica de voltametria de pulso diferencial (DPV) foi possível detectar mercúrio (II) na faixa de 2,5–200 μM. O sensor desenvolvido mostrou-se estável, seletivo e com limite de detecção de 0.52 μM.

ABSTRACT

TERNARY NANOCOMPOSITES BASED ON CELLULOSE NANOCRYSTALS, CONDUCTIVE MATERIALS AND ELECTROSPUN FIBERS APPLIED IN SENSORS FOR DETECTION OF HEAVY METALS IN WATER. The monitoring of water resources destined for consumption is a subject of outmost importance for population and ecosystems life quality maintenance. The degradation of these resources with heavy metals, usually associated with the improper disposal of industrial wastes, is a current issue in Brazil and in the world. The use of strategies arising from nanoscience and nanotechnology can help the development of sensor devices able to provide a rapid and reliable diagnosis of water quality. In this sense, the present thesis reports the development of nanostructured chemical sensors with nanocomposites composed of polyamide 6 (PA6) electrospun fibers, cellulose nanocrystals (CNC) and conductive materials, such as silver nanoparticles (AgNP) and reduced graphene oxide (rGO). The studies revealed the possibility to use CNC as green reagent in the stabilization, reduction and dispersion of conductive species. In this way, CNC were added to AgNP and rGO syntheses, and the resulting hybrid materials were characterized in terms of morphology through scanning and transmission electron microscopy (SEM, FEG-SEM and TEM), and chemical composition using techniques as UV-Vis absorption spectroscopy and FTIR, X-ray diffraction and thermogravimetric analysis (TG). The hybrid materials CNC/AgNP and CNC/rGO were, subsequently, combined with PA6 electrospun fibers. The different possible strategies for combination of these materials were evaluated and the resultant nanocomposites were characterized in terms of morphology by SEM and FEG-SEM, composition by spectroscopy FTIR, interaction between components by differential scanning calorimetry (DSC) and ability of charge transfer by electrochemical impedance spectroscopy (EIS) and cyclic voltammetry (CV). These nanocomposites were applied in the fabrication of sensing platforms which, making use of electrical and electrochemical techniques, enabled the detection of heavy metal ions even under low concentrations. The sensing platforms resultant from distinct combinations of CNC, AGNP and PA6 were arranged to compose an impedimetric electronic tongue. Capacitance data were statistically interpreted using multivariate data analysis, whereby it was possible to classify solution containing lead(II), cadmium(II), copper(II), nickel(II) and pure water. The same sensing array enabled distinguishing pure water and lead solutions under concentrations as low as 10 nmol. L^{-1}. The sensor platform based on CNC, rGO and PA6 was applied to the electrochemical detection of Hg(II). With the use of differential pulse voltammetry (DPV), it was possible to detect mercury (II) in the range of 2.5-200 μM. The developed sensor was stable, selective and showed limit of detection of 0.52 μM.

SUMMARY

PUBLICATIONS

1. Teodoro, K. B. R.; Sanfelice, R. C.; Mattoso, L. H. C.; Correa, D. S. Cellulose Whiskers Influence the Morphology and Antibacterial Properties of Silver Nanoparticles Composites. *J. Nanosci. Nanotechnol.*, 8, 1-8, 2018.
2. Teodoro, K. B. R.; Migliorini, F. L.; Facure, M. H.; Correa, D. S. Conductive electrospun fibers containing cellulose nanowhiskers and reduced graphene oxide for the electrochemical detection of mercury (II). *Carb. Pol.*, 207, 747-754, 2019c.
3. Teodoro, K. B. R; Shimizu, F. M.; Scagion, V. P.; Correa, D. S. "Ternary nanocomposites based on cellulose nanowhiskers, silver nanoparticles and electrospun nanofibers: use in an electronic tongue for heavy metal detection" Sensor Actuator B-Chem. 290:387, 2019b.

OTHER PUBLICATIONS

1. Teodoro, K. B. R.; Migliorini, F. L.; Christinelli, W. A.; Correa, D. S. Detection of hydrogen peroxide (H2O2) using a colorimetric sensor based on cellulose nanowhiskers and silver nanoparticles. *Carb. Pol.* **212**, 235-241, 2019a.

2. Migliorini, F. L.; Teodoro, K. B. R.; Correa, D. S. Optical sensor using cotton cellulose nanowhiskers/gold nanoparticles composite for the selective determination of cadmium (II). *Submmited.*

1. Introduction

1.1. General considerations

A global issue related to water resources degradation lies in the excessive amount of heavy metals in the water, usually related to the improper disposal of industrial wastes, which requires the government to imposes strict legislation aimed at ensuring water of sufficient quality destined for consumption (KARKRA et al., 2017; PENG et al., 2018). In this context, for instance, Brazilian environmental agency established the maximum heavy metal concentrations as 0.01 $mg.L^{-1}$ for lead and 0.0002 $mg.L^{-1}$ for mercury in river waters (CONAMA 357/2005). In relation to effluents disposal, these maximum concentrations are 0.5 $mg.L^{-1}$ for lead and 0.01 $mg.L^{-1}$ for mercury (CONAMA 430/2011).

The importance of heavy metal monitoring has attracted great attention in Brazil due to recent ecologic disasters involving mining dam ruptures, which have led to contamination of important rivers by massive amount of mud containing heavy metal ions, such as iron, manganese, lead, mercury, copper, among others. Since these pollutants are non-biodegradable, living organisms and human health can be seriously affected as consequence of bio-accumulation (ALKMIM-FILHO et al., 2014; JOSE and RAY, 2018; LIU et al., 2017). Although some of these compounds play important role in biological mechanisms, most of them are toxic even under low concentrations, resulting in serious diseases, mutation and even death by poisoning (TCHOUNWOU et al., 2012).

Advances related to sensor device technologies have attracted great attention as a tool for environmental monitoring, providing rapid and reliable diagnostics as an alternative to conventional spectroscopic and chromatographic techniques (LIU et al., 2017; TERRA and MERCANTE, 2017). These advances allow detection of lower concentrations of pollutants (CHAIYO et al., 2016;

KHOSHBIN et al., 2018; MIGLIORINI et al., 2017a). Novel platforms based on nanomaterials have enabled the surface area increasing and amplification of their conductivity, which are desirable in the manufacture of electrical/electrochemical sensors (DING et al., 2010; DU et al., 2017; KAFY et al., 2015; MIGLIORINI et al., 2017a; PAVINATTO et al., 2015; REICH et al., 2018).

In this work the production of ternary nanocomposites based on polyamide fibers (PA6), cellulose nanocrystals (CNC) and conductive materials such as silver nanoparticles (AgNP) and reduced graphene (rGO) were used to manufacture sensors aiming at the detection of low concentrations of heavy metals in water. Few researches can be found in the literature reporting the insertion of the CNC into electrical and electrochemical sensors, owing to the non-conductive nature of these nanostructures. However, a growing number of studies are investigating the properties of composites based in CNC and various functional nanomaterials, which allows a high dispersion of the functional material by the CNC surface, contributing significantly for the exploitation of its properties (ABITBOL et al., 2017; MATSUYAMA et al., 2019; MORALES-NARVÁEZ et al., 2015; POURREZA et al., 2015; TEODORO et al., 2019a).

1.2. Nanostructured chemical sensors

Chemical sensors are devices able to transform physical, chemical or biological stimulus in a measurable analytical signal. The application of sensors and biosensors for monitoring analytes related to contamination and diseases has been extensively explored, once they offer an advantage alternative to conventional analytical techniques such as atomic absorption spectroscopy (AAS), inductively coupled plasma-mass spectrometry (ICP-MS), mass spectrometry (MS) and X-ray fluorescence spectroscopy (XPS), which involve expensive reagents, complex procedures and inflexibility for on-site analysis (TERRA et al., 2017). The advantages are related to facile sample preparation,

simplicity, time and cost efficiency, miniaturization and portability (GOLMOHAMMADI et al., 2017; MERCANTE et al., 2017a).

Considering that certain issues require on-site simultaneous determinations, multicomponent analysis using electronic tongues (E-tongues) appears as a suitable approach to information assessment in an interesting way (KARKRA et al., 2017). The multicomponent analysis is an analytical procedure allowing the extraction of qualitative and quantitative information from an array of non-selective sensors (DI NATALE et al., 1997). Each sensing unit corresponds to a non-specific sensor, in such a way, once immersed in a trial solution, each sensing unit provides a response for each solution-test. The complex data provided describes a characteristic response patterns (fingerprint) for each trial solution, allowing the recognition of liquids of similar composition and detection of substances at very low concentrations.

Advances of nanoscience and nanotechnology have enabled the improvement of overall sensors performance, regarding their main characteristics such as sensitivity, specificity and reproducibility (GOLMOHAMMADI et al., 2017). The analysis of recent scientific researches has shown the preferential employment of optical and electrical transduction for sensing heavy metals (MERCANTE et al., 2017b; NARAYANAN and HAN, 2017; SENTHAMIZHAN et al., 2014; ZUO et al., 2018). Corroborating with this observation, there is a rising number of researches exploring optical and conductive nanomaterials, mainly inorganic materials as metal nanoparticles and carbon-based materials, as graphene and carbon nanotubes (MERCANTE et al., 2017b).

An efficient design of sensor units is a relevant strategy to improve the sensor performance. High surface area, for instance, is a desirable characteristic for sensors and has been widely explored by the use of several nanomaterials. In this context, electrospun fibers have been recently explored as platform to sensors and biosensors (ANDRE et al., 2015; CHEN et al., 2017;

DING et al., 2010; MERCANTE et al., 2017b; SCAGION et al., 2016; TERRA and MERCANTE, 2017), since they can offer a high surface area to interact with analytes, in addition to the possibility of varied surface functionalization.

In this work, we propose the fabrication of distinct sensors architectures based on ternary nanocomposites composed of electrospun fibers, cellulose nanocrystals and conductive materials, and the investigation of their performance in sensing determination of heavy metal ions, which will be discussed in details in the next sections.

1.3. Electrospun fibers

Electrospinning is a well-known processing technique used to fabricate micro- and nanofibers of varied morphologies (GUERRINI et al., 2009; RENEKER and YARIN, 2008; SUBBIAH et al., 2005; TERRA et al., 2017). From the control of the experimental conditions, it is possible to obtain polymer fibers with distinct morphologies, dimensions and functionalities. Electrospun fibers can present micro- and/or nanometric diameters leading to the formation of mats rich in pores and channels, conferring them high surface area (DONG et al., 2012; SUBBIAH et al., 2005).

This technique consists basically on the ejection of a polymer solution from the stretching of a drop as consequence of electrical forces applied on it (YARIN, 2011). The procedure is usually carried out at room temperature and inside a ventilated chamber, in order to facilitate the volatilization of the solvent. The electrospun fibers can be collected on distinct types of collectors, including the rotating one (displayed in Fig. 1.1) or directly deposited onto electrodes surface when intended for sensors application. The scheme of an electrospinning apparatus and its components is displayed in Figure 1.1.

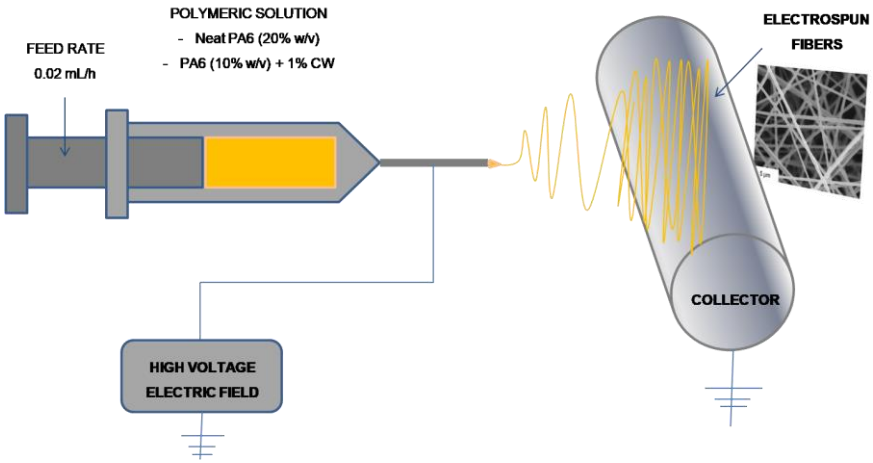

FIGURE 1.1 - Schematic representation of an electrospining apparatus.

Due to their interesting properties, electrospun fibers have been explored for several applications including mechanical reinforcement (DONG et al., 2012; HUANG et al., 2016), sensors (MIGLIORINI et al., 2017a; SINGH et al., 2009) and membranes for wound-dressing (CHENG et al., 2018; WANG; WINDBERGS, 2017), controlled release of drugs and fertilizers (GOH; SHAKIR; HUSSAIN, 2013), among others. The study and application of this type of fibers in sensors aim to explore the high surface area and its consequent increase of sensor sensitivity. However, considering that a great number of sensors designed to detect heavy metals make use of electrical/electrochemical transduction, the insulating properties of most of polymers can hamper the sensing performance. Because of this, the combination of electrospun fibers with conductive materials, as inorganic nanoparticles, carbon-based materials and conductive polymers has shown a possible alternative to overcome the insulating characteristic of this type of fiber.

1.4. Materials employed for the sensor design

1.4.1. Polyamide 6 (PA6)

Polyamides were firstly synthesized by CAROTHERS (1896-1937), a DuPont organic chemist, who synthesized more than 100 polyamide

varieties, including polyamide 66. This was the first commercialized type of polyamide, which was applied to toothbrush bristles and the famous silk socks. In order to attend the required properties of armament industry, the application of polyamides have been extended to reinforce tires and parachute fabrics, for example (FANTONI, 2012). Due to its chemical, mechanical and thermal properties, polyamides had their applications extended to the production of industrial kitchens, screws and gears, fabrics, fishing lines, suture yarns, strings of musical instruments, among others.

Under a chemical approach, polyamides are condensation polymers resultant from polymerization of amines and carboxylic acids. The number associated with the polyamide corresponds to the number of carbons present in the grouper. In the case of polyamide 6 (PA6), the monomer has 6 carbons, including carbonyl carbon (Figure 1.2), and is given the official nomenclature of poly [imino (1-oxohexamethylene)] (SPERLING, 2006). It is a linear homopolymer, in which a large amount of hydrogen-bonding interactions occur intra- and intermolecularly, due to the interaction of the carbon chain hydrogens and nitrogen and oxygen atoms of the amides. Because it is a polymer thermoplastic, the PA6 can be subjected to molding and drawing processes, aiming at the formation of fibers.

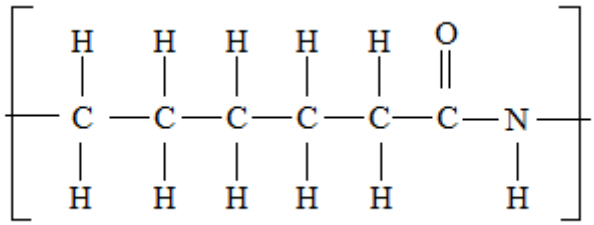

FIGURE 1.2 - Representation of polyamide 6 mer chemical structure.

1.4.2. Silver nanoparticles (AgNP)

Metal nanoparticles have been applied to nanocomposites aiming to explore their conductive and antibacterial properties. The association of nanometric scale to metal particles lead to a increasing of these properties (BECARO et al., 2014). Silver nanoparticles (AgNP), one of the most explored metallic nanoparticles, are synthesized by bottom-up processes, generally by reactions involving aqueous solutions of silver salts (precursor) and reducing and stabilizing compounds (DROGAT et al., 2011; KIMLING et al., 2006; SPAGNOL et al., 2018). Different methods of synthesis of silver nanoparticles have been reported, involving physical, chemical or biological methods, although the chemical reduction is the widest used (AASHRITHA, 2013).

AgNP are mainly synthesized using conventional methodologies as the Turkevich synthesis and the borohydride method. Turkevich synthesis consists in chemical reduction of metallic ions by sodium citrate, which acts as the reducing and the stabilizing agent. The oxidation residues of the citrate anion are adsorbed onto AgNP surface, preventing the aggregation and their uncontrolled growth. The AgNP dimensions obtained by this methodology vary between 60-200 nm (KRUTYAKOV et al., 2008).

The borohydride method, the most explored methodology, requires controlled conditions, in order to avoid the occurrence of uncontrolled agglomeration, since the borohydride shows relatively higher reactivity (in comparison with citrate and carbohydrates) (KRUTYAKOV et al., 2008). The borohydride anion can also act as a stabilizing agent, but it degrades quickly, leading to the agglomeration of AgNP species. For this reason, syntheses involving sodium borohydride require the use of potent stabilizing agents.

A recent trend aims to explore natural compounds as reactants on AgNP synthesis, especially due to their eco-friendly nature, non- toxicity, safer and milder reaction conditions(FARROKHNIA et al., 2017; LIU et al., 2011). As example, carbohydrates have been applied in green synthesis of metal

nanoparticles, once their chemical composition allows their application as stabilizing and also reducing agent (BILIUTA and COSERI, 2019; HASSABO et al., 2015).

Figure 1.3 illustrates a general mechanism involving the reducing of silver cationic species by reducing agent, the following nucleation, controlled coalescence and stabilization, resulting in the typical spherical AgNP with small diameters.

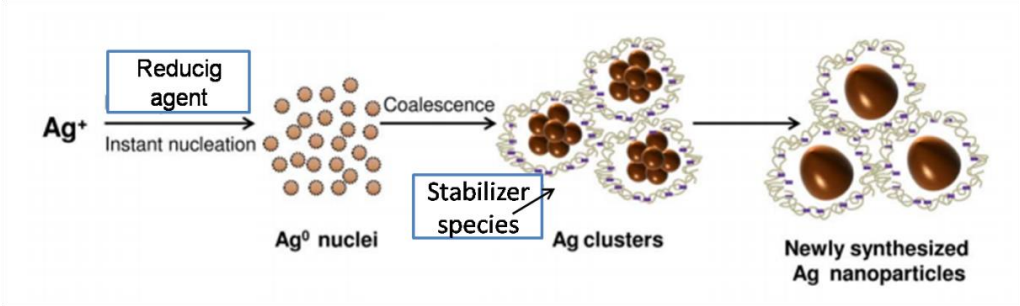

FIGURE 1.3 - Schematic representation of size-controlled silver nanoparticles synthesis (Reprinted with permission from AGNIHOTRI et al. (2014). Copyright (2014) RSC Publishing.

The importance of stabilizing agents in this process arises due the high surface energy of metal nanoparticles, which thermodynamically favors an immediate aggregation for metal-metal specie (JUNIOR et al., 2012). Recent studies have evaluated the use of polymers as stabilizing agent, through interactions between silver and the polymer functional groups. A disadvantage of this method is associated to coating of AgNP by the polymer matrices, hampering the better exploration of their properties (KOGA et al., 2010). Recent researches has shown the better exploration of AgNP properties when they are well-disperse onto nanoscaffolds, as demonstrated by TEODORO et al (2019a), in which cellulose nanocrystals/AgNP hybrids were explored as optical sensing platform for colorimetric detection of hydrogen peroxide (Appendix A).

1.4.3. Reduced graphene oxide (rGO)

Another class of nanomaterials extensively employed in sensor platforms consists of carbon-based materials, such as graphene. Graphene is two-dimensional allotrope of sp2 carbons, present in the constitution of graphite, fullerenes and carbon nanotubes. Each nanosheet of hexagonally rearranged carbons in graphite is called graphene. In these sheets, the electrons are delocalized, which provides the conductive property for this material (ATKINS, 2012).

There are various methods for graphene production, and among them, the synthesis by chemical reduction of graphene oxide (GO) is preferable regarding to the expansion for industrial scale (ALLEN et al. 2009; MOHAN et al., 2018). Experimentally, the graphite exfoliation is first carried out by sonication techniques, in order to obtain the GO nanosheets. The use of a stabilizing agent is required in order to keep the nanosheets well-dispersed. The reduction of the oxygenated surface groups of GO is then carried out, resulting in reduced graphene oxide (rGO). This procedure is illustrated in Figure 1.4. The search alternatives to conventional reducing agents such as hydrazine can be reported and are highly desirable in large-scale syntheses. In this context, recent studies have applied carbohydrate as reducing agents to obtaining o rGO (KAMISAN et al., 2015; SURYABHASKARAM et al. 2014), which was the approach employed in this thesis.

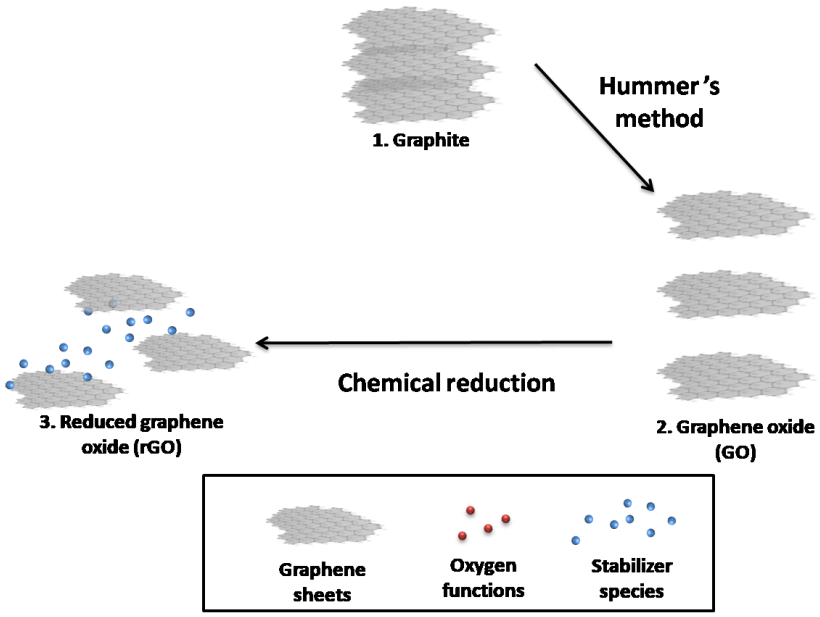

FIGURE 1.4 - Schematic illustration of rGO synthesis from graphite.

1.5. Cellulose nanocrystals (CNC)

Cellulose is the most abundant organic compound on Earth. In general, carbohydrates are the main components produced by plants during the photosynthesis process, constituting an important source of energy for living organisms. In addition, cellulose stores around 40% of available carbon stock of biosphere, representing one of the main sources of this element (EICHHORN, 2011; HUBBE et al., 2008; JONOOBI et al., 2015).

In relation to its chemical structure, carbohydrates are classified as monosaccharides, disaccharides and polysaccharides according to the number of units used to compose the molecule. D-glucose is known as a monosaccharide with formula $C_6H_{12}O_6$ (configuration D refers to the biologically active carbohydrates). The polymerization of β-D-glucopyranose at 1,4-glycosidic bond (β-1,4) results in the cellulose polymer chains (ROY et al., 2009). Figure 1.5 shows a polymeric structure of cellulose, highlighting the so-called *cellobiose*, a disaccharide of glycoses. As a result, is formed a linear homopolymer, with a number of mers (n) ranging from 10,000 to 15,000, depending on the cellulosic source (MOON et al., 2011). The large amount of

hydroxyls present in the cellulose enables strong intermolecular interactions with various materials, including polyamide 6, silver nanoparticles and graphene (KLEMM et al., 2018), as applied in this work.

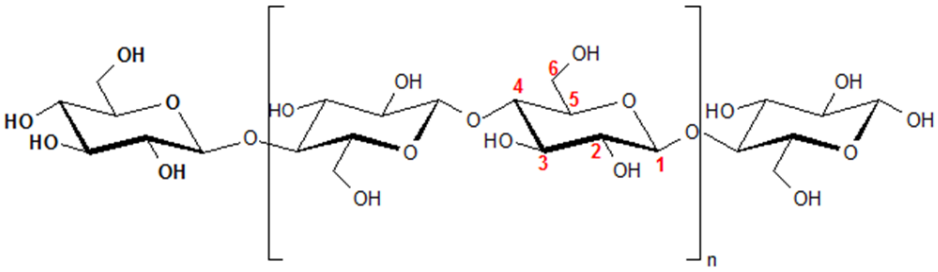

FIGURE 1.5 - Chemical representation of cellulose molecule, highlighting the *cellobiose* dimer and the number of carbons.

Cellulosic nanostructures can be obtained from natural sources. The most explored are the so-called cellulose nanocrystals (CNC), which can be obtained from controlled process of amorphous phase removal, resulting in needle-like structures typical of *whiskers* morphology (JONOOBI et al., 2015; MOON et al., 2011; TEODORO et al., 2017). Acid hydrolysis with strong acids constitutes a traditional method, and the schematic representation shown in Figure 1.6 can exemplify this mechanism.

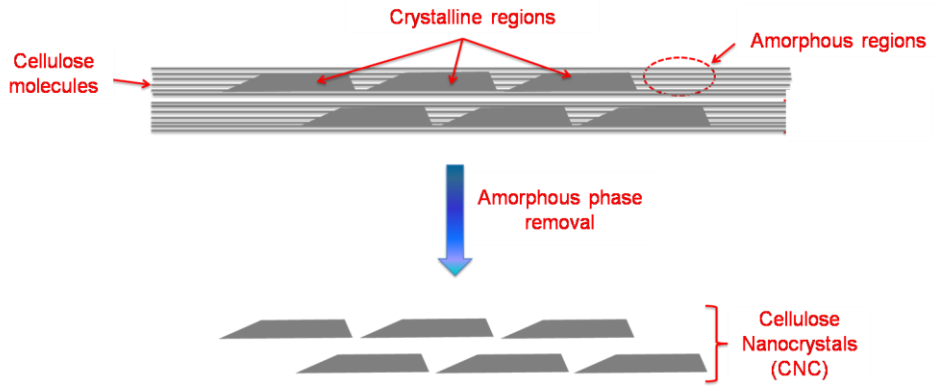

FIGURE 1.6 - Schematic representation of CNC extraction from cellulosic sources.

The literature reveals that these nanostructures can be obtained from different cellulose sources, as plant, animal and bacterial (TINGAUT et al. 2012). Plant sources include agribusiness wastes, such as sugarcane bagasse, palm oil residues and coconut fibers (CAMPOS et al., 2017; CORREA et al., 2010; TEIXEIRA et al., 2011; TEODORO et al., 2011). The use of plant fibers in the development of new materials can result in reduction of costs of the final product, besides promoting the rationalization of these residues, adding value.

2. Goals and Overview

The general goal of this thesis was the incorporation of cellulose nanocrystals functionalized with conductive materials (such as silver nanoparticles and reduced graphene oxide) into high surface area electrospun fibers, aiming at their application in sensors for the detection of heavy metals in water.

Specific Goals

- ✓ Synthesize hybrid materials based on cellulose nanocrystals and conductive materials, as silver nanoparticles and reduced graphene oxide, characterization and investigation of interactions between the components;
- ✓ Investigate the possible methods to combine hybrid materials and electrospun fibers and surface modification of the fibers, and characterization of the resultant ternary nanocomposites;
- ✓ Fabricate sensors by deposition of thin films onto electrodes surface;
- ✓ Evaluate the sensor performance in determining low concentrations of heavy metal ions in water samples.

Chapters Overview

The chapter 3 reports the influence of cellulose nanocrystals in conventional synthesis of silver nanoparticles, as Turkevich and borohydride methods. It was verified that cellulose acts as stabilizing agent, in such way the particles obtained in its presence are well-disperse and with lower diameters. A hybrid formed by cellulose nanocrystals decorated with small silver nanoparticles was obtained, which revealed pronounced antibacterial effects.

The chapter 4 introduces results related to different ways to combine cellulose nanocrystals, conductive materials and polyamide electrospun fibers. The components were combined during electrospinning processing and by immersion of fiber in aqueous suspensions of cellulose/silver nanoparticles hybrid or just silver nanoparticles. The performance of the resultant ternary nanocomposites was evaluated by application of them as sensing units of an electronic tongue for determination of lead in water.

The chapter 5 reports the use of cellulose nanocrystals as reducing and stabilizing agent in green reducing of graphene oxide. The hybrid formed by cellulose nanocrystals/reduced graphene oxide was combined with electrospun polyamide 6 fibers and the potential of application of these architectures as sensing layer was evaluated, and then applied form sensing determination of mercury in water.

3. Synthesis and characterization of cellulose nanocrystals hybrid/silver nanoparticles

***** The content of this chapter is an adaptation of the scientific article entitled: "**Cellulose whiskers influence the morphology and antibacterial properties of silver nanoparticles composites"** by. TEODORO, K. B. R, SANFELICE, R. C., MATTOSO, L. H. C., CORREA, D. S., published in Journal of Nanoscience and Nanotechnology.

Reference: JNN. **2018**, 18 (7), 4876-4883.

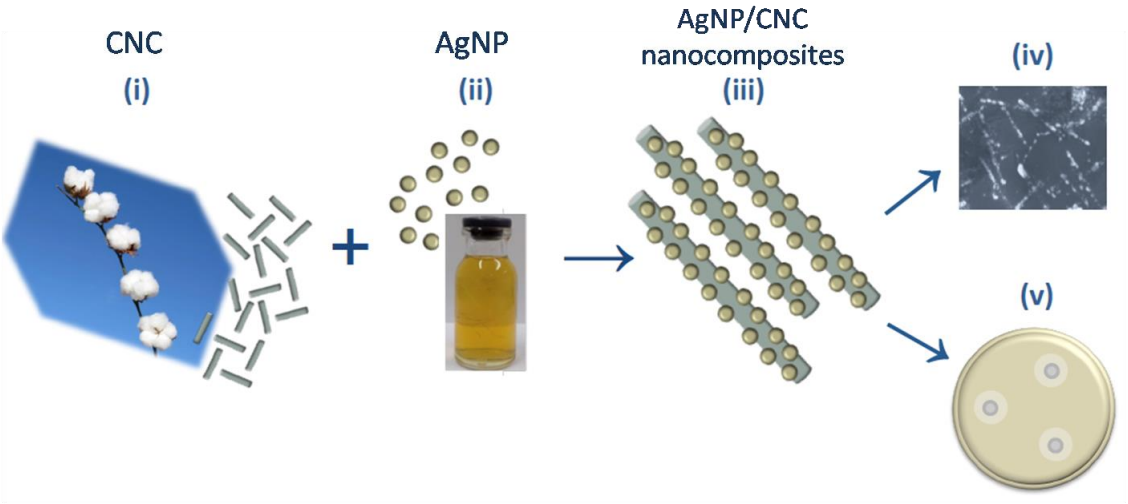

FIGURE 3.1 - Schematic illustration of the synthesis of nanocomposites formed by (i) cellulose nanocrystals (CNC) and (ii) silver nanoparticles, yielding to (iii) AgNP/CNC nanocomposites displaying (iv) varied morphology, according to electron microscopy image, and (v) and antibacterial properties, according to

agar diffusion test. (Reprinted with permission from TEODORO et al. (2018). Copyright (2018) American Society Publishiers.)

3.1. Abstract

Cellulose, the main component of plant cell walls, is a biopolymer widely used for industrial applications, including, food, paper and textile fabrication. More recently, hybrid materials composed of cellulose nanostructures and metal nanoparticles have been applied in diverse areas such as medical and pharmaceutical applications. In this work, cellulose-AgNP hybrid material was synthesized and the influence of cellulose, employed as a stabilizing agent, was investigated. Specifically, cellulose nanocrystals (CNC) were extracted from commercial cotton fibers by acid hydrolysis route, while the AgNP were synthesized by reducing silver salt using sodium citrate and/or sodium borohydride in the presence of CNC. The synthesized CNC/AgNP nanocomposites were characterized in terms of morphology, chemical composition, surface charge and antibacterial properties. The varied synthetic routes generated AgNP with different morphological characteristics in terms of size, shape and coalescence. The particularity of each sample resulted in distinct behaviors for the tested bacteria. Syntheses employing CNC resulted in AgNP/CNC nanocomposites with controlled morphology and improved antibacterial effects against *E. coli* (Gram-negative) and *S. aureus* (Gram-positive), indicating CNC as a promising compound to be used in the syntheses of silver and other metal nanoparticles with controlled morphology and antibacterial properties.

3.2. Introduction

Cellulose is considered the most abundant organic compound in the world, and the simplest natural polymer. This biopolymer consists of long linear chains abundant in hydroxyl groups, which allows them to interact strongly by hydrogen bonds, composing a linearly arrangement known as microfibrils.

Controlled reaction conditions result in extraction of cellulose nanocrystals through a process in which the hierarchical structure of a natural fiber is disrupted, removing non-cellulosic compounds and amorphous cellulose, in order to produce smaller cellulosic structures displaying higher crystallinity. The structures obtained are known as cellulose nanowhiskers or cellulose nanocrystals, and show rod-like shape and nanometric dimensions, resulting in nanostructures with high surface area that have been explored for several applications (HUBBE et al., 2008; JONOOBI et al., 2015) including mechanical reinforcement of polymers (CORREA, A. et al., 2014; SIQUEIRA et al., 2011), membranes for pollutant removal (MAUTNER et al., 2016), hydrogels (ABE and YANO, 2012), land others. The combination between cellulose and silver nanoparticles can result in hybrid materials aiming at applications in antimicrobial wound-healing system (BARUD et al., 2011; BERNDT et al., 2013; MANEERUNG et al. 2008; SURESHKUMAR et al. 2010), antimicrobial hydrogels and aerogels to biomedical and cosmetics (DONG et al., 2013), food package with antimicrobial activity (SIQUEIRA et al., 2014), sensors and biosensors (ARCOT et al., 2015; EDWARDS et al., 2013; LIU et al., 2011; MARZOUK et al., 2016; MORALES-NARVÁEZ et al., 2015).

The application of silver compounds against bacterial propagation is well-known (BERNDT et al., 2013; RAJESHKUMAR and BHARATH, 2017) once it can act against some resistant bacteria strains (RAI et al. 2009). Nowadays, silver nanoparticles can be synthesized using different techniques and reactants, which results in structures with different shape and size and, as consequence, different behavior towards distinct microorganisms (HERMAN and HERMAN, 2014; PAL; TAK; SONG, 2007). In this way, microbiological assays are important to define possible application of these materials, considering their particular properties, which are important for applications in the medical and pharmaceutical areas, and food quality preservation

(JEDRZEJUK et al., 2016; LI et al., 2017) and packaging (BECARO et al., 2016; CANO et al., 2016; KHAN et al., 2016; SIQUEIRA et al., 2014).

Conventional chemical reduction methods to produce AgNP include aqueous solution containing a precursor silver salt combined to reducing and stabilizing agents. Basically, silver cation (Ag^{+}) is reduced to metallic silver (Ag^{0}) by transference of one electron from a reducing agent, while the stabilizing agent acts to avoid the agglomeration and oxidation of metallic silver (LEÓN-SILVA et al., 2016). Traditionally, silver nitrate, sodium citrate and sodium borohydride are used as precursor salt, reducing and stabilizing agent, respectively. Citrate synthesis, known as Turkevich Method, is usually employed for the synthesis of gold nanoparticles (KIMLING et al., 2006), but it has been adapted to produce AgNP. In this method, citrate anions act as reducing and stabilizing agent (AASHRITHA, 2013; KRUTYAKOV et al., 2008) for AgNP, yielding wide range in diameter or size. Although sodium borohydride is the most employed reducing agent for the AgNP synthesis, a rigorous control of reaction conditions (KRUTYAKOV et al., 2008) is required, in addition to the use of another chemical to produce a stable colloidal suspension. In this context, AgNP green-synthesis has been employed in order to decrease the use of hazardous substances usually included in traditional chemical routes (LEÓN-SILVA et al., 2016). The application of cellulosic nanostructures as stabilizing agent for AgNP synthesis follows this context and allows the application of a cheap, biocompatible, biodegradable and nontoxic biomaterial (DONG et al., 2013; KOGA et al., 2010; KOLAROVA et al., 2017; TSAI et al., 2017; ZULKIFLI et al., 2017). However, the control of synthesis conditions is necessary, once some of the nanoparticles properties including size, shape, stability and distribution (LEÓN-SILVA et al., 2016; MORONES et al., 2005; NIKIFOROV et al., 2016; SRIKAR et al., 2016) are closely linked with antimicrobial activity.

Here we report on the effects of cellulose nanocrystals applied in the synthesis of AgNP, using combinations of the conventional reactants sodium citrate and sodium borohydride, and silver nitrate. The effects of cellulose nanocrystals on the AgNP final properties were analyzed by microscopy (FEG-SEM, STEM), UV-Vis absorption spectroscopy and surface charge analysis techniques, which were also correlated to the antimicrobial properties of AgNP/CNC nanocomposites against *E. coli* and *S. aureus.* The emphasis on both microorganisms is because they are foodborne pathogens (IVNITSKI et al., 1999). For instance, although *E. coli* can be present in symbiosis with human body, it is normally associated with foodborne intoxication. The same also applies to *S. aureus*, which can generate toxic extracellular products to human health (ADMINISTRATION, 2012).

3.3. Materials and Methods

3.3.1. Extraction of Cellulose Nanocrystals

Cellulose nanocrystals (CNC) were obtained from commercial white cotton fibers (hydrophilic type, from Apolo Company), by acid hydrolysis according to the methodology described by (TEIXEIRA et al., 2010), which consists in the addition of 5.0 g of cotton in 100 mL of sulphuric acid 60 wt% (Synth). This mixture was kept under mechanical stirring during 75 min., at 40 °C. Next, 500 mL of cold ultrapure water was used to dilute the suspension. The CNC suspension was washed by successive centrifugations at 10,000 rpm for 10 min., and dialyzed in cellulose membrane (Sigma-Aldrich - D9402) using distilled water, until the dispersion reached pH 6–7. Afterward, the suspensions were ultrasonicated for 5 min using a Branson 450 Sonicator (Branson Ultrasonics). Finally, the suspensions of cellulose nanocrystals were frozen and lyophilized using a SuperModuloFreeze Dryer (ThermoElectron) to remove the water content.

3.3.2. Synthesis of silver nanoparticles

Silver nanoparticles (AgNP) were produced by modification of the Turkevich method (AASHRITHA, 2013), in which silver nitrate (Sigma-Aldrich) was used as precursor, and sodium citrate (Synth) was used as reducing and stabilizing agent simultaneously. Some of the AgNP were also obtained by using sodium borohydride (Sigma-Aldrich) or/and citrate as reducing agent, and CNC as stabilizing agent. The distinct reactants used in each synthesis are described in Table 3.1.

TABLE 3.1 - Description of reactants used in each sample for AgNP synthesis

Sample name	Reducing agent	Stabilizing agent
Ag:Cit	Citrate	Citrate
Ag .Cit . CNC	Citrate	Citrate and CNC
Ag .Cit .Bh	Citrate and boroydride	Citrate
Ag .Cit .Bh . CNC	Citrate and borohydride	Citrate and CNC
Ag .Bh . CNC	Borohydride	CNC

The syntheses were performed under reflux, using 200 mL of silver nitrate aqueous solution (1.0×10^{-3} mol.L^{-1}) heated to boiling point. Next, the reducing and stabilizing agents, described in Table 1, were added to the solutions, and kept under constant stirring during 40 minutes. For the methods employing citrate anion, 4 mL of sodium citrate aqueous solution (2.4×10^{-3} mol.L^{-1}) were added to the solution. For the synthesis employing borohydride anion, 2 mL of sodium borohydride solution was slowly added (9.0×10^{-5} mol.L^{-1}) to the solution containing silver precursor. The proportion of reducing agents and silver precursor was 1 mol Ag : 2.5 mol citrate : 0.1 mol borohydrate.

For the synthesis employing CNC, 20 mL of CNC (5.0 $mg.mL^{-1}$), previously ultrasonicated during 5 min, was added to the solution.

3.3.3. Physicochemical Characterization

3.3.3.1. Scanning Transmission Electron Microscopy (STEM)

Morphology of CNC was investigated by STEM. The sample was prepared by dropping a diluted cellulose nanocrystals suspension on a copper grid (400-mesh formvar-carbon) and letting it to dry at room temperature. The sample was stained using a 1.5 % aqueous solution of uranyl acetate and dried at room temperature. STEM analysis of cellulose nanocrystals were performed usng a Tecnai TM G2 F20 (FEI Company, Hillsboro, USA) electron microscope. The images were acquired with a dark-field (DF) detector. The dimensions were calculated using Image-Pro Plus software.

3.3.3.2. Field Emission Gun Scanning Electron Microscopy (FEG-SEM*)*

Morphologies of AgNP and nanocomposites (AgNP:CNC) were investigated by FEG-SEM technique, as illustrated in scheme 1, using a JEOL-JSM 6701F FEG-SEM equipment. One drop of sample suspension was placed on a hot silicon board, and left to dry at room temperature. Next, this board was coupled into a stub by a double-face adhesive carbon tape. The samples were imaged uncoated.

3.3.3.3. Ultraviolet-Visible Absorption Spectroscopy (UV-Vis)

The presence of AgNP in the AgNP/CNC colloidal suspensions was investigated by UV–Vis absorption spectroscopy through monitoring the absorption band centered at 400 nm, which is related to the Surface Plasmon Resonance (SPR) of AgNP (KRUTYAKOV et al., 2008). Aqueous suspensions of samples were placed in a quartz cell of 1 cm of optical path length, using

ultrapure water as blank sample. The spectra were analyzed using OriginPro 8 software.

3.3.3.4. Zeta-Potential Analysis

Changes on surface charges of CNC were estimated through zeta potential analysis. Aqueous suspensions of samples (0.01 % m/m) were employed. The measurements were carried out using a Malvern Zetasizer 3000 NanoZS equipment (Malvern Instruments, UK). The measurements were carried out in triplicate for each suspension.

3.3.3.5. Antimicrobial Activity Tests

The antimicrobial activities of AgNP and AgNP/CNC nanocomposites were evaluated by agar diffusion test, as illustrated in scheme 1. The procedure was performed in accordance with NCCLS document M2-A8 (NCCLS, 2003). The samples were evaluated regarding the ability to inhibit the growth of *S. aureus* (Gram-positive) and *E. coli* (Gram-negative). Laboratory glassware and broth medium were previously sterilized by autoclaving at 121 °C for 15 min, while the procedures were carried out in aseptic environment using a laminar flow cabinet, which was irradiated with UV light during 15 min, as well as the nanocomposites.

Bacterial inoculate from pre-existing cultures available at the Microbiology Laboratory of Embrapa Instrumentation was cultivated in Muller-Hinton broth medium (Himedia). All inocula were incubated for 24 h at 35 °C. By using UV-Vis absorption spectroscopy technique and monitoring the wavelength at 625 nm one can adjust the bacteria concentration to 10^6 cell.mL^{-1}. The bacteria count was made by comparison with the McFarland 0.5 standard solution as optical equivalent. The McFarland 0.5 standard solution displays a turbidity equivalent to 1.5×10^8 colony forming unit (CFU).mL^{-1}. The bacterial inocula were diluted to 1.0×10^6 CFU.mL^{-1}, once this concentration represents

the minimum values to infective dose in food to *E. coli* and *S. aureus*, according U.S. Food and Drugs Administration Institute (FDA) (ADMINISTRATION, 2012). After the measurements, 100 μL of inocula were uniformly spread onto the broth medium.

Three sterilized paper disc were impregnated with aqueous suspension of Ag:Cit, Ag:Cit:CNC, Ag:Cit:Bh, Ag:Cit:Bh:CNC, Ag:Bh:CNC and CNC, and placed equidistantly on the plate containing the gel broth medium, where the microorganisms were inoculated. Two agar plates were prepared for each sample, which were incubated for 24 h at 35 °C.

To complement the results obtained by the disc diffusion method, the minimum concentration inhibition (MIC) analysis was carried out for samples of AgNP/CNC nanocomposites, according to NCCLS document M7-A6 (NCCLS). This experiment consists in determining the lowest concentration of the antibacterial agent capable of inhibiting the growth of the microorganism tested, in this case, *E.coli* and *S. aureus*. The procedure was performed in a sterile microtiter plate, with 96 wells. Equal volumes of 100 μL of broth medium Muller-Hinton, without agar, were distributed in the wells. Next, 100 μL of AgNP samples were added to the first wells of each row, and the mixtures were homogenized. Subsequently, 100 μL of the mixture of the first wells were extracted and placed in the second wells of each row, which procedure was repeated until the twelfth well. Considering the initial concentration as of AgNP as 114 ppm (114 $mg.L^{-1}$), the concentrations of AgNP samples varied from 57 ppm down to 27.8 ppb. Each sample was carried out in duplicate. Next, 10μL of bacteria suspension (10^6 $cell.mL^{-1}$) was inserted in each well, and the final mixtures were homogenized. The plates were incubated for 24 h at 35 °C. Subsequently to the incubation step, 20 μL of triphenyltetrazolium chloride (0.1 %) was added to each well to indicate the development of bacterial growth.

3.4. Results and discussion

Electron micrographs of CNC, AgNP and AgNP/CNC nanocomposites are showed in Fig. 3.2. In Fig. 3.2 (a) is displayed a TEM image of CNC, where the nanostructures exhibit needle-like shape with diameter and length of 15 nm and 185 nm, respectively. Fig. 3.2 (b) displays SEM image of sample Ag:Cit, which presents spherical AgNP with diameters around 66 nm. One can also observe a few nanoparticles with rod-like shape, which may arise from coalescence of spherical nanoparticles. In Fig 3.2 (c) is displayed a SEM image of AgNP obtained by synthesis Ag:Cit:CNC, which spherical AgNP presented smaller diameters (35 nm) compared to the AgNP stabilized with only sodium citrate. CNC helped to stabilize AgNP, improving its dispersion probably due to the interaction of hydroxyl groups of CNC and silver atoms of AgNP.

The use of sodium borohydride in the synthesis leads to formation of smaller nanoparticles, which was verified in images 3.2 (d), (e) and (f), as a consequence of the higher reducing capability of this compound, in comparison to sodium citrate (KRUTYAKOV et al., 2008). The application of both sodium borohydride and sodium citrate in the same reaction system decreased the coalescence of silver nanoparticles, avoiding the formation of rod-like nanoparticles observed in sample Ag:Cit (Fig. 3.2 (b)), and favoring the formation of smaller nanoparticle.

Synthesis Ag:Cit:Bh (Fig. 3.2(d)) and Ag:Cit:Bh:CNC (Fig. 3.2 (e)) yielded AgNP with similar average diameters (23 and 24 nm, respectively), while synthesis Ag:Bh:CNC (Fig. 3.2 (f)) produced AgNP with lower average diameter (15 nm). It is worth noting that synthesis Ag:Cit:Bh:CNC (Fig. 3.2 (e)) produced AgNP exhibiting triangular and spherical shape, which is probably a consequence of competing mechanisms for nanoparticle stabilization led by both citrate and CNC. Synthesis Ag:Bh:CNC (3.2 (f)) provided spherical AgNP lying

along the CNC structures, which does not occur for the others synthesis due to presence of citrate anion.

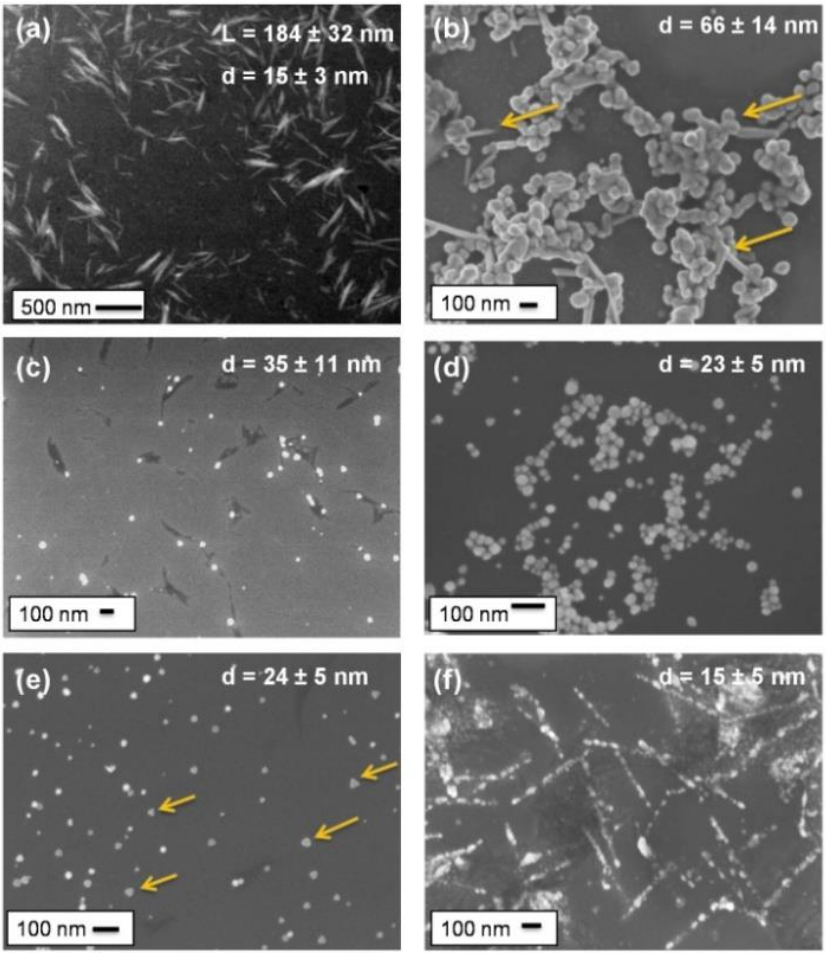

FIGURE 3.2 - Transmission electron microscopy (TEM) image of CNC (a), and scanning electron microscopy (FEG-SEM) images of silver nanoparticles Ag:Cit (b), Ag:Cit:CNC (c), Ag:Cit:Bh (d), Ag:Cit:Bh:CNC (e) and Ag:Bh:CNC (f). Yellow arrows indicate rod-like (image b) and triangular (image e) nanostructures. (Reprinted with permission from TEODORO et al. (2018). Copyright (2018) American Society Publishiers.)

The size distribution of nanoparticle diameters is shown in Figure 3.3. It can be seen that silver nanoparticles reduced by sodium borohydride show a narrower particle size distribution curve, indicating that they have a more

regular size distribution. It is a typical feature of AgNP produced by borohydrate method (KRUTYAKOV et al., 2008).

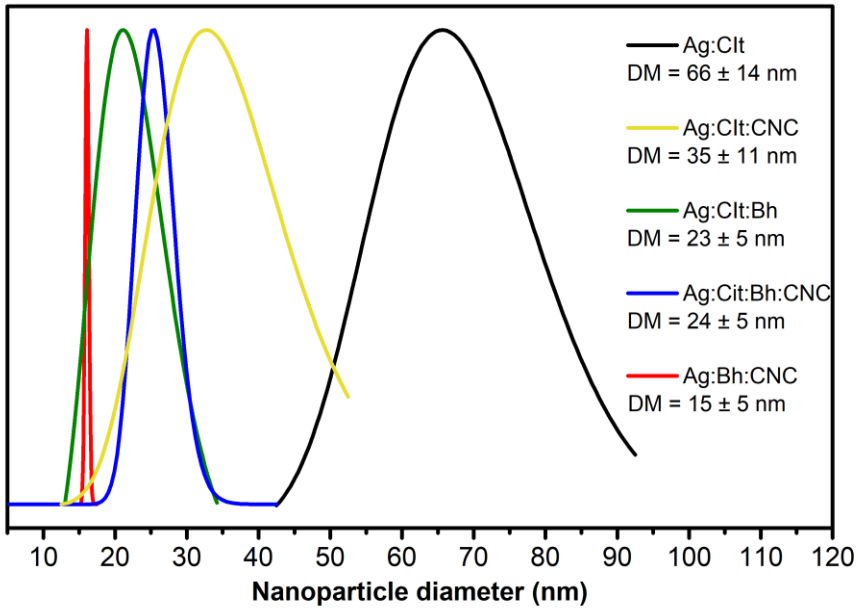

FIGURE 3.3 - Size distribution of silver nanoparticles diameters. (Reprinted with permission from TEODORO et al. (2018). Copyright (2018) American Society Publishiers.)

AgNP suspensions were characterized by UV-Vis absorption spectroscopy and the spectra shown in Figure 3.4 exhibit an absorption band in the range 400-460 nm, typical of silver nanoparticles (AASHRITHA, 2013). The higher morphological inhomogeneity of Ag:Cit sample is reflected by its wider surface plasmon resonance (SPR) band compared to Ag:Cit:CNC, which result is corroborated by the FEG-SEM images displayed in Fig. 3.2, where Ag:Cit:CNC display more homogeneous AgNP.

Ag:Cit:Bh sample showed higher homogeneity of diameters than the other AgNP samples, as can be verified by its narrow absorption band centered at 400 nm. On the other hand, the presence of CNC in the medium (Ag:Cit:Bh:CNC) affected significantly the homogeneity and shapes of AgNP,

yielding the formation of nanotriangles with dimensions of 30 - 40 nm, as displayed by FEG-SEM images of Fig. 3.2 (e). Such fact can be corroborated by the presence of two distinct bands, centered at 425 nm and 472 nm, according to the UV-Vis absorption spectrum for this sample. The first band at 425 nm, regards to the SPR band of spherical AgNP, while the triangular nanoparticles must originate the second band at 472 nm (KRUTYAKOV et al., 2008). As a consequence, such suspension presents a reddish color, in contrast to the typical yellowish color of other AgNP suspensions (see details in Figure 3.4).The UV-Vis spectrum of Ag:Bh:CNC displayed in Figure 3.4 also corroborates the FEG-SEM image (Fig. 3.2 (e)), where the narrow absorption band centered at 408 nm reveals the presence of homogeneous spherical AgNP.

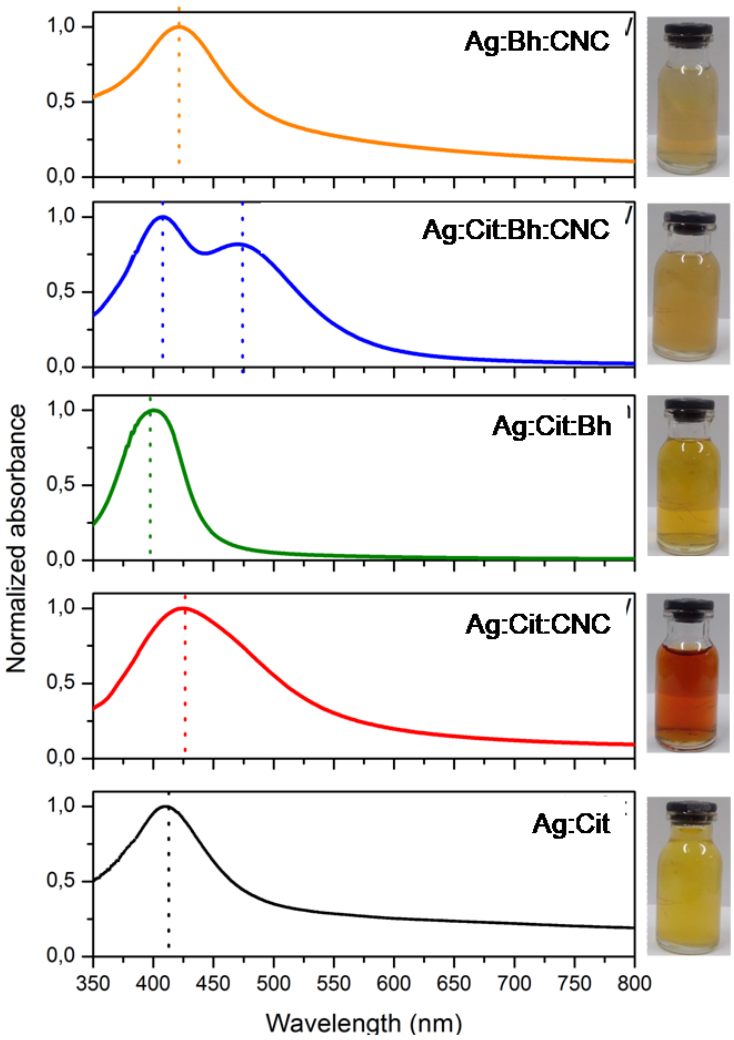

FIGURE 3.4 - UV-Vis absorption spectra of silver nanoparticles obtained by different syntheses. The inset shows the color of distinct AgNP aqueous suspensions (diluted at 1:1). (Reprinted with permission from TEODORO et al. (2018). Copyright (2018) American Society Publishiers.)

Zeta potential values of CNC, AgNP and nanocomposites were measured aiming to verify the surface charge of the nanostructures. All the samples yielded negative zeta potential values, as described in Table 3.2. It is well known that extraction of cellulose nanocrystals using acid hydrolysis with sulphuric acid promotes a partial sulphation of CNC (ROMAN and WINTER, 2004; TEIXEIRA et al., 2010), which contributes to the development of negative charge on the CNC surface, providing a favorable site for AgNP

attachment (PADALKAR et al., 2010). For the other samples, the negative charge derives from the stabilizing agents used for the synthesis of AgNP. Citrate anions encapsulate AgNP by strong electrostatic interaction, neutralizing total charge, which in turn hinders interaction with the hydroxyl groups of cellulose nanocrystals. Borohydride anion can also contribute to the stabilization of AgNP, although it decomposes quickly (KRUTYAKOV et al., 2008) and, therefore, other substances must be employed to act as stabilizing agent (AASHRITHA, 2013; BECARO et al., 2014; MANEERUNG; TOKURA; RUJIRAVANIT, 2008).

The sample that presented the most negative zeta potential was Ag:Cit:Bh:CNC (-43.9 mV), once in this case AgNP were stabilized by both citrate and borohydride anions and had some contribution of hydroxyl and sulphate groups of cellulose.

TABLE 3.2 - Zeta potential values and standard deviation of CNC, AgNP and nanocomposites.

Sample	Zeta potential (mV)
CNC	-25,8 ± 4,5
Ag:Cit	-29,3 ± 7,8
Ag:Cit:CNC	-39,0 ± 9,3
Ag:Cit:Bh	-32,3 ± 6,6
Ag:Cit:Bh:CNC	-43,9 ± 3,9
Ag:Bh:CNC	-26,7 ± 4,2

It is well known that silver and its compounds exhibit strong antimicrobial activities (CANO et al., 2016; JAISWAL et al., 2016; KHAN et al., 2016; SEIL and WEBSTER, 2012; ZEYTUNCU and MORCALI, 2015). Distinct mechanisms on antibacterial activity of silver have been cited in literature. For instance, some authors (DURAN et al., 2010; MANEERUNG et al., 2008) describe that silver ions can interact with thiol groups of enzyme and

proteins used for bacterial respiration and for the transport of substances across the cell membrane and within the cell. These authors also report that the silver ions can attach to the bacterial cell, altering the membrane function and leading to its rupture.

Colonies of *E. coli* and *S. aureus* were employed to verify the antibacterial effects of the distinct AgNP samples synthesized in this work. Antimicrobial properties are influenced by morphology, dimension and concentration of AgNP, as well as by the particular sensitivity of the microorganism investigated. The results of agar diffusion tests are shown in Figures 3.5 and 3.6 to *E. coli* and *S. aureus*, respectively. In general, one notes a more pronounced antibacterial effect of sample Ag:Bh:CNC against both *Escherichia coli* (Fig. 3.5) and *Staphylococcus aureus* (Fig. 3.6), where the clearer zones around the disk indicate that the bacteria growth was inhibited, confirming the strong antibacterial effect of Ag:Bh:CNC.

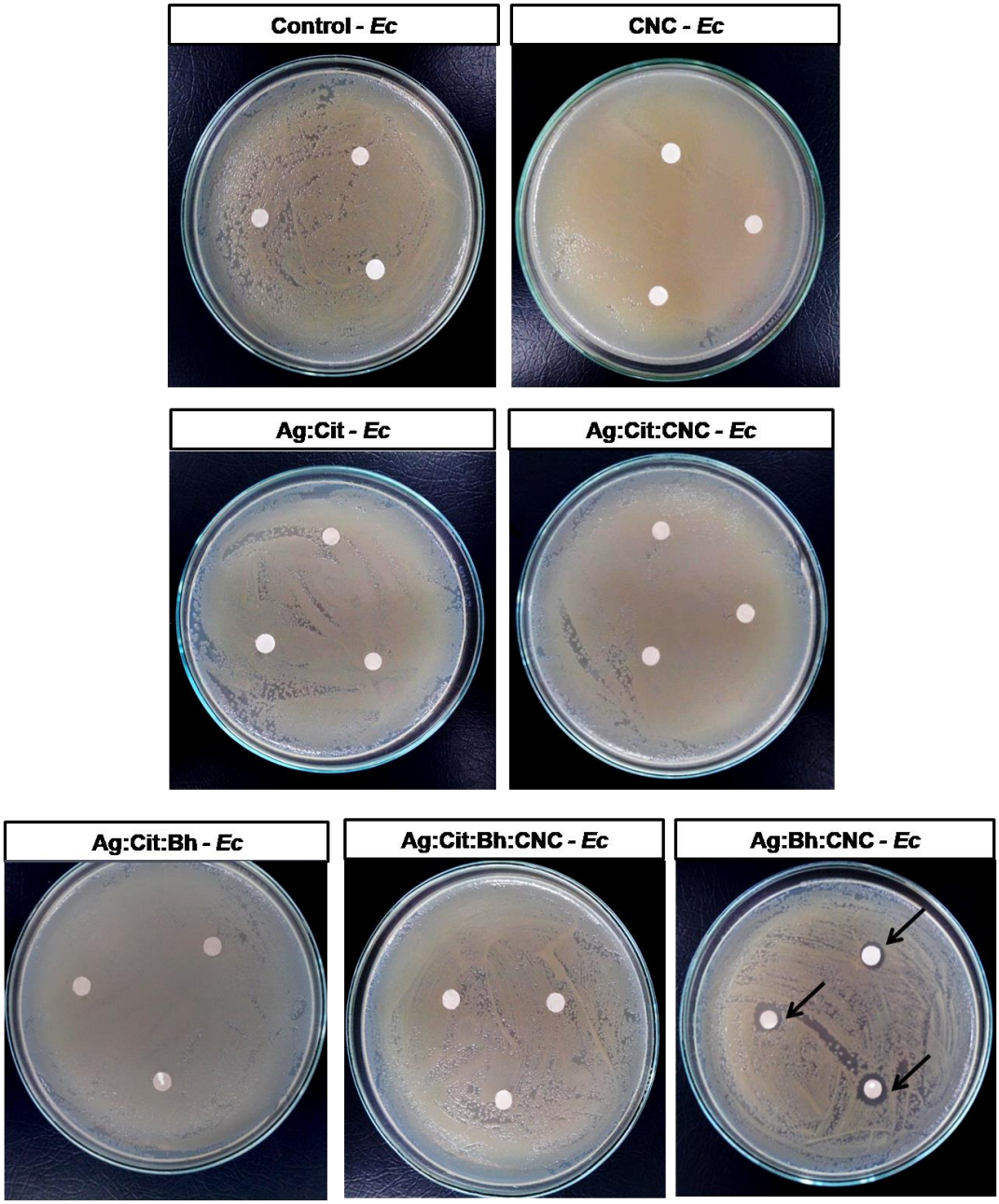

FIGURE 3.5 - Evaluation of antibacterial activity of samples containing silver nanoparticles, by agar diffusion tests. Bacteria investigated: *Escherichia coli*. (Reprinted with permission from TEODORO et al. (2018). Copyright (2018) American Society Publishiers.)

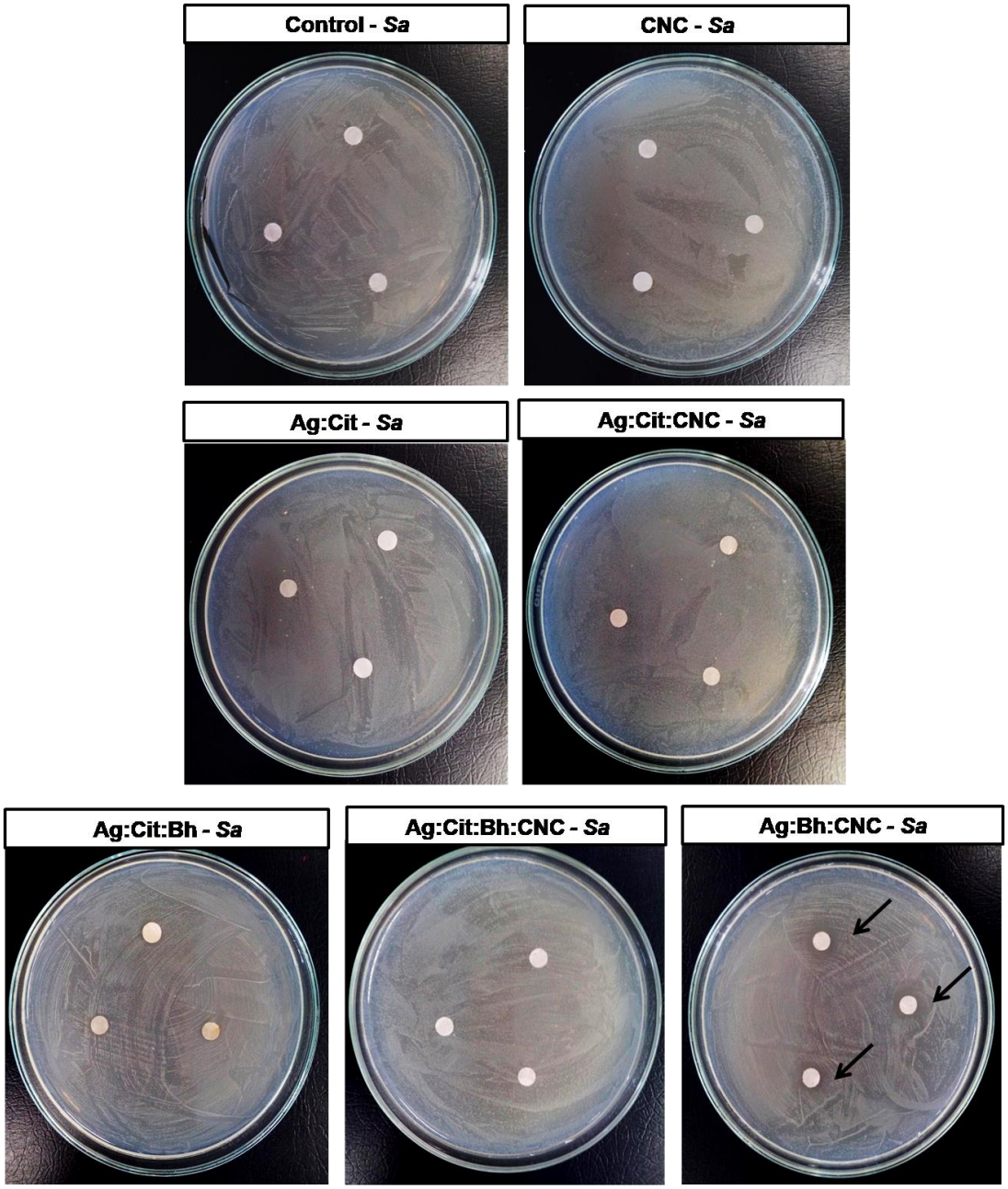

FIGURE 3.6 - Evaluation of antimicrobial activity of samples containing silver nanoparticles, by agar diffusion tests. Bacteria investigated: *Staphylococcus aureus*. (Reprinted with permission from TEODORO et al. (2018). Copyright (2018) American Society Publishiers.)

MIC values obtained for all AgNP samples corroborated the results obtained by agar diffusion test. Ag:Bh:CNC sample was the only to show antibacterial effect, and yielded MIC value of 7.1 ppm to *E. coli*, and 14.2 ppm to *S. aureus*. The main differences between Gram-positive and Gram-negative

bacteria group are in the structure of cell wall. Gram -negative bacteria have a cell wall composed of a thin peptidoglycan layer between the cytoplasm and outer membrane, with dimensions around 2-3 nm. On the other hand, Gram-positive bacteria present a cell wall composed of a thicker peptidoglycan layer, with size around 30 nm, but presents no outer membrane (HAJIPOUR et al., 2012). Silver nanoparticles can attach to most external peptidoglycan layers of Gram-positive bacteria, resulting in a good antibacterial effect (HERMAN; HERMAN, 2014), but small nanoparticles can also penetrate in gram-negative bacteria and act under more than one antibacterial mechanism (MORONES et al., 2005).

Although the scientific literature is not consensual regarding the mechanism involved in antibacterial and bactericidal effects, it is well-know that these effects are dependent on nanoparticle size and shape (PAL et al. 2007), and also on the dispersion (MORONES et al., 2005). Small nanoparticles, as Ag:Bh:CNC, tend to present more pronounced antibacterial effects, once they offer more surface area to interact with thiol groups of bacterial membrane. Moreover, they can penetrate and diffuse more easily than larger particles (DURAN et al., 2010; RAI and YADAV; GADE, 2009), influencing in the respiratory chain and cell division (RAI et al. 2009) . In relation of shape-dependence, it is reported in the literature (PAL et al. 2007) that triangular AgNP can show pronounced antibacterial effects. Ag:Cit:Bh:CNC, which contain triangular AgNP, , did not demonstrate strong antibacterial effects. Such lack of antibacterial effect was probably caused by the larger spherical AgNP nanoparticles found in this samples, compared to the smaller AgNP present in the sample Ag:Bh:CNC.

3.5. Conclusion

In this study, the influence of cellulose nanocrystals applied as a stabilizing agent for the AgNP syntheses was deeply investigated. Conventional

AgNP synthesis employing citrate anion as a reducing and stabilizing agent resulted in low homogeneity of size and shape, due to the nanoparticles coalescence. On the other hand, the combined use of borohydride and citrate anions allowed the production of spherical AgNP with higher homogeneity of diameters. Cellulose nanocrystals in the reaction environment influenced the AgNP formation in different ways. The use of CNC with sodium citrate reduced the AgNP coalescence, yielding spherical nanoparticles. The use of CNC combined with citrate and borohydride resulted in two routes of stabilization, yielding AgNP with spherical and triangular morphologies. In contrast, when CNC was applied as stabilizing agent combined with borohydride as reducing agent (sample Ag:Bh:CNC), AgNP were attached on cellulose nanocrystals surface, yielding spherical AgNP with high homogeneity of shape and small diameters (15 ± 5 nm). As a consequence, Ag:Bh:CNC exhibited a more pronounced antibacterial effect, with minimum inhibitory concentration of 7.1 ppm to *E. coli*, and 14.2 ppm to *S. aureus*. Therefore, the results presented show the CNC biopolymer allowed to produce nanocomposites with good dispersion of AgNP and controlled morphology, small sizes and improved antibacterial properties suitable for applications in wound-healing system and food packaging.

4. Ternary nanocomposites based on cellulose nanocrystals, silver nanoparticles and electrospun fibers: use in an electronic tongue for heavy metal detection

* The content of this chapter is an adaptation of the scientific article entitled: "Ternary nanocomposites based on cellulose nanocrystals, silver nanoparticles and electrospun fibers: use in an electronic tongue for heavy metal detection" by K. B. R. Teodoro, F. M. Shimizu, V. P. Scagion, D. S. Correa, submitted to the Journal Sensors and Actuators B: Chemistry.

Reference: *Sensor Actuator B-Chem. 2019, 290, 387-395.*

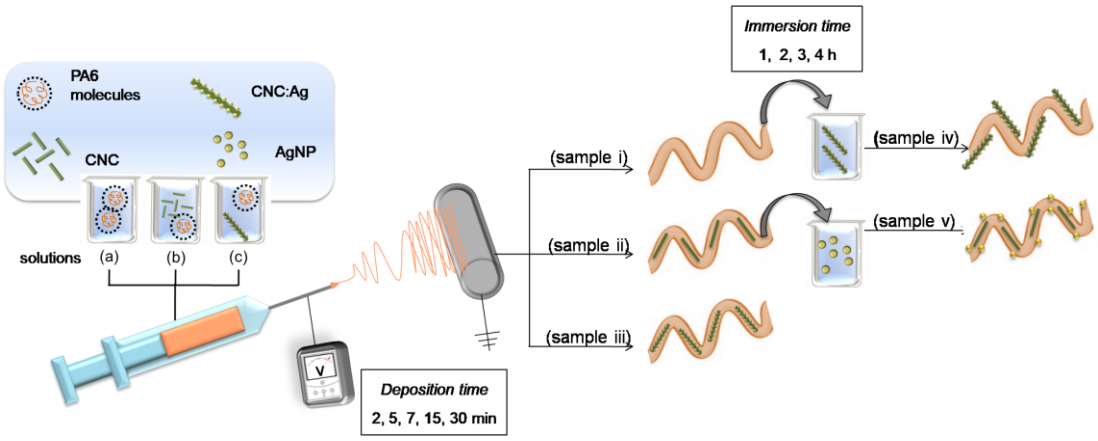

FIGURE 4.7. Experimental setup for ternary nanocomposites fabrication. Samples i - iii represent architectures fabricated by incorporation of nanostructures in the bulk of electrospun fibers, whereas samples iv - v represent electrospun fibers that were surface modified by immersion into the nanostructuressolutions. (Reprinted with permission from TEODORO et al. (2019b). Copyright (2019) Elsevier).

4.1. Abstract

Contamination of water resources with heavy metal ions raises concerns because of their capability to accumulate in living organisms and cause serious health problems. As a consequence, the development of sensitive and reliable sensors capable to provide fast and accessible analysis of water quality regarding heavy metals is highly keen. Nanomaterials advancements have provided considerable improvements in these sensors, enabling efficient detection of different water pollutants even at extremely low concentration. In this work, we evaluated the performance of ternary nanocomposites based on electrospun fibers, cellulose nanocrystals (CNC) and silver nanoparticles as sensing layers used in the electrical detection of heavy metals. These three materials were distinctly combined, resulting in six different sensors, which were arranged to compose an impedimetric electronic tongue. The synergism between the components could be verified by the enhancement of bulk conductance ability when CNC:Ag was combined with electrospun fibers. Adjustments of sensors and frequencies enabled efficient discrimination of distinct heavy metal ions. Moreover, the sensor array could distinguish pure water from aqueous solution contaminated with Pb^{2+} at concentrations as low as of 10 nmol L^{-1}.

4.2. Introduction

A global issue related to water quality is the excessive amount of heavy metals found nowadays in rivers and soils as consequence of improper industrial wastes disposal and other anthropogenic actions (LI et al., 2013; LIN et al. 2017; TCHOUNWOU et al., 2012). Once these pollutants are non-biodegradable, living organisms and human health can be seriously affected as consequence of bio-accumulation (ALKMIM-FILHO et al., 2014; JOSE and RAY, 2018), resulting in serious diseases, mutation and even death by poisoning

(TCHOUNWOU et al., 2012; ZULKIFLI et al. 2018). Lead, specifically, is considered one of the most toxic metals, and can cause cardiovascular diseases, kidney and reproductive dysfunctions (https://www.epa.gov/lead/learn-about-lead#effects). Brazilian environmental agency, for instance, established the maximum lead concentrations for drinking water (SABESP and ANVISA) and effluents discharge (CONAMA) as 0.01 $mg.L^{-1}$ and 0.5 $mg.L^{-1}$, respectively. In this context, heavy metals monitoring in distinct environments becomes of fundamental importance.

Sensors and biosensors (CHAUHAN and SHARMA, 2016; JUSTINO et al. 2017; LU et al., 2018; PENG et al., 2018) are promising alternatives to conventional spectroscopic and chromatographic techniques to monitoring heavy metals in water, where the latter are time consuming and require skilled operators and pre-treatment analysis (LIU et al., 2017). Multi solid-state sensor arrays as electronic tongues (e-tongues) can provide assessment of information from complex signals and, combined with advanced mathematical methods, these devices are capable to distinguish complex and similar samples, providing analysis of water and food quality by an easy and fast qualitative way (DI NATALE et al., 1997; KARKRA et al., 2017; LEGIN et al., 1997; TOKO, 1996). Such devices employ the concept of global selectivity and cross-sensitivity, being formed by distinct sensing units composed of interdigitated electrodes (IDEs) functionalized with different nanomaterials (CORREA, D. et al., 2014; DI ROSA et al., 2017; PODRAZKA et al., 2017). Through electrical transduction, the electronic tongue collects the sample's fingerprint, which is then interpreted by statistical analysis (RIUL-JR et al., 2010). E-tongue approaches have already been used for monitoring varied contaminants in water, including pesticides, medicines and heavy metal residues (FACURE et al., 2017; KARKRA et al., 2017; LVOVA et al., 2016; MARQUES et al., 2017; OLIVEIRA et al., 2012). Specifically, recent studies have reported the detection of very low concentrations (of the order of a few

micrograms per liter) of heavy metal ions in water samples using electrochemical e-tongue devices (ARINO et al., 2017; PÉREZ-RÀFOLS et al., 2017; WILSON et al., 2015).

An efficient design of sensing units is a fundamental strategy to develop E-tongues capable to detect analytes at very low concentrations, which can be achieved by exploring nanostructures and new materials as the active layer. In this work, we report on the development of an e-tongue designed to evaluate lead in water samples, which sensing units were composed by IDE's modified with ternary nanocomposites using polyamide (PA6) electrospun fibers (PA6), cellulose nanocrystals (CNC) and silver nanoparticles (AgNP). Controlled deposition of PA6 electrospun fibers resulted in a thin fiber mat with pores and channels that provide a high surface area to interact with analytes (CHINNAPPAN et al., 2017; MERCANTE et al., 2015; PROMPHET et al., 2015), allowing the detection of very low concentrations of lead. The interest in using nanostructures obtained from sustainable and renewable sources, as cellulose nanocrystals (CNC), is driven by their remarkable properties, which include high aspect ratio, possibility of chemical modification, nontoxicity, insolubility in water and in most common organic solvents, biodegradability, low density and wide abundance (DUFRESNE, 2017; ROY et al., 2009). The negatively charged surface of CNC has been combined to metal nanoparticles in order to work as template/scaffold to keep nanoparticles well-dispersed in different systems (TEODORO et al., 2018), and at the same time to increase electrical conductivity, which allows improvement of electrical conductance (GOULART et al., 2018). Distinct strategies were applied here to combine these materials, resulting in a ternary composite suitable for the e-tongue sensor array employed to detect Pb^{2+}.

4.3. Materials and methods

4.3.1. Materials

Commercial white cotton from Apolo (Brazil), sulphuric acid, sodium citrate, formic acid, lead(II) nitrate, cadmium(II) nitrate, copper(II) nitrate and nickel(II) nitrate were purchased from Labsynth Chemical (Brazil). Ultrapure water was collected from a Merck Milli-Q Direct 8 Water Purification System. Dialysis membrane (D9402), silver nitrate, sodium borohydride and polyamide 6 (20,000 g mol^{-1}) were purchased from Sigma-Aldrich.

4.3.2. Synthesis of Cellulose Nanocrystals (CNC)

CNC were produced via top-down method based on acid hydrolysis of natural fibers. In this experiment, 5.0 g of commercial white cotton were added to 100 mL of 60 wt% H_2SO_4 aqueous solution previously heated at 45 °C. Hydrolysis reaction was performed under constant stirring during 75 min. Cold water (500 mL) was added to reaction mixture, which was then washed by centrifugation at 10,000 rpm for 10 min. Dialysis against distilled water was performed in order to neutralize the CNC suspension, which was then ultrasonicated during 5 min and freeze-dried in a Thermo Fisher Scientific, SuperModulyo220.

4.3.3. Synthesis of CNC:Ag hybrid

CNC:Ag hybrid was produced using a methodology described in (TEODORO et al., 2018). The synthesis was performed under reflux containing 200 mL $AgNO_3$ aqueous solution (1.0 mM). Once reached the boiling point, 20 mL of CNC aqueous suspension (5.0 $mg.mL^{-1}$) was mixed to the reaction system, and 2 mL of sodium borohydride (9.0×10^{-5} $mol.L^{-1}$) was added drop-by-drop, under vigorous stirring. The reaction system was kept under reflux during 40 min and stored in glass flask, protected from light. Figure 4.1 illustrates the proposed architecture of hybrid CNC:Ag.

4.3.4. Synthesis of Silver nanoparticles (AgNP)

AgNP were synthesized following traditional chemical reduction method (KIMLING et al., 2006). The synthesis was performed under reflux containing 200 mL $AgNO_3$ aqueous solution (1.0 mM). Once reached the boiling point, 4 mL of sodium citrate aqueous solution (1.0 mM) was added to reaction system, and 2 mL of sodium borohydride (9.0×10^{-5} $mol.L^{-1}$) immediately prepared was added drop-by-drop, under vigorously stirring. The reactional system was kept under reflux during 40 min and stored in glass flask, protected from light.

4.3.5. CNC, CNC:Ag and AgNP characterization

The morphology of CNC, CNC:Ag and AgNP was investigated by Field Emission Gun Scanning Electron Microscopy (FEG-SEM), using a PHILLIPS-XL30 FEG-SEM microscope. Diluted suspensions (0.5 $mg.mL^{-1}$) of CNC and CNC:Ag were stained with 100 µL of uranyl acetate (1.5 wt%). 1.5 µL of each stained suspension was dripped on a hot silicon board, and left to dry in a desiccator at room temperature. Images were collected using backscattered electrons. Dimensions of CNC, AgNP, CNC:Ag and electrospun fibers were estimated using Image Pro-Plus software and at 100 measurements were used for calculations.

The presence of silver nanoparticles was evaluated by UV-Vis absorption spectroscopy, using an UV-16000 spectrometer Shimadzu spectrometer, software UV Probe 2.31, in which samples were placed in a 1 cm optical path quartz cell and ultrapure water (Millipore system) was used as blank.

Cellulose crystalline structure was evaluated by X-ray diffraction (XRD) technique, using a XRD-6000 Shimadzu diffractometer, employing CuKα radiation (λ = 1.5406 Å) at 30 kV and 30 mA, software XRD-6000. Samples were scanned from 5 up to 40° ($2°.min^{-1}$). The crystallinity index (Ci)

for cellulose was calculated using the Segal equation (Eq. 1) (SEGAL 1959) , measuring the height of I_{200} (2θ= 22.6°) and the minimum intensity at I_{am}(2θ = 18°). I_{200} represents mainly crystalline components, while I_{am} represents the amorphous component.

$$Ci\ (\%) = [1 - (I_{am} / I_{200})] \times 100 \qquad \text{Eq. 1}$$

4.3.6. Production of nanocomposites

Nanocomposites were produced from distinct combinations of PA6, CNC, CNC:Ag and AgNP, using electrospinning as processing technique and immersion in CNC:Ag and AgNP suspensions to promote adsorption of these structures onto the fibers surface. Resulting nanocomposites were obtained as electrospun fibers mats and the ways of combination and correspondent terminologies are described in Figure 4.1 and Table 4.1.

TABLE 4.3- Description of materials' architectures obtained by different combinations of PA6 electrospun fibers, CNC and AgNP used as sensing units of the e-tongue, and correspondent terminology.

Terminology	PA6*	CNC*	AgNP*	Description	Sensing Unit code
Bare	No	No	No	Bare IDE*	el_1
PA6 (2 – 30 min)	Yes	No	No	PA6 electrospun network deposited onto IDE during 2,5, 7, 15, 30 min.	el_2
$(PA6/CNC)_{bulk}$	Yes	Yes	No	CNC incorporated into PA6 fibers during electrospun procedure	el_3
$(PA6/CNC:Ag)_{bulk}$	Yes	Yes	Yes	Hybrid CNC.Ag incorporated into PA6 fibers during electrospinning procedure	el_4
$(PA6)_{im.CNC:Ag}$	Yes	Yes	Yes	PA6 fibers coated with CNC:Ag hybrid after 1-4 hours immersion.	el_5
$(PA6/CNC)_{im.Ag}$	Yes	Yes	Yes	PA6/CNC fibers coated with AgNP after 1-4 hours immersion.	el_6

Fibers were electrospun using a 10.0 wt% PA6 solution, using formic acid as solvent. The processing was made using a homemade electrospinning apparatus with the following parameters: feed rate of 0.02 mL h^{-1}, electrical field of 20 kV, distance of 5 cm between end of needle and collector. Fibers were collected onto aluminum foil, fluorine doped tin oxide (FTO) electrodes and gold interdigited electrodes (IDE) surface, in accordance with each experimental purpose.

In order to produce nanocomposites $(PA6/CNC)_{bulk}$ and $(PA6/CNC:Ag)_{bulk,}$ a mass of 1.0 wt% of CNC or CNC:Ag was added to PA6 solution and ultrasonicated during 5 min, under amplitude of 10 %. Deposition time, ranging from 2 to 30 min, was investigated. The nanocomposites $(PA6)_{imCNC:Ag}$ and $(PA6/CNC)_{imAg}$ were formed by immersion of neat PA6 or $(PA6/CNC)_{bulk}$ electrospun mats onto CNC:Ag or AgNP solutions, respectively. The influence of immersion time was investigated, varying from 1 to 4 hours.

4.3.7. Nanocomposites characterization

Morphological analysis of nanocomposites (electrospun mats collected in aluminum foil during 30 min, using 2-hours immersion time) was investigated with FEG-SEM analysis. Images were obtained in SEM and COMPO mode, operating at 6 kV. Fibers diameters were estimated using Image Pro-Plus software and taking into account 100 measurements. Images of IDE's coated with nanocomposites were evaluated by SEM analysis, using a JEOL 6510 SEM microscope, operating at 15 kV.

The chemical composition of different nanocomposites was elucidated through Fourier Transform Infrared spectroscopy (FTIR) technique, using a Spectrum 1000 Perkin-Elmer spectrometer, software Spectrum, equipped with attenuated total reflection apparatus (ATR). FTIR spectra were obtained in absorbance mode in the range from 4000 - 400 cm^{-1}, using 32 scans and resolution of 2 cm^{-1}. Nanocomposite mats were deposited onto aluminum

foil, then removed from it and placed in an ATR FTIR apparatus for measurements. The presence of AgNP and the investigation of interactions between the components of ternary nanocomposite were evaluated by thermal analysis (TGA) and differential scanning calorimetry (DSC) techniques. TGA analysis was carried out with a TA instrument equipment (TGA Q500), in which the samples (10.0 ± 1 mg) were heated from room temperature until 600 °C at a heating rate of 10 °C.min^{-1}, under inert atmosphere (N_2 - 60 mLmin^{-1}). TG and DTG curves were analyzed using Origin 8 software. DSC was performed using a Q100 TA Instruments, software TA Instrument Explorer. DSC thermograms relative to second heating of PA6 and nanocomposite were collected. Samples (5.0 ± 1.0 mg) were heated from 0 °C to 250 °C using a heating rate of 10 °C.min^{-1}, under nitrogen flow (60 mL.min^{-1}). Crystallinity degree was determined from the melting peak areas, using Eq. 1, described by (CORREA, A. et al., 2014):

$$Ci\ (\%) = (\Delta H_m/\Delta H_m^0) \times 100 \qquad \text{Eq. 2}$$

in which ΔH_m = enthalpy of fusion recorded to each sample, and ΔH_m^0 = heat of fusion of the PA6 considering it 100% crystalline (taken to be 190 J.g^{-1}).

Experimental parameters as fibers deposition time onto electrodes and immersion time required to modify the fibers surface were determined in order to optimize the conductance of nanocomposites. Electrochemical impedance spectroscopy (EIS) and cyclic voltammetry (CV) experiments were performed using a conventional three electrodes electrochemical cell, using an Ag/AgCl (3.0 M KCl) reference electrode, platinum foil as counter electrode and FTO coated with the distinct nanocomposites as working electrode, connected to a Potenciostat Autolab PGSTAT 204 Metrohm, using the software NOVA 1.11. 5.0mM of $[Fe(CN)_6]^{3-/4-}$ dissolved in 0.1 M PBS solution (pH 7)

was prepared. EIS experiments were carried out by applying 10 mV AC voltage in the frequency range of 0.1 Hz to 10 kHz with respect to the open circuit potential (OCP). CV assays were performed in the potential range of -0.4 V to 1.0 V using 50 $mV.s^{-1}$ as scan rate.

4.3.8. Design of sensing units of the e-tongue

The sensing units of e-tongue were designed by modifying gold IDE's surface with distinct nanocomposites, according to Table 4.1. The IDEs were fabricated using conventional photolithography at the Microfabrication Laboratory from Brazilian Nanotechnology National Laboratory (LMF/LNNano/CNPEM). IDEs were comprised by 50 pairs of fingers, each one having the following geometric features: width (*w*) = 10 µm, gap (*s*) between fingers = 10 µm, finger length (*L*) = 3 mm, thickness (*h*) of metal layer = 120 nm (20 nm of Cr and 100 nm of Au), as illustrated in Figure 4.2.

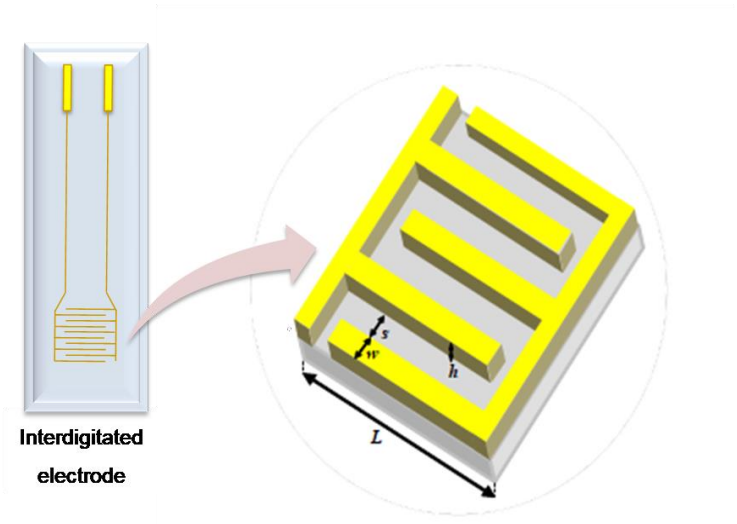

FIGURE 4.8 - Schematic illustration of an Interdigitated Electrode (IDE) and its main geometrical features. They are comprised by 50 pairs of fingers, each one having the following geometric features: width (w) = 10 µm, gap (s) between fingers = 10 µm, finger length (L) = 3 mm, thickness (h) of metal layer = 120 nm (20 nm of Cr and 100 nm of Au). (Reprinted with permission from TEODORO et al. (2019b). Copyright (2019) Elsevier).

4.3.9. Detection experiments

Experiments to discriminate four heavy metal ions (Pb, Cu, Ni, Cd) and different concentrations of lead (10^{-8} to 10^{-3} mol L^{-1}) were performed by electrical impedance spectroscopy, using an impedance/gain-phase analyzer Solartron 1260 A, software SMaRT 3.3.1. Electrical impedance data were collected in the frequency range of 1MHz - 1Hz, under AC electrical voltage of 25 mV. Three measurements per sensing unit were performed, with three independent replicates per sensor. Capacitance data were extracted from impedance information and the whole spectra were statistically interpreted using Principal Components Analysis (PCA) (JOLLIFFE, 1986), Partial least Square (PLS) (GELADI, 1988), Interactive Document Map (IDMAP) (MINGHIM; PAULOVICH; LOPES, 2006) and Parallel Coordinates (PC) techniques (HEINRICH & WEISKOPF, 2013; INSELBERG & DIMSDALE, 1990) using *PEx Sensors* Software (PAULOVICH et al., 2011). Data dimension reduction was performed with PCA and Fastmap techniques employing Euclidean distances.

4.4. Results and Discussion

4.4.1. CNC, CNC:Ag and AgNP characterization

The morphology of CNC, AgNP and CNC:Ag could be elucidated by means of FEG-SEM micrographs shown in Figure 4.3.

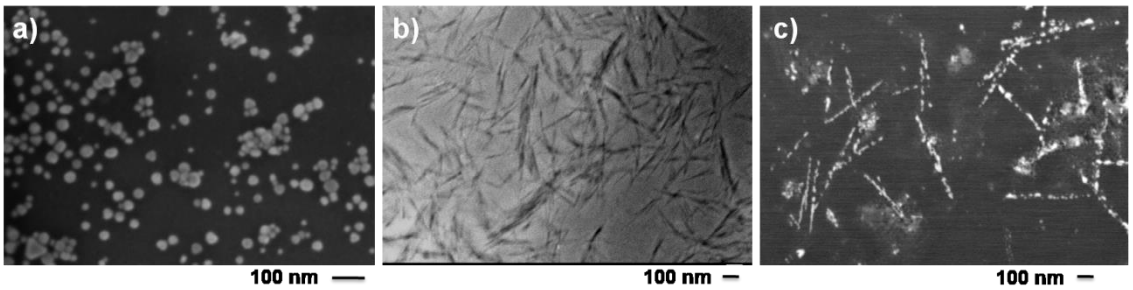

FIGURE 4.9. FEG-SEM micrograph of (a) AgNP, (b) CNC and (c) CNC:Ag hybrid. (Reprinted with permission from TEODORO et al. (2019b). Copyright (2019) Elsevier).

AgNP as spherical nanoparticles, typical of silver nanostructures obtained by chemical reduction method involving citrate and borohydride, is displayed at Figure 4.3 (a). Figure 4.3 (b) shows individual rod-like structures typical of CNC sample, indicating an efficient acid hydrolysis of cotton fibers. CNC:Ag micrography (Figure 4.3-c) displays cellulosic long needles decorated by silver nanoparticles, revealing spherical shape and small diameters with average of 15 ± 5 nm, as verified in previous study (TEODORO et al., 2018). It occurs as consequence of interactions between silver specimens and negatively charged cellulose surface groups (hydroxyl and sulphate), which act as stabilizing agent during the synthesis.

The UV-Vis absorption spectra and XRD diffractograms of AgNP and CNC:Ag samples are presented in Figure 4.4 (a). The well-defined absorption band in the region between 400-425 nm arises from their own localized surface plasmon resonance effect (KRUTYAKOV et al., 2008). The bands verified at 400 nm to AgNP and 410 nm to CNC:Ag samples confirm the successful reduction of silver ions to silver nanoparticles as well as the formation of spherical silver nanoparticles in both samples (KRUTYAKOV et al., 2008).

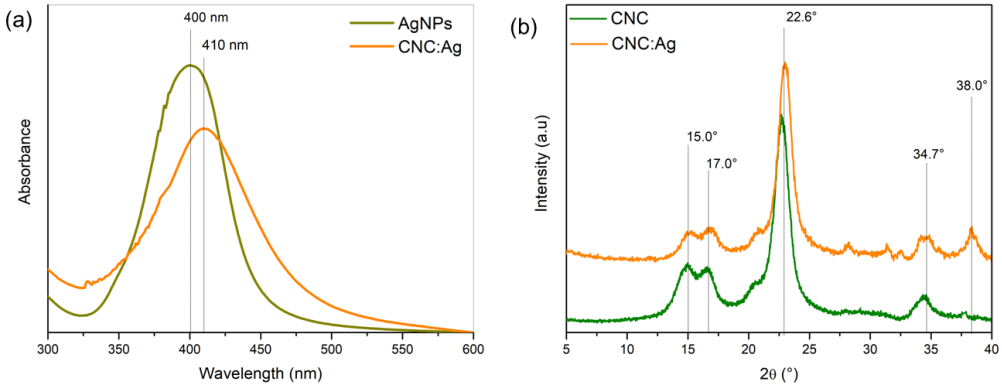

FIGURE 4.10 - (a) UV-Vis absorption spectra and (b) XRD diffractograms of CNC, CNC:Ag and AgNP composition characterization. (Reprinted with permission from TEODORO et al. (2019b). Copyright (2019) Elsevier).

The integrity of cellulose structure after CNC:Ag synthesis was verified with XRD. Diffractograms patterns recorded to CNC and CNC:Ag (Figure 4.4-b) reveal the typical profile of cellulose I polymorphism for both samples. Similar crystallinity index also indicates the integrity of structural, which values were determined as 90.6 % and 93.5 % for CNC and CNC:Ag, respectively. The well-defined crystalline pattern found for CNC arises from the successful removal of non-cellulosic compounds present in natural fibers, plus the degradation of amorphous regions of cellulosic polymer during acid hydrolysis procedure, yielding to crystalline structures whose polymer chains are orientated. Cellulose I polymorphism is composed by triclinic Iα and monoclinic structures Iβ, which reflects in three crystalline peaks at 2θ = 15°, 17°, 22.7°, referent to diffraction caused by $(1\bar{1}0)$, (110) and (200) lattice planes, respectively (JONOOBI et al., 2015). The maintenance of these diffraction patterns for CNC:Ag also indicate that synthesis conditions did not affect the original polymorphism. Moreover, a typical peak at 2θ = 38° reveals the presence of (111) crystallographic plane of face centered cubic structure of metallic silver nanoparticles(XU et al., 2016), confirming the presence of silver nanoparticles in the hybrid.

4.4.2. Nanocomposite characterization

Micrographs of nanocomposites are presented in Figure 4.5, and reveal mats formed by randomly distributed fibers. CNC and CNC:Ag were not visualized in samples $(PA6/CNC)_{bulk}$ and $(PA6/CNC:Ag)_{bulk}$, indicating that these nanostructures were successfully incorporated into bulk, once compatibility and good interactions between CNC and PA6 are expected (CORREA, A. et al., 2014). Diameters of nanocomposites were lower than to neat PA6, which is a consequence of the increase of polymer solution conductivity due to the presence of charged structures (DONG et al., 2012). More regular surface in terms of roughness was verified to $(PA6/CNC)_{bulk}$, It is possible to observe in the sample $(PA6)_{imCNC:Ag}$ the presence of CNC:Ag coating individually the PA6 fibers. The presence of silver nanoparticles was highlighted using backscattered electrons microscope mode, and the correspondent images are shown next to SEM image (left side). No clusters were observed to $(PA6)_{imCNC:Ag}$, in contrast to $(PA6/CNC)_{imAg}$, confirming that CNC:Ag hybrid helps in the silver nanoparticles dispersion.

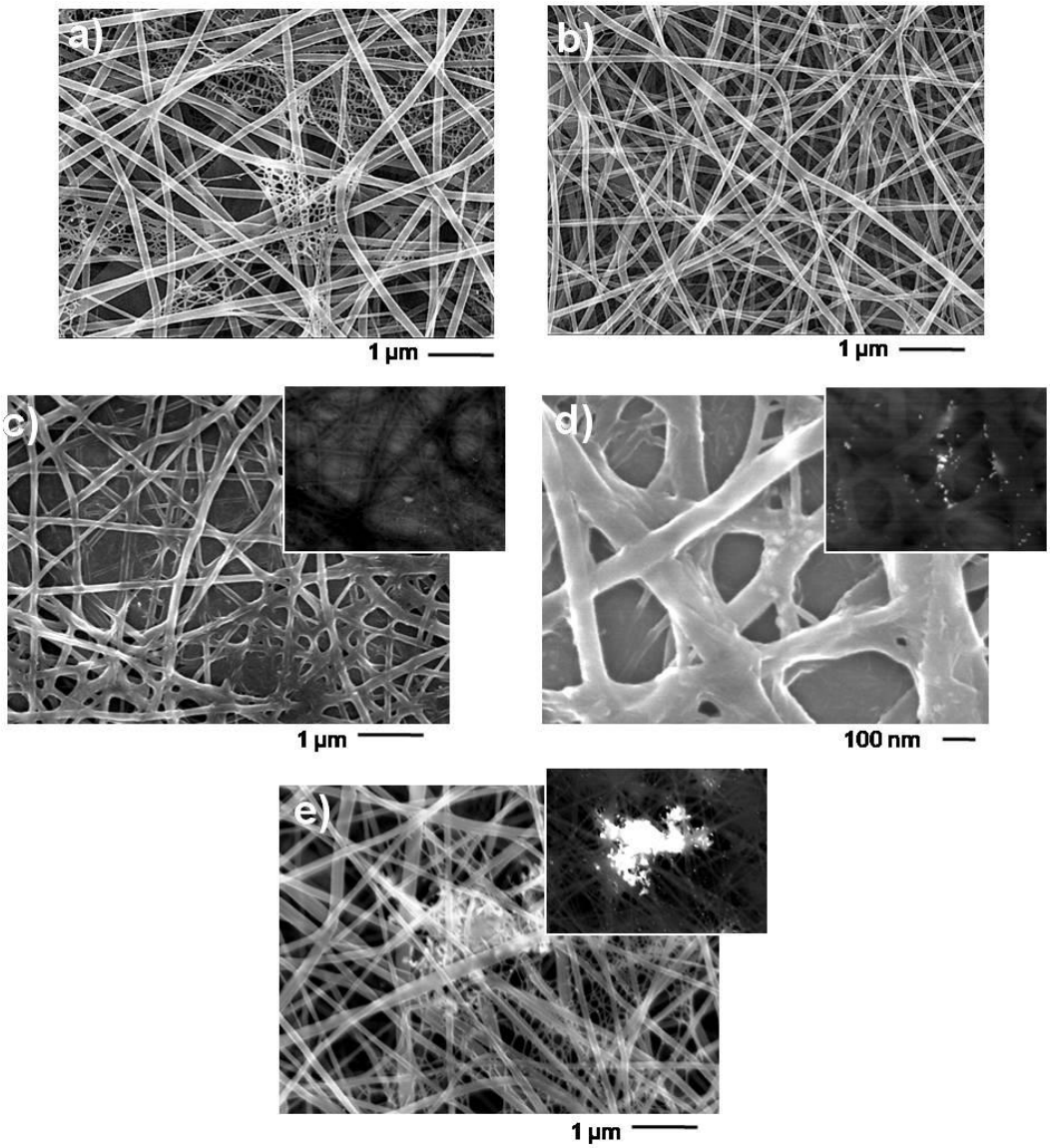

FIGURE 4.11 - FESEM micrographs of nanocomposites: (a) neat PA6 (dav = 81 ± 46 nm), (b) (PA6/CNC)bulk (d= 59.± 20 nm), (c) (PA6/CNC:Ag)bulk (dav = 58 ± 35 nm), (d) (PA6)imCNC:Ag (d_{av} = 72 ± 34 nm), (e) (PA6/CNC)imAgNP (dav = 70 ± 21 nm). Backscattered electrons images of nanocomposites containing silver are shown at upper right side of correspondent micrographs. (Reprinted with permission from TEODORO et al. (2019b). Copyright (2019) Elsevier).

Figure 4.6 displays SEM micrographs of the sensing units composed by IDEs and the distinct nanocomposites (7 min-fiber deposition and 2 hours-immersion in CNC:Ag and AgNP suspensions). The amount of fibers

deposited was enough to modify and coat the IDEs fingers. The use of lower magnification exhibited the structural homogeneity of fibers, except for $(PA6/CNC)_{bulk}$ and $(PA6/CNC)_{imAg}$, which revealed the presence of some fiber defects (beads). However, Figure 4.6 (d) shows that silver nanoparticles favors the formation of free-bead fibers owing probably due to increase of polymer solution conductivity.

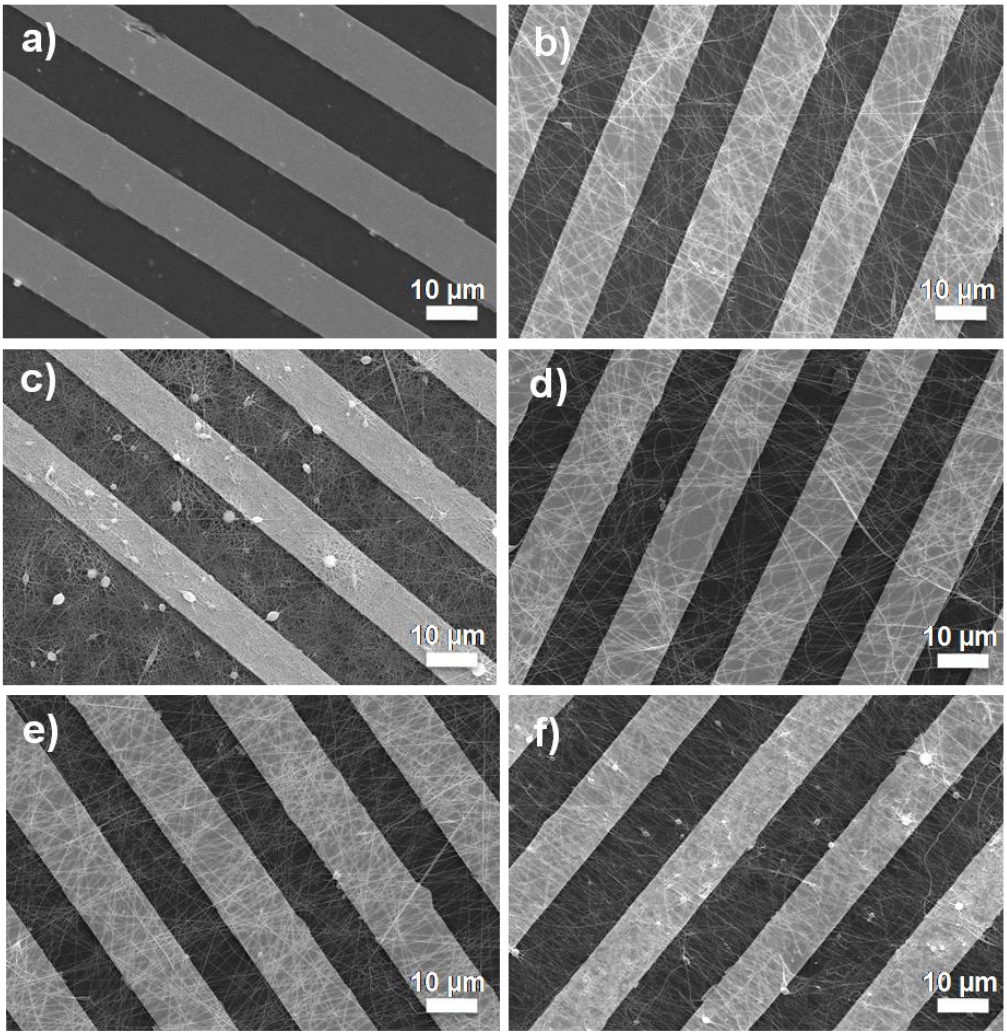

FIGURE 4.12 - SEM micrographs of e-tongue sensing units, which are composed by IDE's coated with nanocomposites as described: (a) bare, (b) PA6, (c) $(PA6/CNC)_{bulk}$, (d) $(PA6/CNC:Ag)_{bulk}$, (e) $(PA6)_{im.CNC:Ag}$ and (f) $(PA6/CNC)_{im.Ag}$. (Reprinted with permission from TEODORO et al. (2019b). Copyright (2019) Elsevier).

FTIR spectra of electrospun fibers confirm the presence of CNC in nanocomposites, which results are displayed in Figure 4.7. The main spectral bands found to electrospun PA6 fibers refer to vibration modes of N-H and C-N amide bonds, amide's carbonyl groups (C=O), and carbonic chain bonds (C-C and C-H). These bands can be verified in PA6 and nanocomposites spectra (i – v), once polyamide is the major component in these materials. Regarding these bonds, 3300 and 3100 cm^{-1} spectral bands arise from free N-H stretching vibrations (CORREA, A. et al., 2014). Axial deformation of aliphatic C-H is also responsible for bands around 2900 cm^{-1} (MIGLIORINI et al., 2017). Most intense bands at 1640 and 1540 cm^{-1} are assigned to amide carbonyl groups (ROTTER and ISHIDA, 1992). Fig 4.7 (b) and (c) display a zoom of nanocomposite spectrum in order to highlight the bands that suggest presence of CNC and CNC:Ag. Bands at 1058, 1160 and 1330 cm^{-1} indicate cellulose C-O-C and C-O vibration modes, as indicated in Figures 4.7 (b and c) (ALEMDAR; SAIN, 2008; TEODORO et al., 2017). Similar spectra were verified for "bulk" and "immersion" nanocomposites.

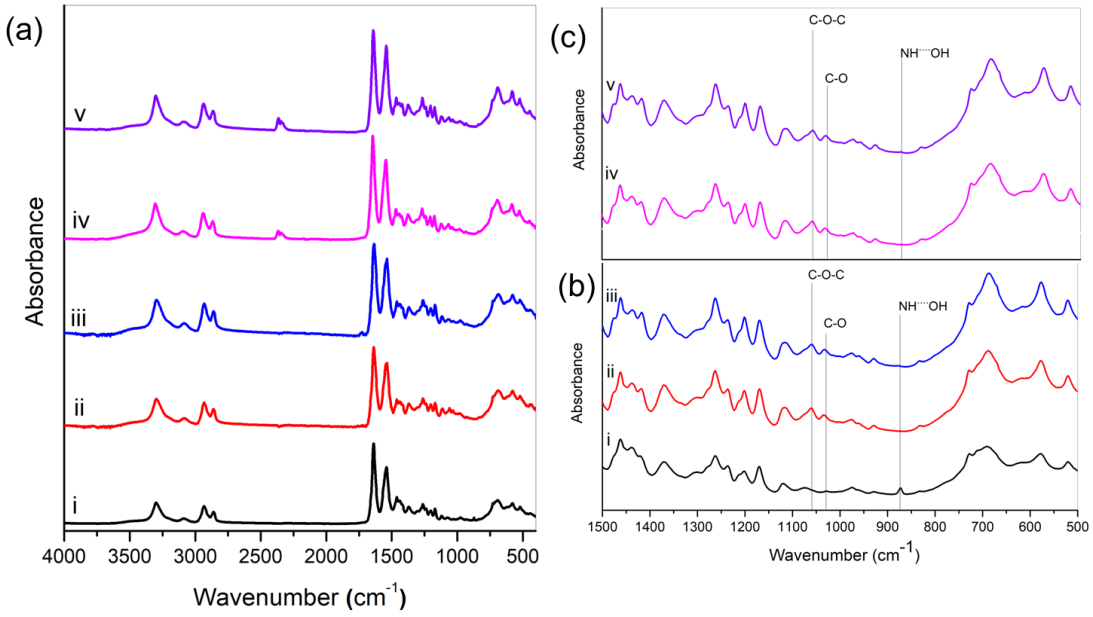

FIGURE 4.13 – (a) FTIR spectra of (i) PA6 electrospun fibers and the nanocomposites: (ii) $(PA6/CNC)_{bulk}$, (iii) $(PA6/CNC:Ag)_{bulk}$, (vi) $(PA6)_{imCNC:Ag}$

and (v) $(PA6/CNC)_{imAgNP}$. Emphasis of 1500-500 cm-1 spectral range for (b) "bulk" composites and for (c) "immersion" nanocomposites. (Reprinted with permission from TEODORO et al. (2019b). Copyright (2019) Elsevier).

Figure 4.8 displays TG/DTG curves obtained from thermogravimetry of nanocomposites. Values referring to initial degradation temperature (T_{onset}) and ashes content at 600 °C are reported in Table 4.2.

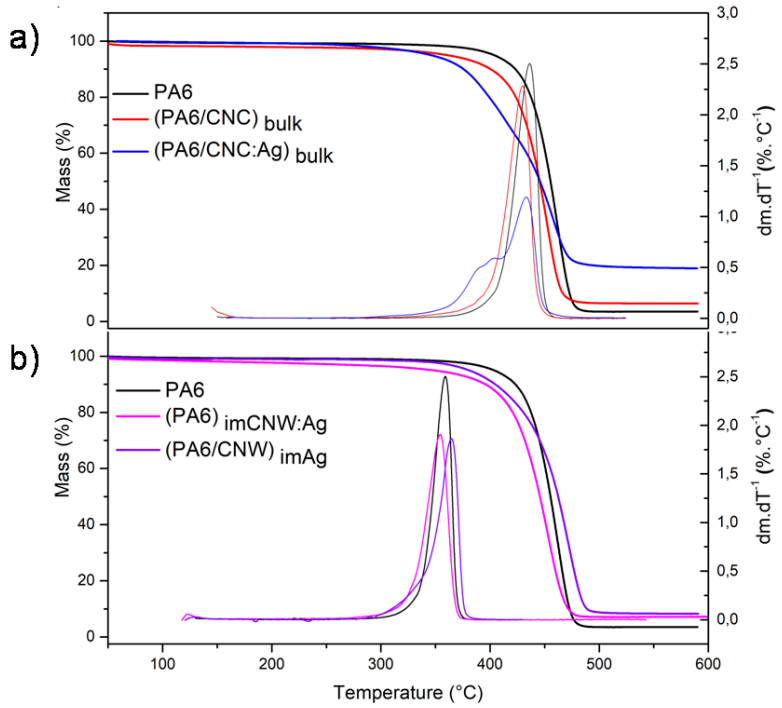

FIGURE 4.14 - TG and DTG curves of PA6 electrospun fibers and the nanocomposites. (Reprinted with permission from TEODORO et al. (2019b). Copyright (2019) Elsevier).

It is possible to observe a major event at around 400 °C as typical profile of polyamide 6 thermal degradation under inert atmosphere (MIGLIORINI et al., 2017b). T_{onset} was estimated as 348 °C for $(PA6/CNC:Ag)_{bulk}$ and 399 °C to neat PA6. Although a slight decrease of T_{onset} could be verified in nanocomposites, the maximum loss rate was kept around

450 °C for all samples, indicating that the presence of nanofiller did not affect significantly the polyamide high thermal stability. Larger amounts of ashes at 600 °C confirm the presence of CNC, CNC:Ag and AgNP, mainly to $(PA6/CNC:Ag)_{bulk}$.

TABLE 4.4 - Values referent to information obtained to from TG/DTG curves to PA6 electrospun fibers and the nanocomposites.

Sample	**T_{onset} (°C)**	**T of maximum loss rate (°C)**	**% ashes at 600 °C**
PA6	399	462	3.56
$(PA6/CNC)_{bulk}$	377	453	6.44
$(PA6/CNC:Ag)_{bulk}$	348	456	18.9
$(PA6)_{imCNC:Ag}$	383	453	7.9
$(PA6/CNC)_{imAg}$	378	472	8.27

DSC analysis was performed in order to monitor potential interactions between PA6 matrix and CNC, CNC:Ag and AgNP as fillers or coatings. Second heating curves are presented in Figure 4.9 and values of melting temperature (T_m), fusion enthalpy (ΔH_m) and crystallinity index (Ci) are described in Table 4.3.

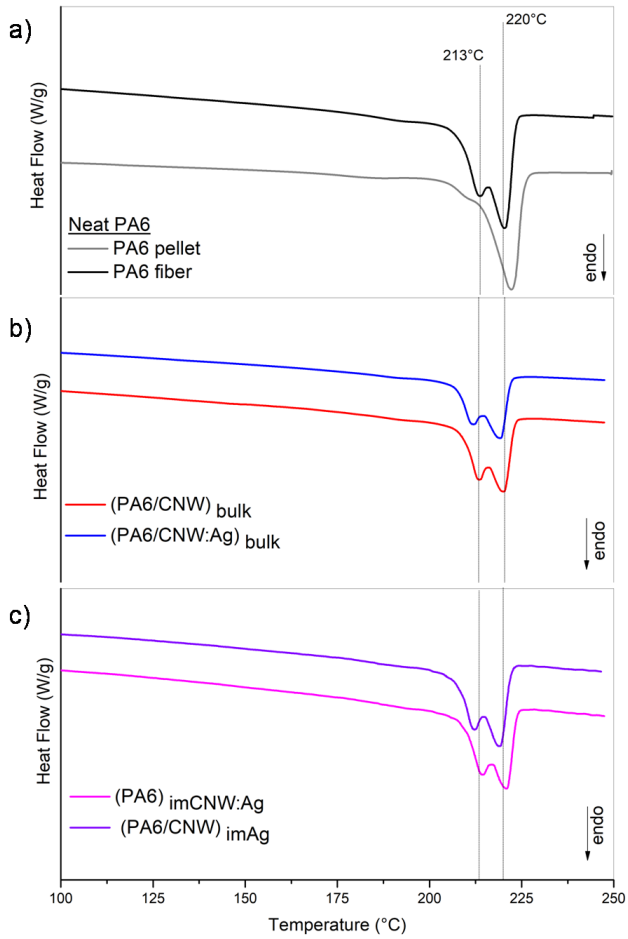

FIGURE 4.15 - Second heating DSC curves of PA6 pellet and electrospun fibers and nanocomposites. (Reprinted with permission from TEODORO et al. (2019b). Copyright (2019) Elsevier).

DSC technique also allows observing processing effects, in this way, neat PA6 were analyzed as electrospun fiber, compared to commercial pellet form. Two major endothermic events are detected to PA6, since the first peak regards to melting of γ metastable crystals and the second and greater peak regards to more stable α-crystals. The main difference between both phases consists in distinct packing, which corresponds to monoclinic planar zigzag conformation to α crystals, and to pseudo-hexagonal helix-conformation to γ phase (SILVA and BRETAS, 2012). The main difference verified between PA6 fibers and pellet regards to an evident increase of γ-phase peak to PA6 fibers, indicating that the electrospinning process induces the reorganization of polymer

chains under this type of crystal. Although cellulose structures can act as nucleation agent, in this case, they can have limited the molecular mobility, hindering the crystals growth (ZHU et al., 2017). As consequence, a substantial decrease of ΔH_m and *Ci* was verified to $(PA6/CNC)_{bulk}$ and $(PA6/CNC:Ag)_{bulk.}$

TABLE 4.5 - Thermal properties and crystallinity index obtained by DSC data of PA6 pellet and electrospun fibers and nanocomposites.

Sample	**Tm α (°C)**	**Tm γ (°C)**	**ΔHm ($J.g^{-1}$)**	**Ci (%)**
PA6 pellet	210	222	52,98	27.9
PA6	213	220	56.7	29.8
$(PA6/CNC)_{bulk}$	213	220	28.5	16.7
$(PA6/CNC:Ag)_{bulk}$	211	218	29.9	17.5
$(PA6)_{imCNC:Ag}$	214	220	41.5	21.8
$(PA6/CNC)_{imAg}$	212	219	41.4	24.2

Nanocomposites were deposited as thin films onto FTO and used as working electrodes for EIS and CV electrochemical experiments. Nyquist plots and cyclic voltammograms displayed in Figure 4.11 and Figure 4.12, respectively, were obtained by employing FTO electrodes coated with the nanocomposites in a conventional electrochemical cell, which works in accordance with a *Randle's equivalent circuit*, as shown in the Scheme in Fig. 4.10 (a), as well as Nyquist plot of neat FTO. Components R_s, C_d, R_{ct} and Z_w regard to electrolyte resistance, double-layer capacitance, bulk resistance and Warburg impedance, respectively (PAVINATTO et al., 2015). In Nyquist plots, resistance R_{ct} corresponds to the semicircular diameter, which is generated either by an electron-transfer process occurring on the electrode interface in electrochemical experiments or by a bulk resistance in impedimetric experiments, in contrast to linear regions of the plot, which contain information regarding diffusional process (WANG et al., 2005).

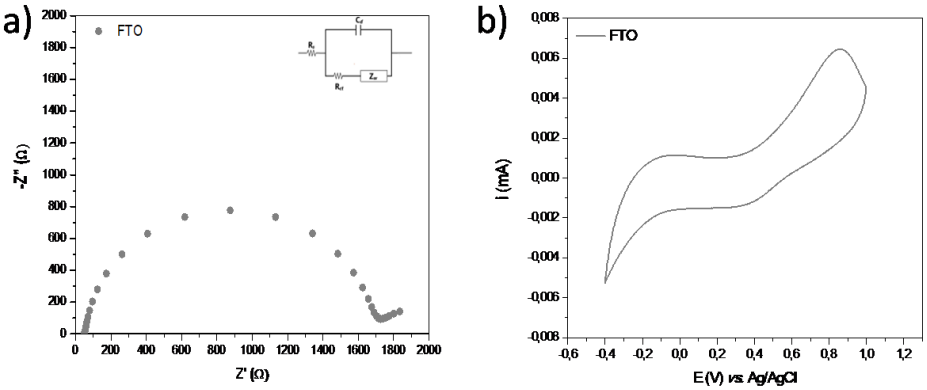

FIGURE 4.16 - (a) Nyquist and (b) Cyclic voltammogram plots for FTO in 5.0 mM $[Fe(CN)_6]^{3-/4-}$ solution dissolved in 0.1 M PBS solution. The inset in Figure 4.10 (a) is the Randle's equivalent circuit model for impedance data. (Reprinted with permission from TEODORO et al. (2019b). Copyright (2019) Elsevier).

The influence of PA6 fibers deposition time onto FTO electrode properties was investigated (Figure 4.11-a) and revealed that longer times of PA6 deposition resulted in enlargement of semicircle due to the electrical insulating properties of this material. A linear increase of R_{ct} values was observed from 7 min on, thus this time was selected as parameter to fiber deposition.

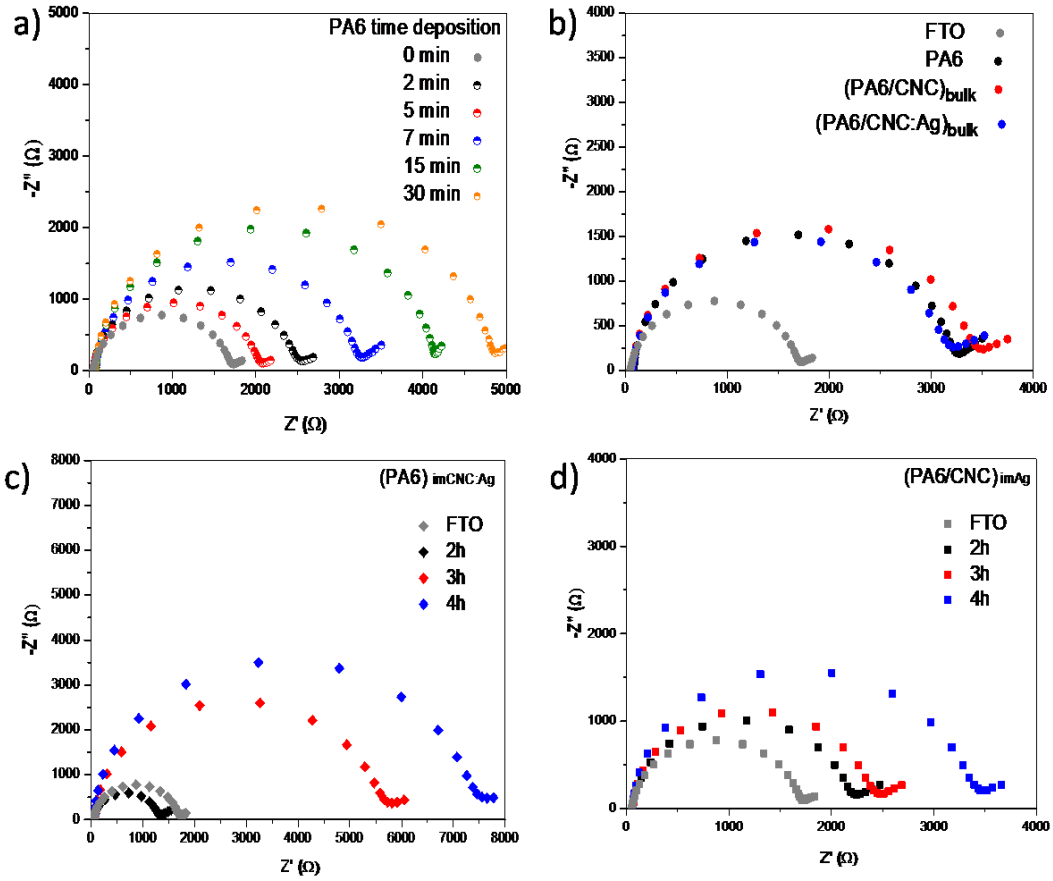

FIGURE 4.17 - EIS Nyquist plots obtained for distinct electrodes regarding (a) time deposition of PA6 electrospun fibers, (b) "bulk" nanocomposites, (c) and (d) immersion time influence. Randle's equivalent circuit model used to fit and analyze impedance data is represented in (a). FTO were used as working electrodes, and experiments were performed using a 5 mmol L−1 $[Fe(CN)6]^{3-/4-}$ solution dissolved in 0.1 M PBS solution. (Reprinted with permission from TEODORO et al. (2019b). Copyright (2019) Elsevier).

The presence of CNC:Ag on the fiber bulk yielded low R_{ct} values (Figure 4.11-b) as a consequence of AgNP electrical conductivity properties. Figures 4.11 (b) and (c) show results related to experimental parameters of $(PA6)_{imCNC:Ag}$ and $(PA6/CNC)_{imAg}$ preparation. The investigation about immersion time revealed an optimized enhancement of conductance for 2-hours immersion to both nanocomposites. These results suggest that longer immersion

times (3 and 4 hours immersion) can impair the distribution of CNC:Ag and AgNP in the nanocomposites.

The electron transfer efficiency of nanocomposites containing silver nanoparticles was also evaluated with cyclic voltammograms, as displayed in Figure 4.12 and Table 4.4.

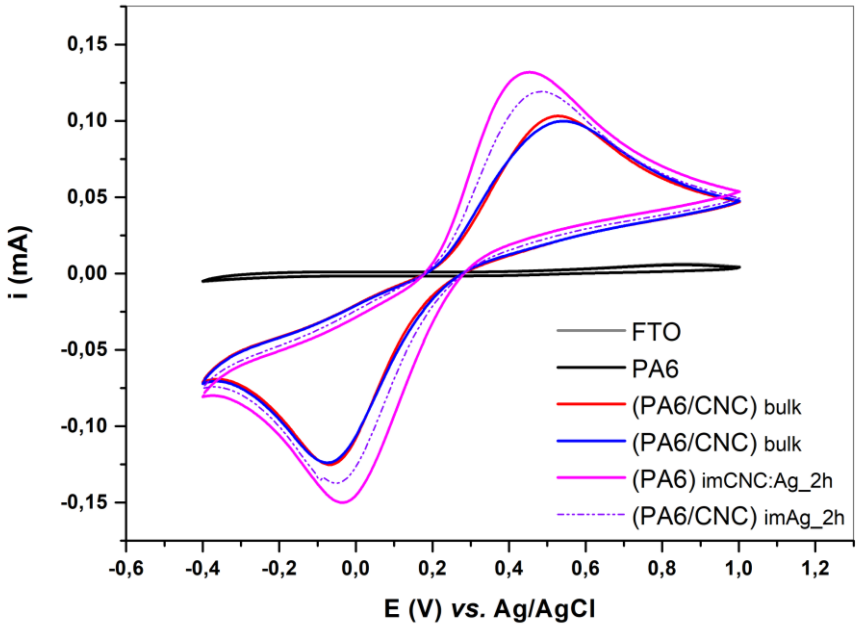

FIGURE 4.18 - Cyclic voltammograms for ternary nanocomposites. The architectures analyzed were obtained in accordance with previous studies, using 7-min deposition time and 2-hours immersion time as fabrication conditions. The experiment was performed in 5.0 mM $[Fe(CN)6]^{3-/4-}$ solution dissolved in 0.1 M PBS solution. (Reprinted with permission from TEODORO et al. (2019b). Copyright (2019) Elsevier).

It is possible to observe an evident increase of current peak occurred when CNC and CNC:Ag was present in the sample, compared to FTO (Figure 4.10 - b) and FTO coated with PA6 fiber. Moreover, $(PA6)_{imCNC:Ag}$ and $(PA6/CNC)_{imAg}$ nanocomposites produced after 2 h of immersion resulted in a higher electron transfer rate and lower peak potential separation (ΔEp),

indicating an enhancement on electron transfer ability. Because of these results, the immersion time of 2 h was chosen to prepare both nanocomposites, $(PA6)_{imCNC:Ag}$ and $(PA6/CNC)_{imAg}$.

TABLE 4.6 - Bulk resistance (R_{ct}) verified by EIS analysis and current peak and peak potential separation data recorded by CV analysis.

Sample	Rct (kΩ)	i_{pc} (mA)	i_{pa} (mA)	ΔEp (V)
FTO	11.7	0.0025	0.0040	0.54
PA6	12.2	0.0036	0.0027	0.51
$(PA6/CNC)_{bulk}$	3.45	0.082	0.13	0.59
$(PA6/CNC:Ag)_{bulk}$	3.19	0.076	0.095	0.62
$(PA6)_{imCNC:Ag}$	1.31	0.106	0.117	0.48
$(PA6/CNC)_{imAg}$	2.23	0.093	0.108	0.52

4.4.3. Ternary nanocomposites used in the electronic tongue

The e-tongue system comprises an array of sensing units used to discriminate liquid samples. The different sensing units prepared using the nanocomposites described in Table 4.1 were employed to detect different heavy metal ions in aqueous solutions. As electrical impedance measurements generate a large amount of data (nearly three hundred spectra), a visual analysis becomes a hard task. One solution is the use of multivariate data analysis to simplify the information visualization of dissimilarities between samples (DI ROSA et al., 2017; HEINRICH and WEISKOPF, 2013; PODRAZKA et al., 2017). Therefore, the experimental data regarding detection of different metals such as Cd^{2+}, Cu^{2+}, Ni^{2+}, and Pb^{2+} ionic solution at 1 $mmol.L^{-1}$ were analyzed with PCA, PLS, IDMAP and PC techniques, as depicted in Figures 4.13, 4.14, 4.15 and 4.16. The calculated silhouette coefficients (-1 i< SC < 1) are 0.90, 0.95, and 0.80, respectively, and according to Rousseuw it means strong data classification (ROUSSEEUW, 1987).

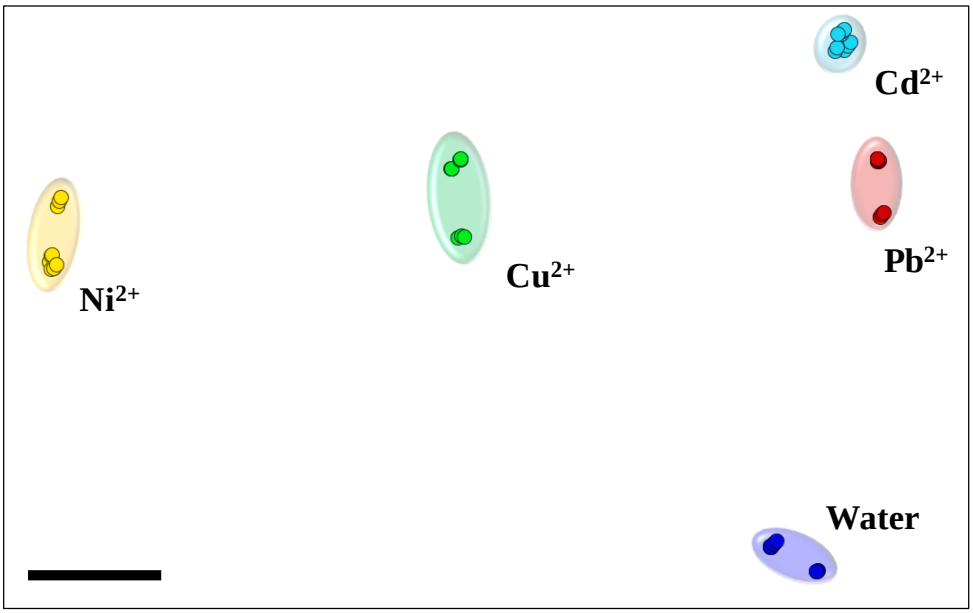

FIGURE 4.19 - PCA plot for different metal solution at concentration of 1 mmol L^{-1}, using the six sensing units. Black bar for guidance only to measure distances between data points. The determined silhouette coefficient is 0.90. (Reprinted with permission from TEODORO et al. (2019b). Copyright (2019) Elsevier).

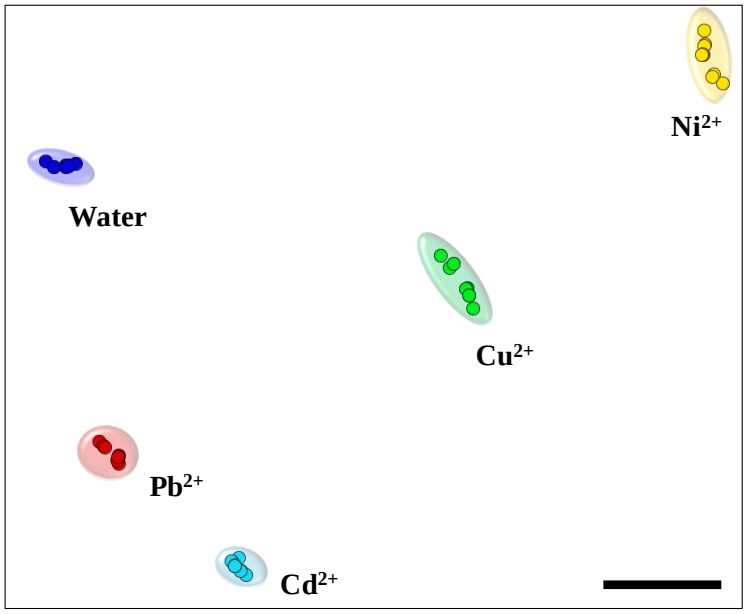

FIGURE 4.20 - PLS plot for different metal solution at concentration of 1 mmol.L^{-1}, using the six sensing units. Black bar is only for guidance to measure distances between data points. The determined silhouette coefficient is 0.95.

(Reprinted with permission from TEODORO et al. (2019b). Copyright (2019) Elsevier).

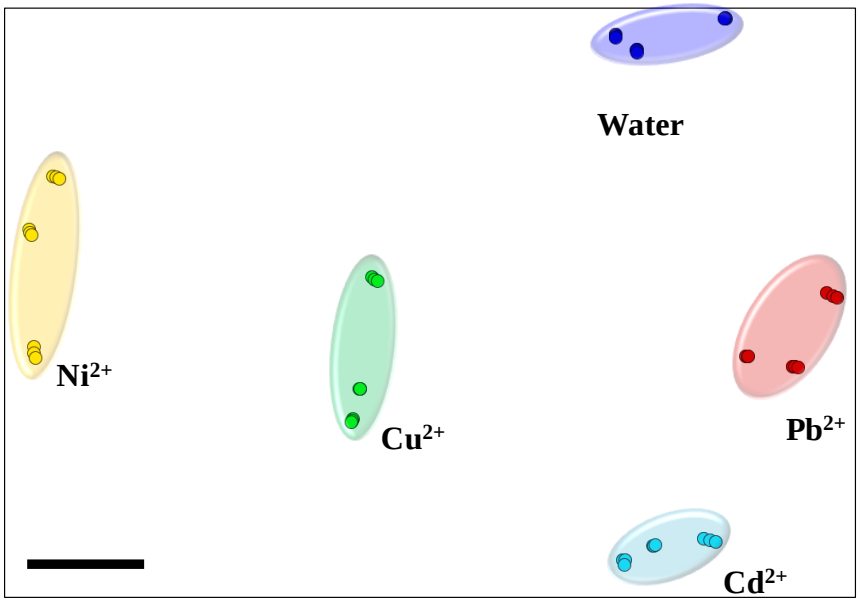

FIGURE 4.21 - IDMAP plot for different metal solution at concentration of 1mmol.L^{-1}, using the six sensing units. Black bar is only a guide to measure distances between data points. The determined silhouette coefficient is 0.81. (Reprinted with permission from TEODORO et al. (2019b). Copyright (2019) Elsevier).

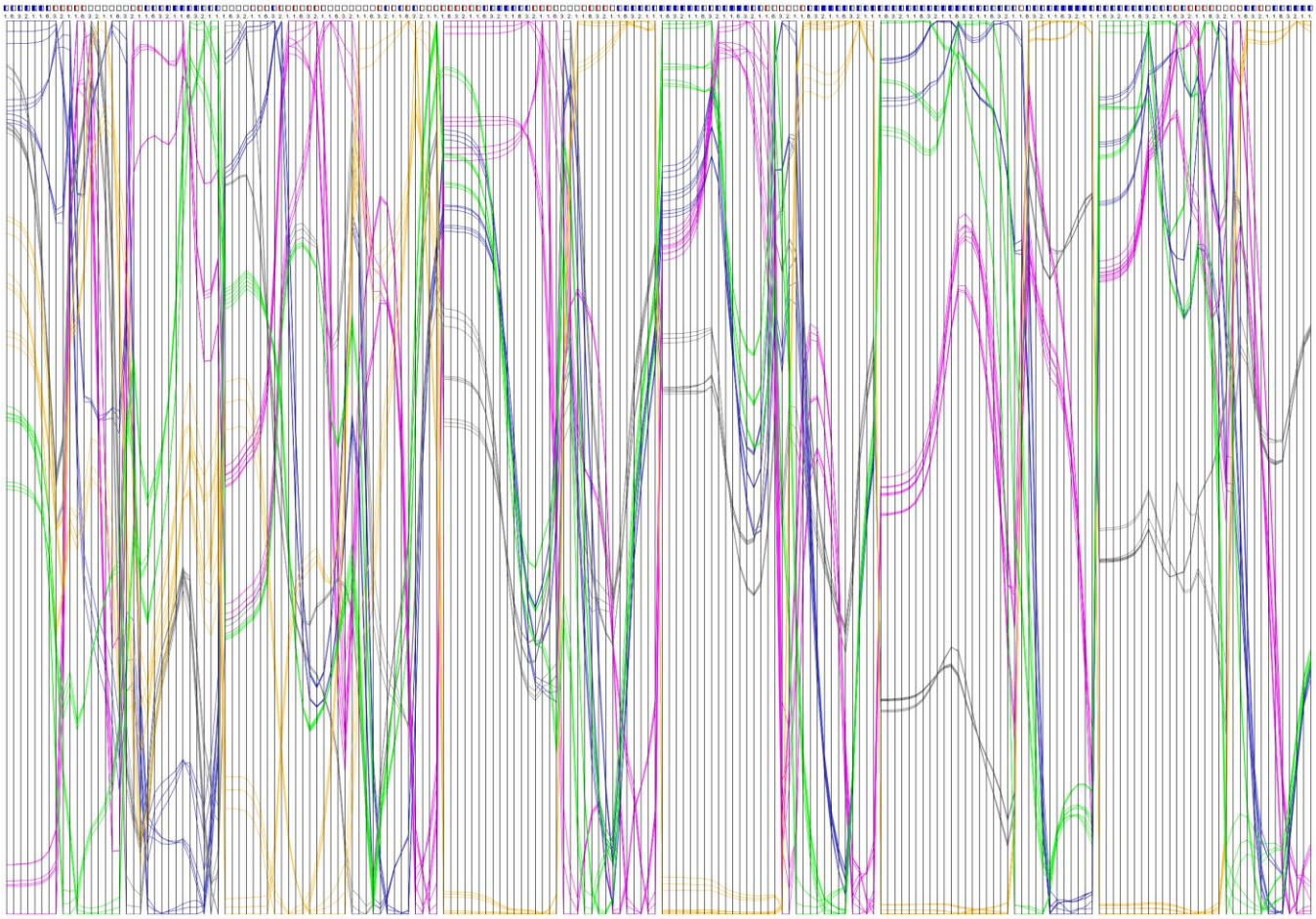

FIGURE 4.22 - PC plot for different metal solution at concentration of 1 mmol.L^{-1}, using the six sensing units. (Reprinted with permission from TEODORO et al. (2019b). Copyright (2019) Elsevier).

Parallel coordinate plots show boxes in blue or red colors, which provide relevant or negligible/hampering information, respective. As considerable number of red boxes can be observed, then we employed the feature selection procedure (DAIKUZONO et al., 2017) to enhance discrimination quality. Figure 4.17 (a) summarizes boxes information and the performance of each sensing unit is then performed in terms of blue boxes, Figure 4.17 (b), and silhouette coefficient, Figure 4.17 (c), where both point to the follow conclusion: *i)* el_2 and el_3 (SC < 0.71) have poor performance, *ii)* el_1 and el_6 are intermediate, and *iii)* el_4 and el_5 are the most sensitive sensing units. These observations can be related to experimental results, which point out that a lower resistance is caused by the presence of silver, mainly for sample $(PA6)_{imCNC:Ag}$, in which silver is more

homogeneously distributed in comparison to sample $(PA6/CNC)_{imAg}$. Lower contribution arises from electrodes coated with electrical insulating materials, as suggested by the high resistance verified by electrochemical experiments.

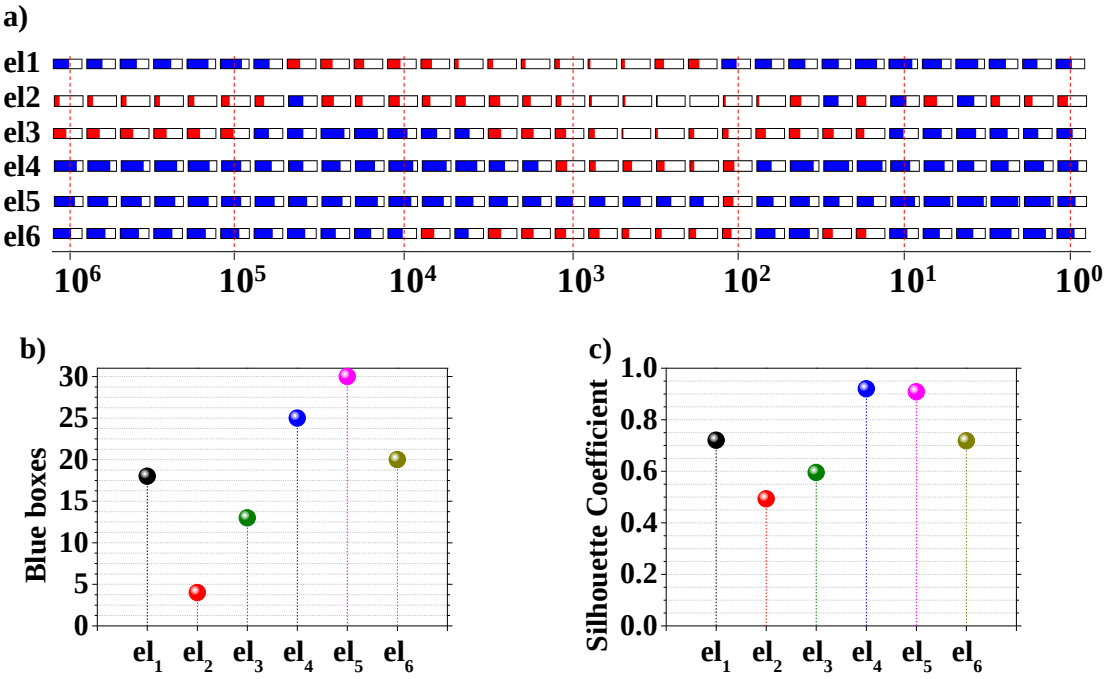

FIGURE 4.23 - a) Blue boxes collected from Parallel Coordinate plot for different metal solution at concentration of 1 mmol.L-1, using the six sensing units. b) Data plot of blue boxes and c) silhouette coefficient of each sensing unit. (Reprinted with permission from TEODORO et al. (2019b). Copyright (2019) Elsevier).

The feature selection of frequencies caused the predominance of blue boxes and a new PLS plot was made (displayed in Figure 4.18), which increased the SC from 0.95 to 0.98 and points were better grouped with low dispersion. The exclusion of el_2 and el_3 also lead to an increase of SC to 0.99 (Figure 4.19).

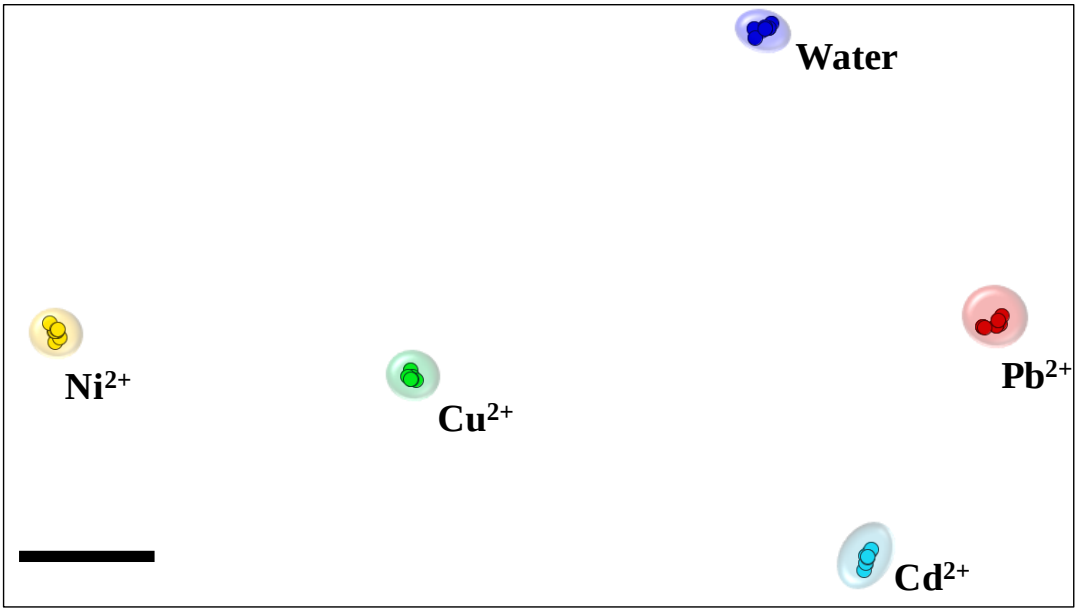

FIGURE 4.24 - PLS plot for different metal ions solution at concentration of 1 mmol.L-1, applying feature selection for frequencies. Black bar is only a guide to measure distances between data points. The determined silhouette coefficient is 0.98. (Reprinted with permission from TEODORO et al. (2019b). Copyright (2019) Elsevier).

Finally the increase of quality discrimination may be obtained with two ways: *i)* exclusion of hampering dimensions or *ii)* discard sensing units with low number of blue boxes or SC lower than 0.71.

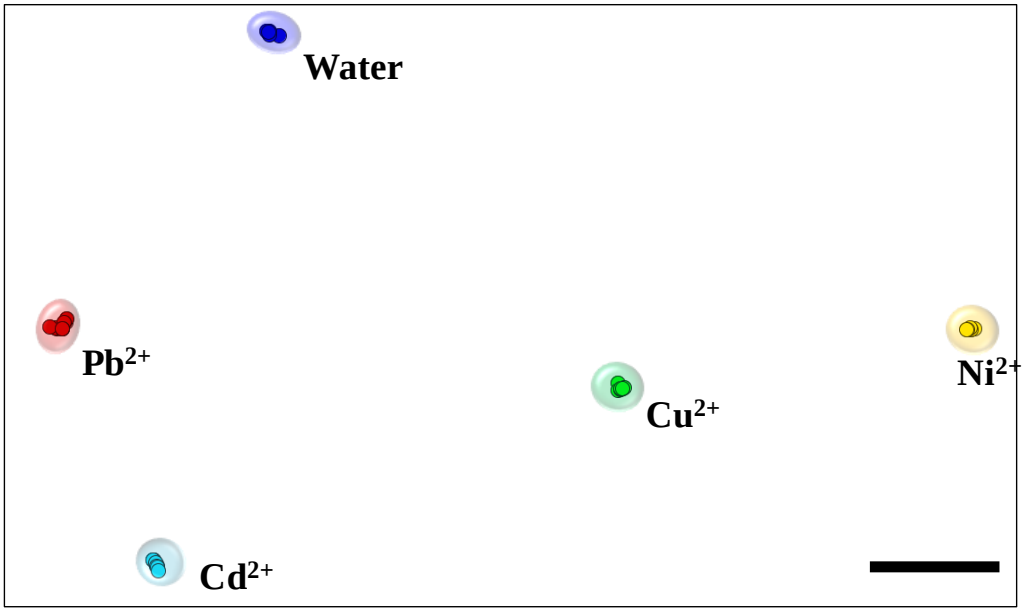

FIGURE 4.25 - PLS plot for different metal solution at concentration of 1 mmol.L-1, applying feature selection for frequencies and sensing units, excluding el2 and el3. Black bar is only a guide to measure distances between data points. The determined silhouette coefficient is 0.99. (Reprinted with permission from TEODORO et al. (2019b). Copyright (2019) Elsevier).

Experiments with different concentrations of Pb^{2+} solution from10^{-8} to 10^{-3} mol.L^{-1} were also performed, which led to a silhouette coefficient of 0.75, as shown in Figure 4.20.

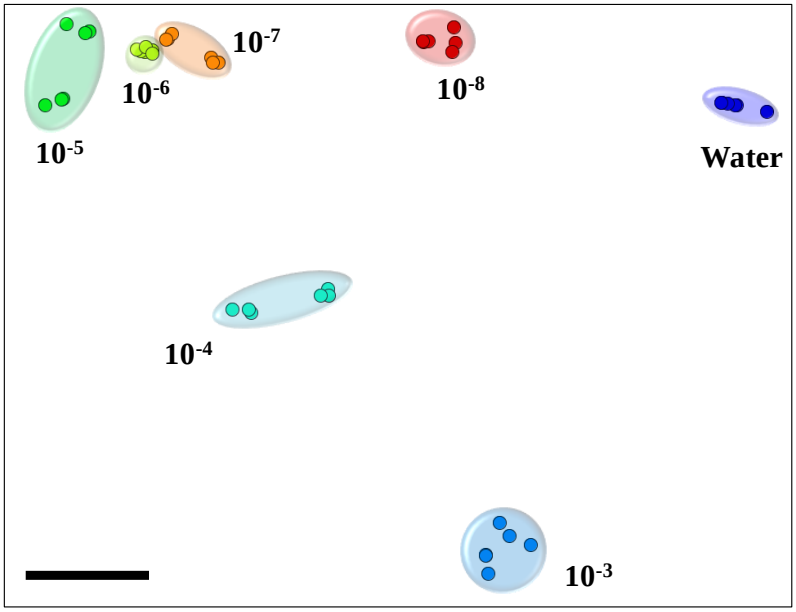

FIGURE 4.26 - PLS plot for different concentration of lead solution from 10^{-8} to 10^{-3} mol.L^{-1}, excluding sensing units number 2 and 3 and using the whole capacitance spectra. Black bar is only a guide to measure distances between data points. The determined silhouette coefficient is 0.75. (Reprinted with permission from TEODORO et al. (2019b). Copyright (2019) Elsevier).

One can note the large distance between samples with and without Pb^{2+}, which makes possible the detection of even lower concentrations of metal ions. In this context, the sensor array developed here has demonstrated the ability to discriminate very low concentrations of heavy metal (10 nmol.L^{-1} or 2.07 µg.L^{-1}), which makes our sensor array comparable to other e-tongues found in the literature with limits of detection as low as 1.5 µg.L^{-1} (SERRANO et al., 2015) and 2.6 µg.L^{-1} (PÉREZ-RÀFOLS et al., 2017). For viewing purposes, capacitance spectra of el_2 and el_5 were plotted in Figure 4.21 to demonstrate information obtained from feature selection procedure, where el_2 presents larger error bar that explains the dispersion of points, while el_5 displays high reproducibility.

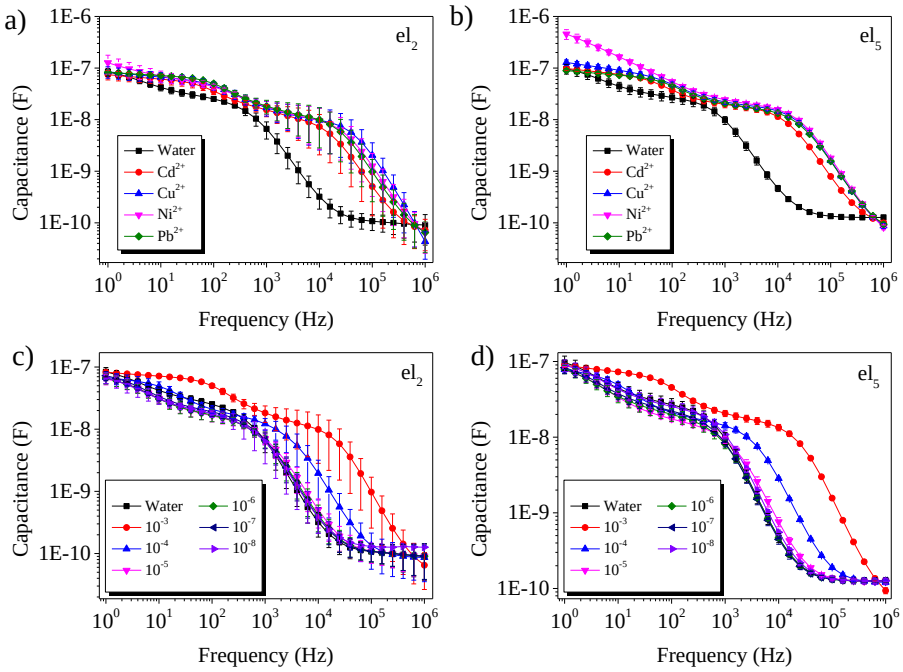

FIGURE 4.27 - Capacitance spectra *vs.* frequency for detecting different metals ions of sensing units (a) el 2 (PA6) and (b) el 5 ($(PA6)_{im\ CNC:Ag}$), and different concentration of lead solutions using sensing unit c) el2 and d) el5. (Reprinted with permission from TEODORO et al. (2019b). Copyright (2019) Elsevier).

4.5. Conclusion

Ternary nanocomposites were produced by distinct combinations of PA6 electrospun fibers, CNC and AgNP, and deposited onto IDEs to be used as sensing units of an e-tongue. The synergism between component materials could be verified, where the presence of CNC:Ag hybrid decrease fiber diameters and improved bulk conductance. These characteristics improved the e-tongue performance to evaluate water contaminated with metal ions, once statistic analysis by Parallel Coordinates revealed that sensors fabricated with only PA6 or PA6 and CNC fibers (el 2 and el 3) contributed negatively to process of samples classification, owing to the insulating nature of these components. Nanocomposites containing the hybrid CNC:Ag (el 4 and el5) were responsible for an improvement of SC and better classification of solutions. The good performance of el5 arises from the better distribution of AgNP onto electrode

surface, due to the use of CNC:Ag hybrid. Additionally, after selection of frequencies and sensing units, it was possible to discriminate different heavy metal ions solutions, and classify lead aqueous solutions of different concentrations, down to nanomolar. Our results point this new architecture combined to multivariate data analysis is highly potential for designing e-tongues aiming at monitoring metal ions in water samples.

5. Conductive electrospun nanofibers containing cellulose nanowhiskers and reduced graphene oxide for the electrochemical detection of mercury (II)

***** The content of this chapter is an adaptation of the scientific article entitled: “Conductive electrospun fibers containing cellulose nanocrystals and reduced graphene oxide for the electrochemical detection of mercury(II)” by K. B. R. Teodoro, F. L. Migliorini, M. H. Facure, D. S. Correa, submmited to the Journal Carbohydrate Polymers.

Reference: *Carb. Pol.* **2019**, 207, 747-754.

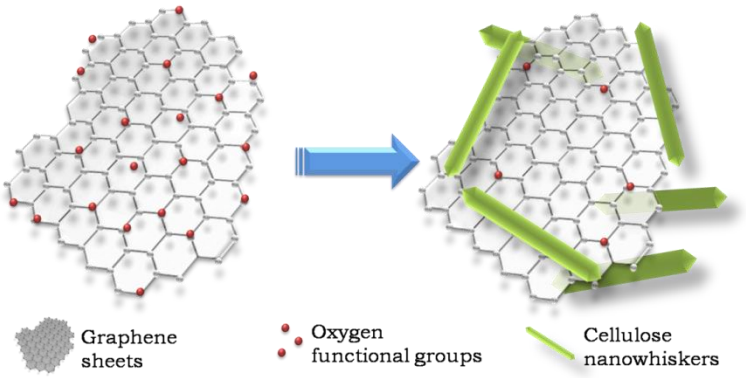

FIGURE 5.1 - Schematic illustration of GO (left side) and CNC:rGO hybrid material (right side). (Reprinted with permission from TEODORO et al. (2019c). Copyright (2019) Elsevier).

5.1. Abstract

Mercury is a heavy metal highly deleterious for the environment being associated to several diseases. Thus, novel and expedite techniques capable of detecting this heavy metal in water, even at trace levels, are highly sought for human and environmental safety purposes. Here we developed a novel electrochemical sensor for detecting mercury(II) using a green hybrid nanoarchitecture composed of reduced graphene oxide (rGO), cellulose nanocrystals (CNC) and polyamide 6 (PA6) electrospun fibers . Scanning transmission electron microscopy (STEM), ultraviolet-visible (UV-VIS) absorption and Fourier transform infrared (FTIR) spectroscopies and termogravimetric analysis (TGA) were employed to elucidate the morphology and composition of CNC:rGO hybrid system. The hybrid composite proved to enhance charge transfer properties, which was evaluated by cyclic voltammetry (CV) experiments. Due to the excellent electrical properties of graphene, the nanocomposite (PA6/CNC:rGO) was applied in the electrochemical detection of very low concentrations of mercury in water samples, improving the sensor sensibility. Moreover, the PA6/CNC/rGO electrode demonstrated stability, high selectivity, low detection limit and wide dynamic linear range for the detection of mercury(II).

5.2. Introduction

Mercury is considered one of the most hazardous heavy metal pollutants (KHOSHBIN et al., 2018), showing high cellular toxicity, once it can accumulate in organs and vital tissues causing several problems to human health, including respiratory disorders, renal failure, reproductive toxicity and even death (LIU et al., 2017; SUN et al., 2018; ZUO et al., 2018). In this way, the development of techniques and materials that can provide a fast and sensitive monitoring of Hg(II) is extremely important. Many techniques have been reported so far for the determination of mercury, such as surface-enhanced

Raman scattering (YANG et al., 2016), atomic absorption spectroscopy (ORANI et al., 2017) and x-ray fluorescence spectrometry (YANG et al., 2017), nonetheless most of these methods include complicated procedures and expensive equipments. In this context, electrochemical techniques have been widely used in the detection of heavy metal ions (BALA and GÓRSKI, 2016; LI et al., 2018; MIGLIORINI et al., 2017; ZUO et al., 2018) due their advantageous features, including high sensitivity, fast response, low cost and easy miniaturization.

Recent investigations have pursued improvements in sensing devices in terms of signal amplification. Electrode surface modification using nanostructured materials is one of the most explored and successful strategies (LI ET AL., 2018; SUN ET AL., 2018). For instance, electrospun fibers enable increasing electrodes surface area and their functionalization with conductive materials can provide signal amplification. As a consequence, sensors with very low limits of detection can be fabricated, in addition to other sensor features improvements as sensitivity, response and recovery time (CHINNAPPAN et al., 2017; MERCANTE et al., 2017a).

Graphene has been extensively explored as a functional material for electrode modification in sensors, owing to their excellent chemical, electrical, optical, thermal and mechanical properties (DESILVA et al., 2017). Graphene is also known by its high adsorption capacity towards heavy metal ions (ZUO et al., 2018), which can also contribute for a better performance of sensing devices. These factors, associated with the low cost of graphite (graphene precursor), have boosted the widespread use of graphene (MOHAN et al., 2018).

The graphene synthesis from graphite requires exfoliation and chemical reactions, involving stabilizing and reducing agents. Conventional methods to reduce graphene oxide include hazardous chemicals as hydrazine (NAG et al., 2018). However, more recently, researches have investigated alternative reducing agents as organic acids, vegetable extracts, protein and

sugars (CHEN et al., 2016; Y. CHEN et al., 2013; DESILVA et al., 2017; LI et al., 2018; ZHU et al., 2010). Sugars and polysaccharides, for instance, have been proven to reduce and stabilize graphene sheets (DESILVA et al., 2017). Cellulose is a low cost, renewable, biodegradable, and nontoxic material with appealing physicochemical properties, including high surface area and reactive chemical groups, which are highly useful for nanocomposites design (TINGAUT et al., 2012). Within this scenario we have synthesized, through a simple and green route, a hybrid material based on cellulose nanocrystals (CNC) and reduced graphene oxide (rGO). The surface molecules of cellulose led to partial reduction of oxygen organic functions of graphene oxide, resulting in rGO, as illustrated in Figure 5.1. The obtained hybrid system was then employed to modify polyamide 6 (PA6) electrospun fibers, which was used in a electrochemical sensor for detecting Hg(II) using differential pulse voltammetry (DPV). The developed sensor showed stability, high selectivity, low detection limit and wide dynamic linear range for the detection of Hg(II).

5.3. Materials and Methods

5.3.1. Reagents

Commercial white cotton from Apolo (Brazil), sulphuric acid (H_2SO_4), formic acid, lead(II) nitrate, cadmium(II) nitrate, copper(II) nitrate and mercury(II) acetate were purchased from LabSynth Chemical (Brazil). Graphite flakes, potassium permanganate (KMnO4), hydrochloric acid (HCl) and hydrogen peroxide (H_2O_2) used in the synthesis of graphene oxide were purchased from Dinamica, Brazil. Dialysis membrane (D9402) and polyamide 6 (20,000 g mol^{-1}) were purchased from Sigma-Aldrich. All chemicals were used as received, and ultrapure water (Millipore system) was used as to prepare all aqueous solutions.

5.3.2. Synthesis of CNC/rGO hybrid material

CNC was obtained by conventional acid hydrolysis of white cotton fibers, in which 5.0 g of cotton were mixed to 100 mL of 60 wt% H_2SO_4 aqueous solution. The reaction was performed under constant temperature (45 °C) and vigorous stirring during 75 min. The reaction was stopped by adding 500 mL of cold water, which suspension was then purified by centrifugation at 10,000 rpm for 10 min. Dialysis against distilled water was used to neutralize the CNC suspension. Next, CNC aqueous suspension was sonicated (Branson) during 5 min and freeze-dried (Thermo Fisher Scientific, SuperModulyo220).

GO was previously synthesized from graphite powder by adaptations of Hummer's method, accordingly to procedure described in previous works from our group (FACURE et al., 2017). The green reduction of GO was performed under reflux containing 160 mL of ultrapure water, 25 mL of GO aqueous suspension (0.5 mg mL^{-1}) and 15 mL of CNC aqueous suspension (5.0 mg.mL^{-1}). Once homogenized, 0.5 mL of NH_4OH 10% w/v was added and the reaction was performed during 72 h. Aliquots (1 mL) were collected at 1, 2, 4, 24, 48 and 72 hours of reaction. The reducing process was then studied by monitoring the spectral band at around 230-270 nm, using a UV-16000 Shimadzu spectrophotometer, software UV Probe 2.31.

5.3.3. PA6/CNC:rGO nanocomposite

The nanocomposite PA6/CNC:rGO was prepared by initially producing PA6 electrospun fibers followed by physical adsorption of CNC:rGO hybrid material onto PA6 fibers surface. Specifically, PA6 fibers were produced by electrospinning using a solution of 10.0 % of PA6 (wt% in respect to solvent) in formic acid. A homemade electrospinning apparatus was employed with the following parameters: feed rate of 0.02 mL h^{-1}, electrical field of 20 kV, working distance of 5 cm. Electrospun fibers were collected onto aluminum foil and fluorine doped tin oxide (FTO) electrodes (deposition time of 40 min). The physical adsorption of CNC:rGO onto PA6 fibers occurred by immersion of neat

PA6 electrospun mats onto CNC:rGO solution. The influence of immersion time was investigated, varying from 1 to 4 hours.

5.3.4. Materials characterization

The morphology of CNC and CNC:rGO was investigated by Scanning Transmission Electron Microscopy (STEM), using a Tecnai TM G2 F20 (FEI Company, Hillsboro, USA) electron microscope. The samples were prepared from diluted suspension of CNC and CNC:rGO, stained with uranyl acetate (1.5 wt%). The stained suspension was dripped on a copper grid and let to dry at room temperature. The images were acquired with a dark-field (DF) detector.

The reduction of GO was studied by monitoring the absorption band around 230-270 nm using UV-Vis absorption spectroscopy (UV-16000 spectrometer Shimadzu spectrometer, software UV Probe 2.31). The samples were placed in a 1 cm optical path quartz cell and ultrapure water (Millipore system) was used as blank.

Chemical composition of CNC:rGO was investigated through Fourier Transform Infrared spectroscopy (FTIR) technique, using a Spectrum 1000 Perkin-Elmer spectrometer, equipped with attenuated total reflection apparatus (ATR). FTIR spectra were obtained in absorbance mode in the range from 4000 - 400 cm^{-1}, using 32 scans and resolution of 2 cm^{-1}.

Cellulose crystalline structure was evaluated by X-ray diffraction (XRD) technique, using a XRD-6000 Shimadzu diffractometer, employing CuKα radiation (λ = 1.5406 Å) at 30 kV and 30 mA, software XRD-6000. The sample was scanned from 5 up to 40° (2°.min^{-1}).

Morphological analysis of PA6/CNC:rGO nanocomposite was investigated by SEM analysis, using a JEOL 6510 SEM microscope, operating at 15 kV. Fibers diameters were estimated using Image J software and taking into account 100 measurements.

5.3.5. Electrochemical experiments

Cyclic voltammetry (CV) experiments were performed using a conventional three electrodes electrochemical cell, using Ag/AgCl (3.0 M KCl) as reference electrode, platinum foil as counter electrode and *fluorine tin-oxide electrode* (FTO) (area = 0.25 cm^2) coated with PA6/CNC:rGO as working electrode, connected to a Potenciostat Autolab PGSTAT 204 Metrohm, using the software NOVA 1.11. 5.0 mM of $[Fe(CN)_6]^{3-/4-}$ dissolved in acetate buffer was prepared. CV assays were performed in the potential range of -0.2 V to 0.6 V using 30 $mV.s^{-1}$ as scan rate.

The electrochemical essay of Hg(II) detection was performed using 0.1 mol L^{-1} acetate buffer (pH 5.0) at room temperature. DPV measurements were carried out from -0.1 to 0.3 V using pulse amplitude of 50 mV, pulse width 0.4 s and pulse period of 0.5 s.

5.4. Results and Discussion

5.4.1. CNC:rGO hybrid material characterization

Figure 5.2 shows the morphology of CNC:rGO hybrid material, which needle-like structures with diameter and length of 15 nm and 185 nm, respectively, are related to cellulose nanocrystals (TEODORO et al., 2018) and typical rGO sheets (FACURE et al., 2017). The preferential location of rGO sheets at CNC regions can indicate the existence of interactions between both materials (PENG et al., 2012). The good dispersion of rGO sheets can be also result of this synergism.

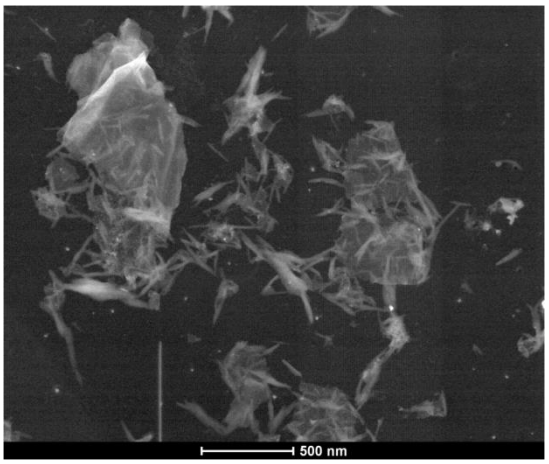

FIGURE 5.2 - STEM micrography of CNC:rGO hybrid obtained after 72h of reaction. (Reprinted with permission from TEODORO et al. (2019c). Copyright (2019) Elsevier).

UV-Vis absorption spectra of CNC:rGO obtained under different reaction times are presented in Figure 5.3. The UV–Vis spectrum of GO exhibits a characteristic absorption peak near 230−240 nm due to the π-π* transitions of the C = C aromatic rings and a shoulder near 290−300 nm corresponding to the n−π* transitions of the C = O bonds. Upon reduction, the 230−240 nm band redshifts to 260−290 nm due to an increase in restored carbon network conjugation length, while the 290−300 nm band disappears or decreases in intensity, because of the elimination of C = O bonds. (PENG et al., 2012; TRUSOVAS et al., 2016). Nonetheless, the redshift of 230 to 260 nm is observed after 48 and 72 h of reaction, indicating the presence of reduced species (ZHU et al., 2010).

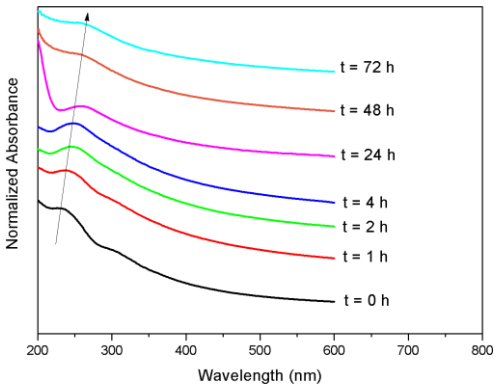

FIGURE 5.3 - UV-Vis absorption spectra of CNC:rGO obtained under different reaction times. (Reprinted with permission from TEODORO et al. (2019c). Copyright (2019) Elsevier).

FTIR spectra of CNC, GO and CNC:rGO are displayed in Figure 5.4. CNC:rGO spectrum is composed by a group of spectral bands of both CNC and rGO, however, the notable decrease of bands attributed to oxygen groups, as at 1374 cm^{-1} (hydroxyl groups), 1210 cm^{-1} (epoxy groups), 1730 cm^{-1} (carbonyl groups) (KAMISAN et al., 2015) and the broad band at 3414 cm^{-1} of O-H stretching and intermolecular hydrogen bonds (KAFY et al., 2016), indicates the partial reduction of graphene oxide. Spectral band at 1633 cm^{-1} indicates the stretching vibrations of C=C of rGO (ZHANG et al., 2015). The presence of 1730 cm^{-1} spectral band can be attributed to remaining oxygen groups in rGO.

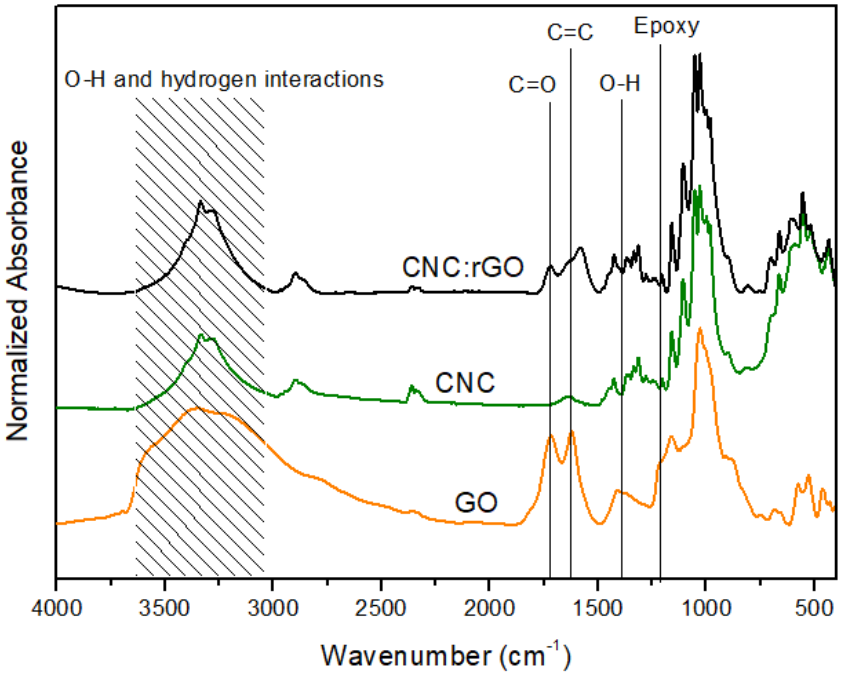

FIGURE 5.4 – FTIR spectra of GO, CNC and CNC:rGO. (Reprinted with permission from TEODORO et al. (2019c). Copyright (2019) Elsevier).

The XRD pattern of CNC:rGO is displayed in Figure 5.5. It exhibits cellulose I profile, with typical crystalline peaks at 2θ = 15°, 16.5°, 22.7°, related to diffraction caused by $(1\bar{1}0)$, (110) and (200) lattice planes of triclinic Iα and monoclinic structures Iβ (JONOOBI et al., 2015; SHIN et al., 2008). This fact indicates that CNC crystalline structures were preserved during reaction conditions. Peaks related to GO layers (10.6° and 23.8°) were not observed in CNC:rGO diffractogram (STOBINSKI et al., 2014). Such result reveals the presence of rGO layers onto cellulose, as a consequence of efficient reduction and stabilization by strong hydrogen bond interactions between cellulose and rGO (Chen et al., 2013). A decrement of interlayer spacing due to the removal of the oxygen functionalities of the GO surface can lead to a shift of GO mean peak at 10.6° to 23 - 25°.

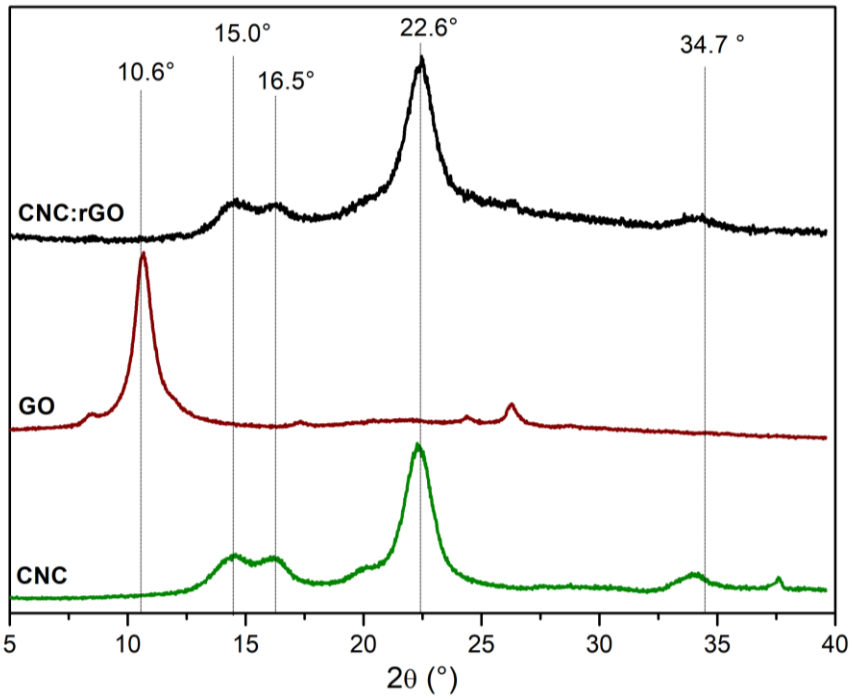

FIGURE 5.5 - XRD pattern of CNC, GO and CNC:rGO. (Reprinted with permission from TEODORO et al. (2019c). Copyright (2019) Elsevier).

5.4.2. Sensing platform characterization

Micrographs of neat PA6 fibers and PA6/CNC:rGO nanocomposite are displayed in Figure 5.6. Neat PA6 mats (Figure 5.6-a) are constituted by randomly distributed fibers, which display smooth and bead-free surface and homogeneity in terms of size, with average diameter of 130 ± 32 nm. Representative region of nanocomposite PA6/CNC:rGO is shown in Figure 5.6 (b), and it is possible to observe the presence of rGO sheets in random spots of the mat. The physical adsorption was strong, once the mats were washed three times and CNC:rGO remained onto the fibers surface. The occurrence of strong interaction between CNC and PA6 it is attributed to strong hydrogen bonds between cellulose hydroxyl groups and amide groups of PA6 (CORREA, A. et al., 2014).

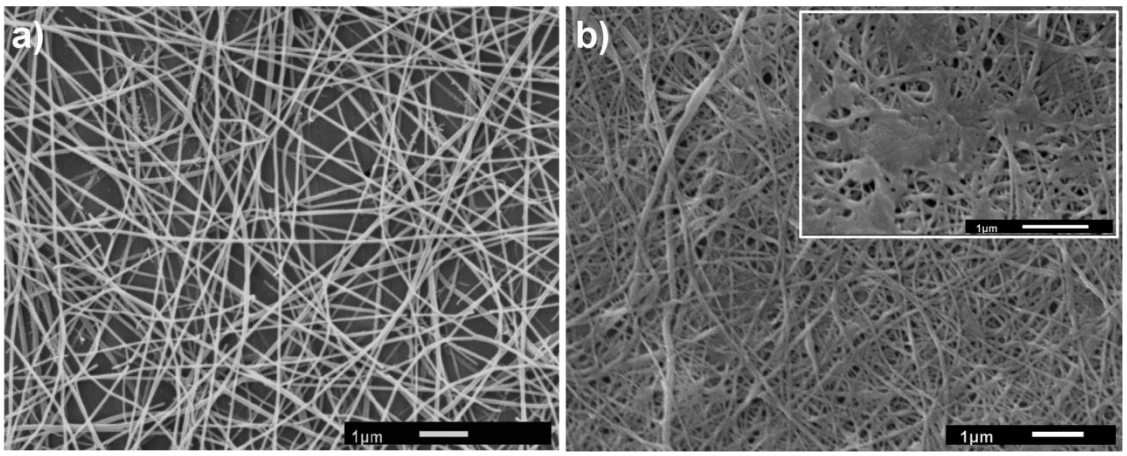

FIGURE 5.6 - SEM image of (a) neat PA6 and (b) PA6/CNC:rGO nanocomposites. The higher magnification (20,000 x) image inserted in (b) emphasizes regions related to rGO sheets. (Reprinted with permission from TEODORO et al. (2019c). Copyright (2019) Elsevier).

The electron transfer ability of PA6/CNC:rGO nanocomposites was evaluated by cyclic voltammetry. The influence of CNC:rGO time adsorption was investigated and the resultant cycle voltammograms are displayed in Figure 5.7. The quasi-reversible (BARD and FAULKNER, 2000) one-electron redox behavior is exhibited to all samples, although an evident increase of current peak occurred as consequence of incorporation of CNC:rGO hybrid material. Moreover, nanocomposites produced after 2 h of adsorption resulted in a higher electron transfer rate and lower peak potential separation (ΔEp), indicating an enhancement on electron transfer ability. Adsorption times of 3 and 4 h have not showed significant improvement, and therefore 2 hours was chosen as condition to prepare the sensing platform.

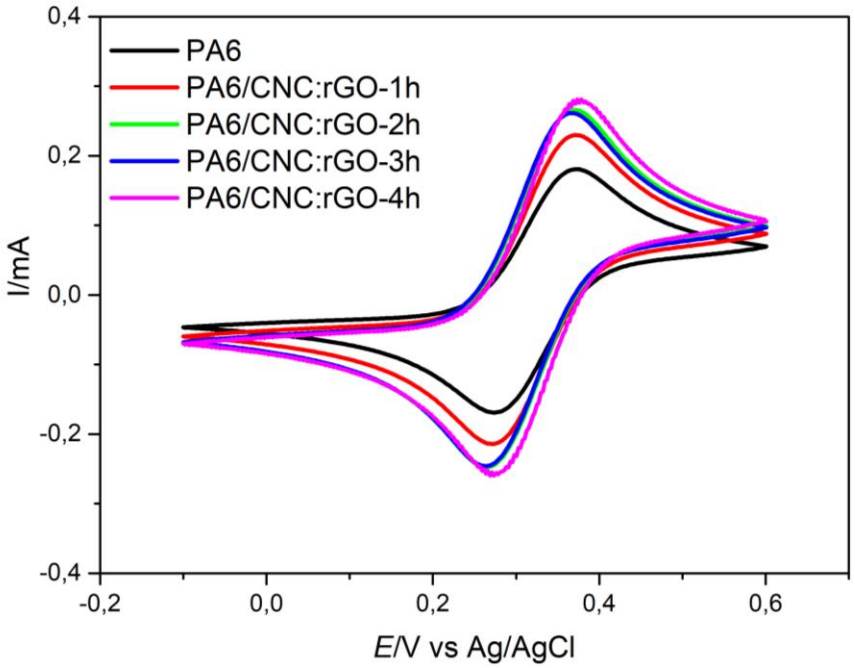

FIGURE 5.7 - Cyclic voltammograms of PA6/CNC:rGO nanocomposites. The influence of time adsorption of 1, 2, 3 and 4h were investigated. The experiment was performed in 5.0 mM $[Fe(CN)6]^{3-/4-}$ solution dissolved in 0.1 M acetate buffer solution. (Reprinted with permission from TEODORO et al. (2019c). Copyright (2019) Elsevier).

5.4.3. Electrochemical detection of Hg(II)

DPV was employed to evaluate the analytical performance of the PA6/CNC:rGO hybrid platform for the detection of Hg(II). As illustrated in Figure 5.8, the anodic peak currents increased with higher concentrations of Hg(II). Moreover, it was found that the anodic peak currents were proportional to the bulk concentration of Hg(II) in the range of 2.5–75 μM. The linear regression equations can be expressed as I (A) = 8.37×10^{-7} [Hg] (μM) + 6.60×10^{-6}, with linear correlation coefficients (R^2) of 0.994.

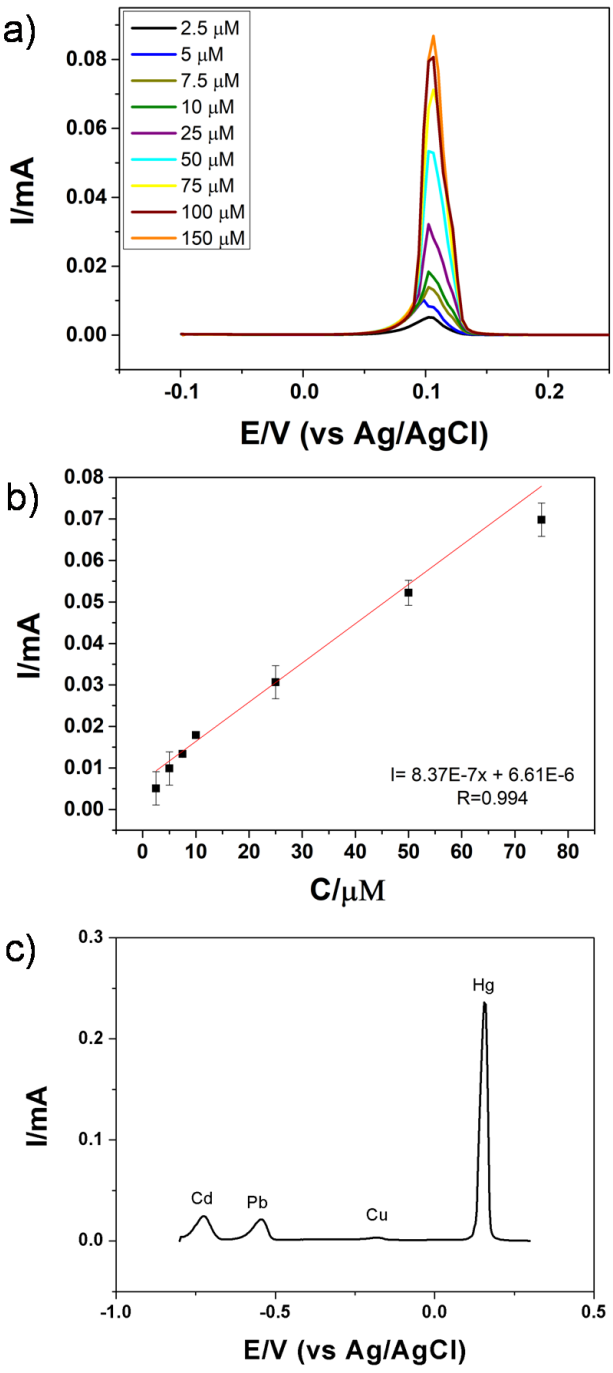

FIGURE 5.8 - (a) DPV curves for different concentrations of Hg(II) using PA6/CNC:rGO hybrid platform, in 0.1 mol.L^{-1} acetate buffer and (b) the linear relationship between the peak current versus Hg(II) concentrations. (c) DPV curves of PA6/CNC:rGO for Hg(II) detection in the presence of interferents Cd(II), Pb(II) and Cu(II). (Reprinted with permission from TEODORO et al. (2019c). Copyright (2019) Elsevier).

The limit of detection (LOD) was calculated using the following equation (DIRECÇÃO, 2005):

$$LOD = 3.3\ \sigma/S \qquad \text{(Eq. 1)}$$

where σ is the standard deviation of DPV signal (measurements of three replicates), and S is the slope of the calibration curve. Therefore, the LOD was calculated as 0.52 μM, in a concentration range of 2.5 – 200 μM, which is comparable to some recent reported works available in literature, as described in Table 5.1. Moreover, the analytical performance of the proposed sensor was compared with some previously reported Hg(II) sensors available in the literature. As can be observed in Table 5.1, the performance of the PA6/CNC:rGO hybrid sensing platform is comparable to other previous works. These results indicate that the PA6/CNC:rGO hybrid material is a potential platform to be used in electrochemical sensor for detecting Hg(II).

TABLE 5.1 - Analytical performance of different electrochemical sensing platforms for measurements of Hg(II)

Sensing Platform	**Analytical method**	**LOD (μM)**	**Linear Range (μM)**	**REF**
Cu_7S_4-Au@S-MoS_2/GCE	SWASV	0.19	0.36–3.68	(Cui, Xu, & Wang, 2017)
CNF/AuNPs	LSV	0.03	0.1-1.2	(Sánchez-Calvo, Fernández-Abedul, Blanco-López, & Costa-García, 2019)
Carbon PEG-SH/SePs/AuNPs paper electrodes	DPV	0.005	0.07-17.5	(Bui, Brockgreitens, Ahmed, & Abbas, 2016)
PA6/CNW:rGO onto FTO	DPV	0.52	2.5–200	This work

5.4.4. Interference studies

To investigate the selectivity of the PA6/CNC:rGO hybrid sensing platform for the detection of Hg(II) the DPV technique was used again. The chosen interferents were cadmium (Cd(II)), lead (Pb(II)) and copper (Cu(II)), once they are highly toxic and can be found in various contaminated environments (TERRA et al. 2017; WEI et al., 2012). This study was performed by using a solution containing Hg(II) and also the other interfering metals, each one in a concentration of 75 µM in acetate buffer. In figure 5.8(c) it is possible to observe a complete separation of the reduction peaks for each metal. It is worth mentioning that the reduction potential for each metal is also in agreement with the literature (WEI et al., 2012). From these results we demonstrated the efficiency of our sensing platform containing PA6/CNC:rGO hybrid material for the detection of Hg(II), even in the presence of other interfering metals.

5.4.5. Real sample analysis

To evaluate the performance of the sensing platform for real environmental analysis, measurements of Hg(II) detection were made using tap and river water samples using the standard addition method (CHAIYO et al., 2016). The river water sample was collected from the Monjolinho River (located in São Carlos - São Paulo / Brazil) and filter using a paper filter (J Prolab JP42). A concentration of Hg(II) (50 µM) was added to the water samples. The recovery tests percentage varies from 97% to river water to 102% to tap water, showing good response for the developed platform in real-life sample analysis.

5.5. Conclusion

A novel sensing platform was developed aiming at the electrochemical detection of Hg (II). The sensor was based on cellulose

nanocrystals/reduced graphene oxide and polyamide 6 electrospun fibers. The use of cellulose nanocrystals as reducing agent of rGO could be confirmed by the presence of reduced species of graphene oxide, revealed by UV absorption spectroscopy and FTIR analysis. Conductive properties of the hybrid nanomaterial were explored in an electrochemical sensor, which demonstrated good charge transfer and capability of detecting low concentrations of mercury in water samples. Detection essays revealed that the sensor was capable to detect Hg (II) with a low limit of detection of 0.52 µM in a concentration range of 2.5 – 200 µM. The selectivity of the developed sensor for detecting Hg (II) was demonstrated even in the presence of interfering metals, including Cd (II), Pb (II) and Cu (II). Moreover, the novel sensing platform has been proven useful for detecting Hg (II) in real samples, including in river and tap water, indicating its potential for environmental sensing applications.

6. General Conclusions and future perspectives

In the present thesis we demonstrated the fabrication of ternary nanocomposites based on polyamide electrospun fibers (PA6), cellulose nanocrystals (CNC) and conductive materials, as silver nanoparticles (AgNP) and reduced graphene oxide (rGO), to be used in sensors to evaluate the presence of low concentration of heavy metal ions in water samples. Additionally, a few remarks deserve to be highlighted:

- CNC as long needles with high surface area and a significant negative charge were obtained, leading to a low tendency of agglomeration and availability to interact with other materials;
- CNC can influence the AgNP synthesis in different ways, as promoting the dispersion and stabilization of AgNP. A hybrid structure composed by CNC decorated with well-disperse AgNP was obtained, which revealed a pronounced antibacterial effect, in comparison with AgNP obtained by traditional methods;
- CNC could act as stabilizing and reducing agent in rGO synthesis, which resultant material was composed by well-disperse rGO nanosheets preferentially attached to CNC needles;
- In respect of the possible ways to combine CNC/conductive materials and PA6 electrospun fibers, it was observed that the inclusion of CNC:AgNP to the bulk of PA6 fibers revealed good dispersion of AgNP, nonetheless electrochemical analysis revealed that conductive properties were affected, once AgNP were coated with PA6 matrix. The modification of PA6 surface with CNC/AgNP and CNC/rGO revealed low agglomeration of conductive species, reflecting in low resistance values associated to EIS analysis.

- The feature selection associated to an electronic tongue constituted by sensors modified with nanocomposites allowed evaluating their performance as sensing layer to detect heavy metals in water. The study revealed the negative contribution of units composed by PA6 and CNC (or both), considering the insulating properties of these materials. In the same way, a better contribution of films containing CNC:AgNP hybrid was verified, as consequence the good distribution of AgNP. The optimized electronic tongue allowed a strong data classification of different heavy metals solutions down to nanomolar concentrations.

- The ternary nanocomposite PA6/CNC:rGO showed the random distribution of CNC:rGO onto PA6 fibers, which led to its ability to charge transfer. The application of this nanocomposite as an electrochemical sensor demonstrated capability of detecting low concentrations of mercury, with limit of detection of 0.52 µM. This sensor was selective for mercury and has been proven useful for detecting mercury in real samples, including in river and tap water.

6. References

AASHRITHA S. “Synthesis of Silver Nanoparticles By Chemical Reduction Method and Their Antifungal Activity”. Int. Res. J. Pharm., **4**:111, 2013.

ABE K., YANO H. “Cellulose nanofiber-based hydrogels with high mechanical strength”. Cellulose. **19**:1907, 2012.

ABITBOL T., MARWAY H. S., KEDZIOR S. A., YANG X., FRANEY A., GRAY D. G., CRANSTON E. D. “Hybrid fluorescent nanoparticles from quantum dots coupled to cellulose nanocrystals”. Cellulose. **24**:1287, 2017.

ABITBOL T., PALERMO A., MORAN-MIRABAL J. M., CRANSTON E. D. “Fluorescent labeling and characterization of cellulose nanocrystals with varying charge contents”. Biomacromolecules. **14**:3278, 2013.

AFKHAMI A., BAGHERI H., KHOSHSAFAR H., SABER-TEHRANI M., TABATABAEE M., SHIRZADMEHR A. “Simultaneous trace-levels determination of Hg(II) and Pb(II) ions in various samples using a modified carbon paste electrode based on multi-walled carbon nanotubes and a new synthesized Schiff base”. Anal Chim Acta **746**:98, 2012.

AGNIHOTRI S., MUKHERJI S., MUKHERJI S. “Size-controlled silver nanoparticles synthesized over the range 5-100 nm using the same protocol and their antibacterial efficacy”. RSC Adv. **4**:3974, 2014.

ALEMDAR A., SAIN M. “Isolation and characterization of nanofibers from agricultural residues - Wheat straw and soy hulls”. Bioresour. Technol. **99**:1664, 2008.

ALKMIM-FILHO J. F., GERMANO A., DIBAI W. L. S., VARGAS E. A., MELO M. M. “Heavy metals investigation in bovine tissues in Brazil”. Food Sci. Technol. **34**:110, 2014.

ALLEN M. J., TUNG V. C., KANER R. B. “Honeycomb carbon -- A study of graphene”. Chem. Rev. **110**:132, 2009.

AMIRJANI A., BAGHERI M., HEYDARI M., HESARAKI S. “Label-free surface plasmon resonance detection of hydrogen peroxide; A bio-inspired approach”. Sensor Actuator B-Chem **227**:373, 2016.

ANDRE R. S., PAVINATTO A., MERCANTE L. A., PARIS E. C., MATTOSO L. H. C., CORREA D. S. “Improving the electrochemical properties of polyamide 6/polyaniline electrospun nanofibers by surface modification with ZnO nanoparticles”. RSC Adv. **5**:73875, 2015.

ARCOT L. R., UDDIN K. M. A., CHEN X., WENCHAO X,. XIANMING K., JOHANSSON L. S., RAS R. H. A., ROJAS O. J. “Paper-based plasmon-enhanced protein sensing by controlled nucleation of silver nanoparticles on cellulose”. Cellulose. **22**:4027, 2015.

ARINO C., SERRANO N., DIAZ-CRUZ J. M., ESTEBAN M. Voltammetric determination of metal ions beyond mercury electrodes. A review. Anal. Chim. Acta. **990**:11, 2017.

ASADPOUR-ZEYNALI K., AMINI R. “A novel voltammetric sensor for mercury(II) based on mercaptocarboxylic acid intercalated layered double hydroxide nanoparticles modified electrode”. Sensor Actuator B-Chem. **246**:961, 2017.

ATKINS P.; JONES L. Princípios de Química: Questionando a vida moderna e o meio ambiente. 5ª ed. Bookman, 2012. p.211.

BALA A., GÓRSKI L. “Determination of mercury cation using electrode modified with phosphorothioate oligonucleotide”. Sensor Actuator B-Chem. **230**:731, 2016.

BARD A. J., FAULKNER L. R. “Electrochemical Methods: Fundamentals and Applications” 2a ed. Wiley, 2000. p. 864.

BARUD H. S., REGIANI T., MARQUES R. F. C., LUSTRI W. R., MESSADDEQ Y., RIBEIRO S. J. L. “Antimicrobial Bacterial Cellulose-Silver Nanoparticles Composite Membranes”. J. Nanomater. **2011**:1, 2011.

BECARO A. A., JONSSON C. M., PUTI F. C., SIQUEIRA M. C., MATTOSO L. H. C., CORREA D. S., FERREIRA M. D. “Toxicity of PVA-stabilized silver nanoparticles to algae and microcrustaceans”. Environ. Nanotechnology., Monit Manag **3**:22, 2014.

BECARO A. A., PUTI F. C., PANOSSO A. R,. GERN J. C., BRANDÃO H. M., CORREA D. S., FERREIRA M. D. “Postharvest Quality of Fresh-Cut Carrots Packaged in Plastic Films Containing Silver Nanoparticles”. Food Bioprocess. Technol. **9**:637, 2016.

BERNDT S., WESARG F., WIEGAND C., KRALISCH D., MÜLLER F. A. “Antimicrobial porous hybrids consisting of bacterial nanocellulose and silver nanoparticles”. Cellulose. **20**:771, 2013.

BIGDELI A., GHASEMI F., GOLMOHAMMADI H., ABBASI-MOAYED S., NEJAD M. A. F., FAHIMI-KASHANI N., JAFARINEJAD S., SHAHRAJABIAN M., HORMOZI-NEZHAD M. R. “Nanoparticle-based optical sensor arrays”. Nanoscale. **9**:16546, 2017.

BILIUTA G., COSERI S. “Cellulose: A ubiquitous platform for ecofriendly metal nanoparticles preparation”. Coord. Chem. Rev. **383**:155–173, 2019.

BUI, M. P. N., BROCKGREITENS, J., AHMED, S., & ABBAS, A. “Dual detection of nitrate and mercury in water using disposable electrochemical sensors.” Biosensors and Bioelectronics, **85**, 280–286, 2016.

BUSCHLE- DILLER G., ZERONIAN S. H. “Enhancing the reactivity and strength of cotton fibers”. J. Appl. Polym. Sci. **45**:967, 1992.

CAMPOS A., SENA NETO A. R., RODRIGUES V. B., KUANA V. A., CORREA A. C., TAKAHASHI M. C., MATTOSO L. H. C., MARCONCINI J. M. “Production of Cellulose Nanowhiskers from Oil Palm Mesocarp Fibers by Acid Hydrolysis and Microfluidization”. J. Nanosci. Nanotechnol. **17**:4970, 2017.

CANO A., CHÁFER M., CHIRALT A., GONZÁLEZ-MARTÍNEZ C. "Development and characterization of active fi lms based on starch-PVA, containing silver nanoparticles". Food Packag. Shelf. Life. **10**:16, 2016.

CHAIYO S., MEHMETI E., ZAGAR K., SIANGPROH W., CHAILAPAKUL O., KALCHER K. "Electrochemical sensors for the simultaneous determination of zinc, cadmium and lead using a Nafion/ionic liquid/graphene composite modified screen-printed carbon electrode". Anal. Chim. Acta. **918**:26, 2016.

CHAUHAN P., SHARMA S. "Nanomaterials for Sensing Applications". J. Nanomedicine. Res. **3**:1–8, 2016.

CHEN C., TANG Y., VLAHOVIC B., YAN F. "Electrospun Polymer Nanofibers Decorated with Noble Metal Nanoparticles for Chemical Sensing". Nanoscale. Res. Lett. **12**: 451, 2017.

CHEN L., LAI C., MARCHEWKA R., BERRY R. M., TAM K. C. "CdS quantum dot-functionalized cellulose nanocrystal films for anti-counterfeiting applications". Nanoscale. **8**:13288, 2016.

CHEN Y., PÖTSCHKE P., PIONTECK J., VOIT B., QI H. "Smart cellulose/graphene composites fabricated by: In situ chemical reduction of graphene oxide for multiple sensing applications". J. Mater. Chem. A. **6**:7777, 2013.

CHENG H., YANG X., CHE X., YANG M., ZHAI G. "Biomedical application and controlled drug release of electrospun fibrous materials". Mater. Sci. Eng. C. **90**:750, 2018.

CHINNAPPAN A., BASKAR C., BASKAR S., RATHEESH G., RAMAKRISHNA S. "An overview of electrospun nanofibers and their application in energy storage, sensors and wearable/flexible electronics". J. Mater. Chem. C. **5**:12657, 2017.

CLSI "Performance Standards for Antimicrobial Disk Susceptibility Tests; Approved Standard" 12nd ed. Wayne, PA. 2003.

CLSI “Methods for Dilution Antimicrobial Susceptibility Tests for Bacteria That Grow Aerobically; Approved Standard” 6th ed. Wayne, PA. 2012.

CORREA A. C., TEIXEIRA E. M., PESSAN L. A., MATTOSO L. H. C. “Cellulose nanofibers from curaua fibers”. Cellulose. **17**:1183, 2010.

CORREA A. C., TEIXEIRA E. M., CARMONA V. B., TEODORO K. B. R., RIBEIRO C., MATTOSO L. H. C., MARCONCINI J. M. “Obtaining nanocomposites of polyamide 6 and cellulose whiskers via extrusion and injection molding”. Cellulose. **21**:311, 2014.

CORREA D. S., MEDEIROS E. S., OLIVEIRA J. E., PATERNO L. G., MATTOSO L. H. C. “Nanostructured Conjugated Polymers in Chemical Sensors: Synthesis , Properties and Applications”. J. Nanosci. Nanotechnol. **14**:6509, 2014.

CUI, J., XU, S., WANG, L. Monolayer MoS2 decorated Cu7S4-Au nanocatalysts for sensitive and selective detection of mercury(II). Sci. China Mater., 60(4), 352–360, 2017.

DAIKUZONO C. M., SHIMIZU F. M., MANZOLI A., RIUL A., PIAZZETTA M. H. O., GOBBI A. L., CORREA D. S., PAULOVICH F. V., OLIVEIRA O. N. “Information Visualization and Feature Selection Methods Applied to Detect Gliadin in Gluten-Containing Foodstu ff with a Microfluidic Electronic Tongue”. Appl. Mater. Interfaces. **9**:19646, 2017.

SILVA K. K. H., HUANG H. H., JOSHI R. K., YOSHIMURA M. “Chemical reduction of graphene oxide using green reductants”. Carbon. **119**:190, 2017.

DEVARAYAN K., KIM B. S. “Reversible and universal pH sensing cellulose nanofibers for health monitor”. Sensor Actuator B-Chem. **209**:281, 2015.

DI NATALE C., MACAGNANO A., DAVIDE F., D’AMICO A., LEGIN A., VLASOV Y., RUDNITSKAYA A., SELEZENEV B. “Multicomponent analysis on polluted waters by means of an electronic tongue”. Sensor Actuator B-Chem. **44**:423, 1997.

DI ROSA A. R., LEONE F., CHELI F., CHIOFALO V. “Fusion of electronic nose, electronic tongue and computer vision for animal source food authentication and quality assessment – A review”. J. Food. Eng. **210**:62, 2017.

DING B., WANG M., WANG X., YU J., SUN G. “Electrospun nanomaterials for ultrasensitive sensors”. Mater. Today. **13**:16, 2010.

COMITÉ DE DIRECÇÃO ICH - ICH Topic Q2 (R1) “Validation of analytical procedures: text and methodology”. International Conference on Harmonization. 2005.

DONG H., SNYDER J. F., TRAN D. T., LEADORE J. L. “Hydrogel, aerogel and film of cellulose nanofibrils functionalized with silver nanoparticles”. Carbohydr. Polym. **95**:760, 2013.

DONG H., STRAWHECKER K. E., SNYDER J. F., ORLICKI J. A., REINER R. S., RUDIE A. W. “Cellulose nanocrystals as a reinforcing material for electrospun poly(methyl methacrylate) fibers: Formation, properties and nanomechanical characterization”. Carbohydr. Polym. **87**:2488, 2012.

DONG S., ROMAN M. “Fluorescently labeled cellulose nanocrystals for bioimaging applications”. J. Am. Chem. Soc. **129**:13810, 2007.

DROGAT N., GRANET R., SOL V., MEMMI A., SAAD N., KLEIN K. C., BRESSOLLIER P., KRAUSZ P. “Antimicrobial silver nanoparticles generated on cellulose nanocrystals”. J. Nanoparticle. Res. **13**:1557, 2011.

DU X., ZHANG Z., LIU W., DENG Y. “Nanocellulose-based conductive materials and their emerging applications in energy devices - A review”. Nano Energy. **35**:299, 2017.

DUFRESNE A. “Cellulose nanomaterial reinforced polymer nanocomposites”. Curr. Opin. Colloid. Interface. Sci. **29**:1–8, 2017.

DURAN N., MARCATO P. D., CONTI R., ALVES O. L., COSTA F. T. M., BROCCHI M. “Potential Use of Silver Nanoparticles on Pathogenic Bacteria, their Toxicity and Possible Mechanisms of Action”. J. Braz. Chem. Soc **21**:949, 2010.

EDWARDS J. V., PREVOST N., FRENCH A., CONCHA M., DELUCCA A., WU Q. “Nanocellulose-Based Biosensors : Design , Preparation , and Activity of Peptide-Linked Cotton Cellulose Nanocrystals Having Fluorimetric and Colorimetric Elastase Detection Sensitivity.” Engineering. 2013:20, 2013.

EICHHORN S. J. “Cellulose nanowhiskers: promising materials for advanced applications”. Soft Matter. **7**:303, 2011.

FACURE M. H. M., MERCANTE L. A., MATTOSO L. H. C., CORREA D. S. “Detection of trace levels of organophosphate pesticides using an electronic tongue based on graphene hybrid nanocomposites”. Talanta. **167**:59, 2017.

FANTONI R. F. “Como a poliamida substituiu a seda: uma história da descoberta da poliamida 66”. Polímeros. **22**:1–6, 2012.

FARROKHNIA M., KARIMI S., MOMENI S., KHALILILAGHAB S. “Colorimetric sensor assay for detection of hydrogen peroxide using green synthesis of silver chloride nanoparticles: Experimental and theoretical evidence”. Sensor Actuator B-Chem. **246**:979, 2017.

FDA U.S. Food and Drug Administration “Foodborne Pathogenic Microorganisms and Natural Toxins” IN: Bad Bug Book 2nd ed. 2012. P. 91.

GELADI P. “Notes on the history and nature of partial least squares (PLS) modeling”. J. Chemom. **2**:231, 1988.

GOH Y. F. SHAKIR I. HUSSAIN R. “Electrospun fibers for tissue engineering, drug delivery, and wound dressing”. J. Mater. Sci. **48**:3027, 2013.

GOLMOHAMMADI H., MORALES-NARVÁEZ E., NAGHDI T., MERKOÇI A. “Nanocellulose in Sensing and Biosensing”. Chem. Mater. **29**:5426, 2017.

GOULART L. A., GONÇALVES R., CORREA A. A., PEREIRA E. C., MASCARO L. H. “Synergic effect of silver nanoparticles and carbon nanotubes on the simultaneous voltammetric determination of hydroquinone, catechol, bisphenol A and phenol”. Microchim. Acta. **185**:12, 2018.

GUERRINI L. M., BRANCIFORTI M. C., CANOVA T., BRETAS R. E. S. "Electrospinning and characterization of polyamide 66 nanofibers with different molecular weights". Mater. Res. **12**:181, 2009.

GUO J., LIU D., FILPPONEN I., JOHANSSON L. S., MALHO J. M., QURAISHI S., LIEBNER F., SANTOS H. A., ROJAS O. J. "Photoluminescent Hybrids of Cellulose Nanocrystals and Carbon Quantum Dots as Cytocompatible Probes for in Vitro Bioimaging". Biomacromolecules. **18**:2045, 2017.

HAJIPOUR M. J., FROMM K. M., ASHKARRAN A. A., ABERASTURI D. J., LARRAMENDI I. R., ROJO T. "Antibacterial properties of nanoparticles". Trends. Biotechnol. **30**:499, 2012.

HASSABO A. G., NADA A. A., IBRAHIM H. M., ABOU-ZEID N. Y. "Impregnation of silver nanoparticles into polysaccharide substrates and their properties". Carbohydr. Polym. **122**:343, 2015.

HEINRICH J., WEISKOPF D. "State of the Art of Parallel Coordinates". Eurographics. **1**:95, 2013.

HERMAN A., HERMAN A. P. "Nanoparticles as Antimicrobial Agents : Their Toxicity and Mechanisms of Action". J. Nanosci. Nanotechnol. **14**:946, 2014.

HSU C. L., CHANG K. S., KUO J. C. "Determination of hydrogen peroxide residues in aseptically packaged beverages using an amperometric sensor based on a palladium electrode". Food Control. **19**:223, 2008.

HUANG S., ZHOU L., LI M. C., WU Q., KOJIMA Y., ZHOU D. "Preparation and properties of electrospun poly (vinyl pyrrolidone)/cellulose nanocrystal/silver nanoparticle composite fibers". Materials. 9 (7):523, 2016.

HUBBE M. A., ROJAS O. J., LUCIA L. A., SAIN M. "Cellulosic Nanocomposites: a Review". Bioresources. **3**:929, 2008.

INSELBERG A., DIMSDALE B. "Parallel coordinates: a tool for visualizing multi-dimensional geometry". IN: Proceedings of the First IEEE Conference on Visualization: Visualization. IEEE, San Francisco, 1990. p. 361.

IVNITSKI D., ABDEL-HAMID I., ATANASOV P., WILKINS E. “Biosensors for detection of pathogenic bacteria.” Biosens. Bioelectron. **14**:599, 1999.

JAISWAL M., KOUL V., DINDA A. K. “In vitro and in vivo investigational studies of a nanocomposite-hydrogel-based dressing with a silver-coated chitosan wafer for full-thickness skin wounds”. J. Appl. Polym. Sci. 133 (21): 43472, 2016.

JEDRZEJUK A., RABIZA-SWIDER J., SKUTNIK E., LUKASZEWSKA A. “Some factors affecting longevity of cut lilacs. Postharvest”. Biol. Technol. **111**:247, 2016.

JOLLIFFE I. T. “Principal Component Analysis and Factor Analysis”. In: Principal Component Analysis. New York, Springer New York, 1986. p 115.

JONOOBI M., OLADI R., DAVOUDPOUR Y., OKSMAN K., DUFRESNE A., HAMZEH Y., DAVOODI R. “Different preparation methods and properties of nanostructured cellulose from various natural resources and residues: a review”. Cellulose. **22**:935, 2015.

JOSE A., RAY J. G. “Toxic heavy metals in human blood in relation to certain food and environmental samples in Kerala, South India”. Environ. Sci. Pollut. Res. **25**:7946, 2018.

JUNIOR M. A. M., SANTOS L. S. S., GONÇALVES M. C., NOGUEIRA A. F. “Preparation of silver and gold nanoparticles: a simple method to introduce nanotechnology into teaching laboratories”. Quim. Nova. **35**:1872, 2012.

JUSTINO C. I. L., DUARTE A. C., ROCHA-SANTOS T. A. P. “Recent progress in biosensors for environmental monitoring: A review”. Sensors. 17(12):2918, 2017.

KAFY A., AKTHER A., SHISHIR M. I. R., KIM H. C., YUN Y., KIM J. “Cellulose nanocrystal/graphene oxide composite film as humidity sensor”. Sensor Actuator A-Phys **247**:221, 2016.

KAFY A., SADASIVUNI K. K., AKTHER A., MIN S. K., KIM J. "Cellulose/graphene nanocomposite as multifunctional electronic and solvent sensor material". Mater. Lett. **159**:20, 2015.

KAMISAN A. I., KAMISAN A., RUSLINDA M. A., KUDIN T. I. T., HASSAN O. H., HALIM N. A., YAHYA M. Z. A. "Synthesis of Graphene via Green Reduction of Graphene Oxide with Simple Sugars". Adv. Mater. Res. **1107**:542, 2015.

KARIMI A., HUSAIN S. W., HOSSEINI M., AZAR P. A., GANJALI M. R. "Rapid and sensitive detection of hydrogen peroxide in milk by Enzyme-free electrochemiluminescence sensor based on a polypyrrole-cerium oxide nanocomposite". Sensor Actuator B-Chem **271**:90, 2018.

KARKRA R., KUMAR P., BANSOD B. K. S., BAGCHI S., SHARMA P., KRISHNA C. R. "Classification of heavy metal ions present in multi-frequency multi-electrode potable water data using evolutionary algorithm". Appl. Water. Sci. **7**:3679, 2017.

KHAN B. A., CHEVALI V. S., NA H., ZHU J., WARNER P., WANG H. "Processing and properties of antibacterial silver nanoparticle-loaded hemp hurd/poly (lactic acid) biocomposites". Compos. Part. B. **100**:10, 2016.

KHOSHBIN Z., HOUSAINDOKHT M. R., VERDIAN A., BOZORGMEHR M. R. "Simultaneous detection and determination of mercury (II) and lead (II) ions through the achievement of novel functional nucleic acid-based biosensors". Biosens. Bioelectron. **116**:130, 2018.

KIMLING J., MAIER M., OKENVE B., KOTAIDIS V., BALLOT H., PLECH A. "Turkevich Method for Gold Nanoparticle Synthesis". J. Phys. Chem. **110**:15700, 2006.

KLEMM D., CRANSTON E. D., FISCHER D., GAMA M., KEDZIOR S. A., KRALISCH D., KRAMER F., KONDO T., LINDSTROM T., NIETZSCHE S., PETZOLD-WELCKE K., RAUCHFUB F. "Nanocellulose as a natural source

for groundbreaking applications in materials science: Today's state". Mater Today. 21(7):720, 2018.

KOGA H., TOKUNAGA E., HIDAKA M., UMEMURA Y., SAITO T., ISOGAI A., KITAOKA T. "Topochemical synthesis and catalysis of metal nanoparticles exposed on crystalline cellulose nanofibers". Chem. Commun. **46**:8567, 2010.

KOLAROVA K., SAMEC D., KVITEK O., REZNICKOVA A., RIMPELOVA S., SVORCIK V. "Preparation and characterization of silver nanoparticles in methyl cellulose matrix and their antibacterial activity and their antibacterial activity". Jpn. J. Appl. Phys. 56(6S1):06GG09, 2017.

KOSHY O., POTTATHARA Y. B., THOMAS S., PETOVAR B., FINSGAR M. "A Flexible, Disposable Hydrogen Peroxide Sensor on Graphene Nanoplatelet-Coated Cellulose". Curr. Anal. Chem. **13**:480, 2017.

KRUTYAKOV Y. A., KUDRINSKIY A. A., OLENIN A. Y., LISICHKIN G. V. "Synthesis and properties of silver nanoparticles: advances and prospects". Russ. Chem. Rev. **77**:233, 2008.

LEE J. H., HUYNH-NGUYEN B. C., KO E., KIM J. H., SEONG G. H. "Fabrication of flexible, transparent silver nanowire electrodes for amperometric detection of hydrogen peroxide". Sensor Actuator B-Chem. **224**:789, 2016.

LEGIN A., RUDNITSKAYA A., VLASOV Y. G., DI NATALE C., DAVIDE F., D'AMICO A. "Tasting of beverages using an electronic tongue". Sensor Actuator B-Chem. **44**:291, 1997.

LEÓN-SILVA S., FERNÁNDEZ-LUQUEÑO F., LÓPEZ-VALDEZ F. "Silver Nanoparticles (AgNP) in the Environment : a Review of Potential Risks on Human and Environmental Health". Water, Air, Soil Pollut. **227**:306, 2016.

LI B., JIN X., LIN J., CHEN Z. "Green reduction of graphene oxide by sugarcane bagasse extract and its application for the removal of cadmium in aqueous solution". J Clean Prod. **189**:128, 2018.

LI H., LI H., LIU J., LUO Z., JOYCE D., HE S. “Nano-silver treatments reduced bacterial colonization and bio fi lm formation at the stem-ends of cut gladiolus ‘ Eerde ’ spikes”. Postharvest Biol Technol. **123**:102, 2017.

LI L., LIU D., SHI A., YOU T. “Simultaneous stripping determination of cadmium and lead ions based on the N-doped carbon quantum dots-graphene oxide hybrid”. Sensor Actuator B-Chem. **255**:1762, 2018.

LI M., GOU H., AL-OGAIDI I., WU N. “Nanostructured sensors for detection of heavy metals: A review”. Sustain Chem Eng. **1**:713, 2013.

LI S. M., JIA N., MA M. G., ZHANG Z., LIU Q. H., SUN R. C. “Cellulose-silver nanocomposites: Microwave-assisted synthesis, characterization, their thermal stability, and antimicrobial property”. Carbohydr Polym. **86**:441, 2011.

LIANG A., LIU Q., WEN G., JIANG Z. “The surface-plasmon-resonance effect of nanogold/silver and its analytical applications”. TrAC - Trends Anal Chem. **37**:32, 2012.

LIN W. C., LI Z., BURNS M. A. “A Drinking Water Sensor for Lead and Other Heavy Metals”. Anal Chem. **89**:8748, 2017.

LIU H., DING Y., YANG B., LIU Z., LIU Q., ZHANG X. “Colorimetric and ultrasensitive detection of H_2O_2 based on Au/Co_3O4-CeOx nanocomposites with enhanced peroxidase-like performance”. Sensor Actuator B-Chem. **271**:336, 2018.

LIU H., WANG D., SONG Z., SHANG S. “Preparation of silver nanoparticles on cellulose nanocrystals and the application in electrochemical detection of DNA hybridization”. Cellulose. **18**:67, 2011.

LIU Y., DENG Y., DONG H., LIU K., HE N. “Progress on sensors based on nanomaterials for rapid detection of heavy metal ions”. Sci China Chem. **60**:329, 2017.

LU Y., LIANG X., NIYUNGEKO C., ZHOU J., XU J., TIAN G. “A review of the identification and detection of heavy metal ions in the environment by voltammetry”. Talanta. **178**:324, 2018.

LVOVA L., GONÇALVES C. G., PETROPOULOS K., MICHELI L., VOLPE G., KIRSANOV D., LEGIN A., VIAGGIU E., CONGESTRI R., GUZZELLA L., POZZONI F., PALLESCHI G., DI NATALE C., PAOLESSE R. "Electronic tongue for microcystin screening in waters". Biosens Bioelectron. **80**:154, 2016.

MAHMOUDIAN M. R., BASIRUN W. J., ALIAS Y. "A sensitive electrochemical Hg^{2+} ions sensor based on polypyrrole coated nanospherical platinum". RSC Adv. **6**:36459, 2016.

MANEERUNG T., TOKURA S., RUJIRAVANIT R. "Impregnation of silver nanoparticles into bacterial cellulose for antimicrobial wound dressing". Carbohydr Polym. **72**:43, 2008.

MARQUES I., MAGALHÂES-MOTA G., PIRES F., SÉRIO S., RIBEIRO P. A., RAPOSO M. "Detection of traces of triclosan in water". Appl Surf Sci. **421**:142, 2017.

MARTINS M. A., TEIXEIRA E. M., CORREA A. C., FERREIRA M., MATTOSO L. H. C. "Extraction and characterization of cellulose whiskers from commercial cotton fibers". J Mater Sci. **46**:7858, 2011.

MARZOUK W., SAKLY N., ROUDESLI S., OUADA H. B., MAJDOUB H. "Ag-nanocomposite based on carboxymethylcellulose for humidity detection : Green synthesis and sensing performances". J Appl Polym Sci. **133**:1–9, 2016.

MATSUYAMA K., MOROTOMI K., INOUE S., NAKASHIMA M., NAKASHIMA H., OKUYAMA T., KATO T., MUTO H., SUGIYAMA H. "Antibacterial and antifungal properties of Ag nanoparticle-loaded cellulose nanofiber aerogels prepared by supercritical CO2 drying". J Supercrit Fluids. **143**:1–7, 2019.

MAUTNER A., MAPLES H. A., SEHAQUI H., ZIMMERMANN T., LARRAYA U. P., MATHEW A. P., LAI C. Y., LI K., BISMARCK A. "Nitrate removal from water using a nanopaper ion-exchanger". Environ Sci Water Res Technol. **2**:117, 2016.

MERCANTE L. A., PAVINATTO A., IWAKI L. E. O., SCAGION V. P., ZUCOLOTTO V., OLIVEIRA O. N., MATTOSO L. H. C., CORREA D. S. “Electrospun polyamide 6/poly(allylamine hydrochloride) nanofibers functionalized with carbon nanotubes for electrochemical detection of dopamine”. Appl Mater Interfaces. 7:4784, 2015.

MERCANTE L. A., SCAGION V. P., MIGLIORINI F. L., MATTOSO L. H. C., CORREA D. S. “Electrospinning-based (bio)sensors for food and agricultural applications: A review”. Trends Anal Chem. **91**:91, 2017a.

MERCANTE L. A., FACURE M. H. M., SANFELICE R. C., MIGLIORINI F. L., MATTOSO L. H. C., CORREA D. S. “One-pot preparation of PEDOT:PSS-reduced graphene decorated with Au nanoparticles for enzymatic electrochemical sensing of H_2O_2”. Appl Surf Sci. **407**:162, 2017b.

MIGLIORINI F. L., SANFELICE R. C., PAVINATTO A., STEFFENS J., STEFFENS C., CORREA D. S. “Voltammetric cadmium(II) sensor based on a fluorine doped tin oxide electrode modified with polyamide 6/chitosan electrospun nanofibers and gold nanoparticles”. Microchim Acta. **184**:1077, 2017.

MINGHIM R., PAULOVICH F. V., LOPES A. A. “Content-based text mapping using multi-dimensional projections for exploration of document collections”. **6060**:60600S, 2006.

MOHAN V. B., LAU K., HUI D., BHATTACHARYYA D. “Graphene-based materials and their composites: A review on production, applications and product limitations”. Compos Part B Eng. **142**:200, 2018.

MOON R. J., MARTINI A., NAIRN J., SIMONSEN J., YOUNGBLOOD J. “Cellulose nanomaterials review: structure, properties and nanocomposites” **40**:3941, 2011.

MORALES-NARVÁEZ E., GOLMOHAMMADI H., NAGHDI T., YOUSEFI H., KOSTIV U., HORÁK D., POURREZA N., MERKOÇI A. “Nanopaper as an Optical Sensing Platform”. ACS Nano. **9**:7296, 2015.

MORONES J. R., ELECHIGUERRA J. L., CAMACHO A., HOLT K., KOURI J. B., RAMIREZ J. T., YACAMAN M. J. “The bactericidal effect of silver nanoparticles”. Nanotechnol **16**:2346, 2005.

NAG A., MITRA A., MUKHOPADHYAY S. C. “Graphene and its sensor-based applications: A review”. Sensor Actuator A-Phys. **270**:177, 2018.

NAIK A. N., PATRA S., KANEKAR A. S., SEN D., RAMAGIRI S. V., BELLARE J. R., MAZUMDER S., GOSWAMI A. “Nafion membrane incorporated with silver nanoparticles as optical test strip for dissolved hydrogen peroxide: Preparation, deployment and the mechanism of action”. Sensor Actuator B-Chem. **255**:605, 2018.

NARAYANAN K. B., HAN S. S. “Colorimetric detection of manganese (II) ions using alginate-stabilized silver nanoparticles”. Res Chem Intermed. **43**:5665, 2017.

NIKIFOROV A., DENG X., XIONG Q., CVELBAR U., DEGEYTER N., MORENT R., LEYS C. “Non-thermal plasma technology for the development of antimicrobial surfaces : a review”. J Phys D Appl Phys **49**:204002, 2016.

NITINAIVINIJ K., PARNKLANG T., THAMMACHAROEN C., EKGASIT S., WONGRAVEE K. “Colorimetric determination of hydrogen peroxide by morphological decomposition of silver nanoprisms coupled with chromaticity analysis”. Anal Methods. **6**:9816, 2014.

OLIVEIRA J. E., SCAGION V. P., GRASSI V., CORREA D. S., MATTOSO L. H. C. “Modification of electrospun nylon nanofibers using layer-by-layer films for application in flow injection electronic tongue: Detection of paraoxon pesticide in corn crop”. Sensor Actuator B-Chem. **171–172**:249, 2012.

ORANI A. M., MANDJUKOV P., VASSILEVA E. “Determination of selected trace elements in marine biota samples with the application of fast temperature programs and solid sampling continuous source high resolution atomic absorption spectroscopy: method validation”. Int J Environ Anal Chem. **97**:710, 2017.

PADALKAR S., CAPADONA J. R., ROWAN S. J., WEDER C., WON Y. H., STANCIU L. A., MOON R. J. “Natural biopolymers: Novel templates for the synthesis of nanostructures”. Langmuir. **26**:8497, 2010.

PAL S., TAK Y. K., SONG J. M. “Does the antibacterial activity of silver nanoparticles depend on the shape of the nanoparticle? A study of the gram-negative bacterium Escherichia coli”. J Biol Chem. **73**:1712, 2007.

PAULOVICH F. V., MORAES M. L., MAKI R. M., FERREIRA M., OVIVEIRA-JR O. N., OLIVEIRA M. C. F. “Information visualization techniques for sensing and biosensing”. Analyst. 136:1344, 2011.

PAVINATTO A., MERCANTE L. A., LEANDRO C. S., MATTOSO L. H. C., CORREA D. S. “Layer-by-Layer assembled films of chitosan and multi-walled carbon nanotubes for the electrochemical detection of 17 α –ethinylestradiol”. J Electroanal Chem. **755**:215, 2015.

PENG B., TANG L., ZENG G., ZHOU Y., ZHANG Y., LONG B., FANG S., CHEN S., YU J. “Current progress in aptasensors for heavy metal ions based on photoelectrochemical method: A review”. Curr Anal Chem. **14**:4, 2018.

PENG H., MENG L., NIU L., LU Q. “Simultaneous reduction and surface functionalization of graphene oxide by natural cellulose with the assistance of the ionic liquid”. J Phys Chem C. **116**:16294, 2012.

PÉREZ-RÀFOLS C., SERRANO N., DÍAZ-CRUZ J. M., ARIÑO C., ESTEBAN M. “A screen-printed voltammetric electronic tongue for the analysis of complex mixtures of metal ions”. Sensor Actuator B-Chem. **250**:393, 2017.

PODRAZKA M., BÁCZYŃSKA E., KUNDYS M., JELEŃ P. S., NERY E. W. “Electronic tongue-A tool for all tastes?” Biosensors. **8**:1–24, 2017.

POURREZA N., GOLMOHAMMADI H., NAGHDI T., YOUSEFI H. “Green in-situ synthesized silver nanoparticles embedded in bacterial cellulose nanopaper as a bionanocomposite plasmonic sensor”. Biosens Bioelectron. **74**:353, 2015.

PROMPHET N., RATTANARAT P., CHAILAPAKUL O., RANGKUPAN R., RODTHONGKUM N. “An electrochemical sensor based on graphene/polyaniline/polystyrene nanoporous fibers modified electrode for simultaneous determination of lead and cadmium”. Sensor Actuator B-Chem. **207**:526, 2015.

RAGAVAN K. V., AHMED S. R., WENG X., NEETHIRAJAN S. “Chitosan as a peroxidase mimic: Paper based sensor for the detection of hydrogen peroxide”. Sensor Actuator B-Chem. **272**:8–13, 2018.

RAI M., YADAV A., GADE A. “Silver nanoparticles as a new generation of antimicrobials”. Biotechnol Adv. **27**:76, 2009.

RAJESHKUMAR S., BHARATH L. V. “Mechanism of plant-mediated synthesis of silver nanoparticles – A review on biomolecules involved, characterisation and antibacterial activity”. Chem Biol Interact. **273**:219, 2017.

REICH S., YU J., DING B., LANGNER M., BURGARD M., GREINER A., JIANG S., WANG X., AGARWAL S. “Polymer nanofibre composite nonwovens with metal-like electrical conductivity”. Flex Electron. **2**:3, 2018.

RENEKER D. H., YARIN A. L. “Electrospinning jets and polymer nanofibers”. Polymer. **49**:2387, 2008.

RIUL-JR A., DANTAS C. A. R., MIYAZAKI C. M., OLIVEIRA-JR O. N. “Recents advances in electronic tongues”. Analyst. **135**:2481, 2010.

ROMAN M., WINTER W. T. “Effect of sulfate groups from sulfuric acid hydrolysis on the thermal degradation behaviour of bacterial cellulose”. Biomacromolecules. 5(5):1671, 2004.

ROTTER G., ISHIDA H. “FTIR separation of nylon- 6 chain conformations: Clarification of the mesomorphous and γ- crystalline phases”. J Polym Sci Part B Polym Phys. **30**:489, 1992.

ROUSSEEUW P. J. “Silhouettes: A graphical aid to the interpretation and validation of cluster analysis”. J Comput Appl Math. **20**:53, 1987.

ROY D., SEMSARILAR M., GUTHRIE J. T., PERRIER S. “Cellulose modification by polymer grafting: a review”. Chem. Soc. Rev. **38**:2046, 2009.

SAHOO P. K., SAHOO S., SATPATI A. K., BAHADUR D. “Solvothermal synthesis of reduced graphene oxide/Au nanocomposite-modified electrode for the determination of inorganic mercury and electrochemical oxidation of toxic phenolic compounds”. Electrochim Acta. **180**:1023, 2015.

SÁNCHEZ-CALVO, A., FERNÁNDEZ-ABEDUL, M. T., BLANCO-LÓPEZ, M. C., & COSTA-GARCÍA, A. Paper-based electrochemical transducer modified with nanomaterials for mercury determination in environmental waters. Sensor Actuator B-Chem, **290**, 87–92, 2019.

SCAGION V. P., MERCANTE L. A., SAKAMOTO K. Y., OLIVEIRA J. E., FONSECA F. J., MATTOSO L. H. C., FERREIRA M. D., CORREA D. S. “An electronic tongue based on conducting electrospun nanofibers for detecting tetracycline in milk samples”. RSC Adv. **6**:103740, 2016.

SEIL J. T., WEBSTER T. J. “Antimicrobial applications of nanotechnology: Methods and literature”. Int J Nanomedicine. **7**:2767, 2012.

SENTHAMIZHAN A., CELEBIOGLU A., UYAR T. “Flexible and highly stable electrospun nanofibrous membrane incorporating gold nanoclusters as an efficient probe for visual colorimetric detection of Hg(II)”. J Mater Chem A. 2:12717, 2014.

SERRANO N., GONZÁLEZ-CALABUIG A., DEL VALLE M. “Crown ether-modified electrodes for the simultaneous stripping voltammetric determination of Cd(II), Pb(II) and Cu(II)”. Talanta. **138**:130, 2015.

SHEN D., XIAO R., GU S., ZHANG H. “The Overview of Thermal Decomposition of Cellulose in Lignocellulosic Biomass”. IN: Cellulose - Biomass Conversion, Theo van de Ven and John Kadla (Eds), IntechOpen. 2013.

SHIN Y., BAE I. T., AREY B. W., EXARHOS G. J. “Facile stabilization of gold-silver alloy nanoparticles on cellulose nanocrystals”. J Phys Chem C. **112**:4844, 2008.

SILVA A. B., BRETAS R. E. S. “Preparation and characterization of PA6/PAni-TSA nanofibers”. Synth Met. **162**:1537, 2012.

SINGH R., PRASAD R., SUMANA G., ARORA K., SOOD S., GUPTA R. K., MALHOTRA B. D. “STD sensor based on Biosensors and Bioelectronic nucleic acid functionalized nanostructured polyaniline”. Biosens Bioelectron. **24**:2232, 2009.

SIQUEIRA G., TAPIN-LINGUA S., BRAS J., SILVA P. D., DUFRESNE A. “Mechanical properties of natural rubber nanocomposites reinforced with cellulosic nanoparticles obtained from combined mechanical shearing, and enzymatic and acid hydrolysis of sisal fibers”. Cellulose. **18**:57, 2011.

SIQUEIRA M. C., COELHO G. F., MOURA M. R., BRESOLIN J. D., HUBINGER S. Z., MARCONCINI J. M., MATTOSO L. H. C. “Evaluation of Antimicrobial Activity of Silver Nanoparticles for Carboxymethylcellulose Film Applications in Food Packaging”. J Nanosci Nanotechnol. **14**:5512, 2014.

SPAGNOL C., FRAGAL E. H., PEREIRA A. G. B., NAKAMURA C. V., MUNIZ E. C., FOLLMANN H. D. M., SILVA R., RUBIRA A. F. “Cellulose nanowhiskers decorated with silver nanoparticles as an additive to antibacterial polymers membranes fabricated by electrospinning”. J Colloid Interface Sci. **531:**705, 2018.

SPERLING L. H. Introduction to physical polymer”, 4a ed. John Wiley & Sons, 2006. p.28.

SRIKAR S. K., GIRI D. D., PAL D. B., MISHRA P. K., UPADHYAY S. N. “Green Synthesis of Silver Nanoparticles : A Review”. Green Sustain Chem. **6**:34, 2016.

STOBINSKI L., LESIAK B., MALOLEPSZY A., MAZURKIEWICZ M., MIERZWA B., ZEMEK J., JIRICEK P., BIELOSHAPKA I. “Graphene oxide

and reduced graphene oxide studied by the XRD, TEM and electron spectroscopy methods". J Electron Spectros Relat Phenomena. **195**:145, 2014.

SUBBIAH T., BHAT G. S., TOCK R. W., PARAMESWARAN S., RAMKUMAR S. S. "Electrospinning of nanofibers". J Appl Polym Sci. **96**:557, 2005.

SUN M., LI Z., WU S., GU Y., LI Y. "Simultaneous detection of Pb^{2+}, $Cu^{2+}$and Hg^{2+} by differential pulse voltammetry at an indium tin oxide glass electrode modified by hydroxyapatite". Electrochim Acta. **283**:1223, 2018.

SURESHKUMAR M., SISWANTO D. Y., LEE C. "Magnetic antimicrobial nanocomposite based on bacterial cellulose and silver nanoparticles". J Mater Chem. **20**:6948, 2010.

SURYABHASKARAM D., CHERUKU R., GOVINDARAJ G. "Sugar Assisted Graphene : A Green Synthesis Approach". Int J ChemTech Res. **6**:3291, 2014.

TCHOUNWOU P. B., YEDJOU C. G., PATLOLLA A. K., SUTTON D. J. "Heavy Metals Toxicity and the Environment". Mol Clin Environ Toxicol. **101**:133, 2012.

TEIXEIRA E. M., BONDANCIA T. J., TEODORO K. B. R., CORREA A. C., MARCONCINI J. M., MATTOSO L .H. C. "Sugarcane bagasse whiskers: Extraction and characterizations". Ind Crops Prod. **33**:63, 2011.

TEIXEIRA E. M., CORREA A. C., MANZOLI A., LIMA LEITE F., OLIVEIRA C. R., MATTOSO L. H. C. "Cellulose nanofibers from white and naturally colored cotton fibers". Cellulose. **17**:595, 2010.

TEODORO K. B. R., TEIXEIRA E. M., CORREA A. C., CAMPOS A., MARCONCINI J. M., MATTOSO L. H. C. "Whiskers de fibra de sisal obtidos sob diferentes condições de hidrólise ácida: efeito do tempo e da temperatura de extração". Polímeros. **21**:280, 2011.

TEODORO K. B. R., CAMPOS A., CORREA A. C., TEIXEIRA E. M., MARCONCINI J. M., MATTOSO L. H. C. "Surface Functionalization of Cellulose Whiskers for Nonpolar Composites Applications". IN: Handbook of

Composites from Renewable Materials - Volume 4: Functionalization. Thakur VK, Thakur MK, Kessler MR (Eds) Scrivener Publishing LLC, 217. p 199.

TEODORO K. B. R., SANFELICE R. C., MATTOSO L. H. C., CORREA D. S. "Cellulose Whiskers Influence the Morphology and Antibacterial Properties of Silver Nanoparticles Composites". J Nanosci Nanotechnol. 18(7):4876, 2018.

TEODORO K. B. R., MIGLIORINI F. L., CHRISTINELLI W. A., CORREA D. S. "Detection of hydrogen peroxide (H_2O_2) using a colorimetric sensor based on cellulose nanowhiskers and silver nanoparticles". Carbohydr Polym. **212**:235, 2019a.

TEODORO K. B. R., SHIMIZU F. M., SCAGION V. P., CORREA, D. S. "Ternary nanocomposites based on cellulose nanocrystals, silver nanoparticles and electrospun fibers: use in an electronic tongue for heavy metal detection". Sensor Actuator B-Chem. **290**:387, 2019 b.

TEODORO K. B. R.; MIGLIORINI F. L., FACURE M. H. M., CORREA D. S. "Conductive electrospun fibers containing cellulose nanocrystals and reduced graphene oxide for the electrochemical detection of mercury(II)". Carbohydr Polym. **207**:747, 2019c.

TERRA I. A. A., MERCANTE L. A. "Fluorescent and Colorimetric Electrospun Nanofibers for Heavy-Metal Sensing". Biosensors. 7(4):E61, 2017.

TERRA I. A. A., MERCANTE L. A., ANDRE R. S., CORREA D. S. "Optically active electrospun nanofibers for heavy metals sensing". **7**:1, 2017.

TINGAUT P., ZIMMERMANN T., SÈBE G. "Cellulose nanocrystals and microfibrillated cellulose as building blocks for the design of hierarchical functional materials". J Mater Chem. **22**:20105, 2012.

TOKO K. "Taste sensor with global selectivity". Mater Sci Eng C. **4**:69, 1996.

TRUSOVAS R., RACIUKAITIS G., NIAURA G., BARKAUSKAS J., VALUSIS G., PAULIUKAITE R. "Recent Advances in Laser Utilization in the Chemical Modification of Graphene Oxide and Its Applications". Adv Opt Mater. **4**:37, 2016.

TSAI T., HUANG T., CHANG C., HO N. Y., TSENG Y. “Antibacterial cellulose paper made with silver-coated gold nanoparticles”. Sci Rep. **7**:1–10, 2017.

VAN DEN BERG O., SCHROETER M., CAPADONA J. R., WEDER C. “Nanocomposites based on cellulose whiskers and (semi)conducting conjugated polymers”. J Mater Chem **17**:2746, 2007.

WANG J., WINDBERGS M. “Functional electrospun fibers for the treatment of human skin wounds”. Eur J Pharm Biopharm. **119**:283, 2017.

WANG Q., MOSER J-E., GRÄTZEL M. “Electrochemical Impedance Spectroscopic Analysis of Dye-Sensitized Solar Cells”. J Phys Chem B. **109**:14945, 2005.

WEI J., YANG D., CHEN H., GAO Y., LI H. “Stripping voltammetric determination of mercury(II) based on SWCNT-PhSH modified gold electrode. Sensor Actuator B-Chem. **190**:968, 2014.

WEI Y., GAO C., MENG F. L., LI H. H., WANG L., LIU J. H., HUANG X. J. “SnO_2/reduced graphene oxide nanocomposite for the simultaneous electrochemical detection of cadmium(II), lead(II), copper(II), and mercury(II): An interesting favorable mutual interference”. J Phys Chem C. **116**:1034, 2012.

WILSON D., ALEGRET S., DELVALLE M. “Simultaneous Titration of Ternary Mixtures of Pb(II), Cd(II) and Cu(II) with Potentiometric Electronic Tongue Detection”. Electroanalysis. **27**:336, 2015.

XU F., WENG B., MATERON L. A., KUANG A., TRUJILLO J. A., LOZANO K. “Fabrication of cellulose fine fiber based membranes embedded with silver nanoparticles via Forcespinning”. J Polym Eng. **36**:269, 2016.

YAN Y., YU H., ZHANG K., SUN M., ZHANG Y., WANG X., WANG S. “Dual-emissive nanohybrid of carbon dots and gold nanoclusters for sensitive determination of mercuric”. Nano Res. **9**:2088, 2016.

YANG H., YAN R., CHEN H., LEE D. H., ZHENG C. “Characteristics of hemicellulose, cellulose and lignin pyrolysis”. Fuel. **86**:1781, 2007.

YANG S., DAI X., STOGIN B. B., WONG T-S. “Ultrasensitive surface-enhanced Raman scattering detection in common fluids”. Proc Natl Acad Sci. **113**:268, 2016.

YANG Y., HAN A., LI R., FANG G., LIU J., WANG S. “Synthesis of highly fluorescent gold nanoclusters and their use in sensitive analysis of metal ions”. Analyst. **142**:4486, 2017.

YARIN A. L. “Coaxial electrospinning and emulsion electrospinning of core-shell fibers”. Polym Adv Technol. **22**:310, 2011.

ZEYTUNCU B., MORCALI M. H. “Fabrication and Characterization of Antibacterial Polyurethane Acrylate-based Materials.” Mater Res. **18**:867, 2015.

ZHANG C., ZHANG R. Z., MA Y. Q., GUAN W. B., WU X. L., LIU X., LI H., DU Y. L., PAN C. P. “Preparation of cellulose/graphene composite and its applications for triazine pesticides adsorption from water”. ACS Sustain Chem Eng. **3**:396, 2015.

ZHANG L., LI L. “Colorimetric detection of hydrogen peroxide using silver nanoparticles with three different morphologies”. Anal Methods. **8**:6691, 2016.

ZHAO J., WEI Z., FENG X., MIAO M., SUN L., CAO S., SHI L., FANG J. “Luminescent and transparent nanopaper based on rare-earth up-converting nanoparticle grafted nanofibrillated cellulose derived from garlic skin”. Appl Mater Interfaces. **6**:14945, 2014.

ZHU C., GUO S., FANG Y., DONG S. “Reducing sugar: New functional molecules for the green synthesis of graphene nanosheets”. ACS Nano. **4**:2429, 2010.

ZHU R., YADAMA V., LIU H., LIN R. J. T., HARPER D. P. “Fabrication and characterization of Nylon 6/cellulose nanofibrils melt-spun nanocomposite filaments”. Compos Part A Appl Sci Manuf. **97**:111, 2017.

ZULKIFLI F. H., HUSSAIN F. S. J., ZEYOHANNES S. S., RASAD M. S. B. A., YUSUFF M. M. “A facile synthesis method of hydroxyethyl cellulose-silver

nanoparticle scaffolds for skin tissue engineering applications". Mater Sci Eng C. **79**:151, 2017.

ZULKIFLI S. N., RAHIM H. A., LAU W. "Detection of contaminants in water supply: A review on state-of-the-art monitoring technologies and their applications". Sensor Actuator B-Chem. **255**:2657, 2018.

ZUO Y., XU J., XING H., DUAN X., LU L., YE G., JIA H., YU Y. "Simple and green synthesis of piperazine-grafted reduced graphene oxide and its application for the detection of Hg(II)". Nanotechnology. **29**:165502, 2018.

APPENDIX A

Article published in the Journal Carbohydrate Polymers – Elsevier

This Appendix presents the scientific article entitled: "**Detection of hydrogen peroxide (H_2O_2) using a colorimetric sensor based on cellulose nanowhiskers and silver nanoparticles**" by K. B. R. Teodoro, F. L. Migliorini, W. A. Christinelli, D. S. Correa, published in the Journal Carbohydrate Polymers.

Reference: *Carb. Pol.* **2019**, 212, 235-241.

Abstract

Hydrogen peroxide (H_2O_2) is an important compound for several industrial sectors, but it becomes harmful to human health under high concentrations. Thus, the development of simple, low cost and fast analytical methods capable to detect and monitor H_2O_2 is fundamentally important. In the present study, we report a simple route for synthesizing silver nanoparticles (AgNPs) in the presence of a nanostructured polysaccharide (cellulose nanowhiskers) to produce a hybrid material, which was employed as a colorimetric probe for H_2O_2 detection. Our results revealed that AgNPs tend to experience catalytic decomposition when exposed to H_2O_2, causing a decrease of AgNPs absorption band at 410 nm in accordance with H_2O_2 concentration. This decrease was linearly dependent on H_2O_2 concentration (0.01-30 μM and 60-600 μM), yielding limits of detection of 0.014 μM and 112 μM, respectively. The easy-to-interpret H_2O_2 sensor also proved to be suitable for real samples analysis even in the presence of other interfering substances.

Keywords: *cellulose nanowhiskers; silver nanoparticles; hydrogen peroxide monitoring; optical sensor; colorimetric sensor.*

1. Introduction

The monitoring of hydrogen peroxide (H_2O_2) has gained importance in the last years, once this compound is employed in several industrial sectors (KARIMI et al., 2018; MERCANTE et al., 2017b; RAGAVAN et al., 2018) being associated with advanced oxidation processes (AOPs) for water treatment, biochemical procedures (DIRECÇÃO, 2005; NITINAIVINIJ et al., 2014) and sterilizing procedures in the food industry (HSU; CHANG; KUO, 2008). For instance, H_2O_2 is applied to preserve raw milk, albeit its excess can lead to the undesirable degradation of folic acid present in milk (KARIMI et al., 2018). Additionally, H_2O_2 in high concentration can be deleterious to human health, leading, for instance, to cellular damage in tissues (ZHANG; LI, 2016) and also some serious diseases including diabetes, cancer and cardiovascular disorder (LIU et al., 2018). In this way, the development of simple, low cost and fast analytical methods capable to monitoring H_2O_2, even at very low concentration, is fundamentally important. Several techniques including electrochemistry (HSU; CHANG; KUO, 2008; LEE et al., 2016; MERCANTE et al., 2017b), chemiluminescene (KARIMI et al., 2018) and spectrometry (FARROKHNIA et al., 2017; LIU et al., 2018; UZER et al., 2017, KOSHY et al., 2016) have been employed for the determination of hydrogen peroxide. Colorimetric sensors, on the other hand, can be a remarkable alternative for monitoring H_2O_2, once they are low cost devices and show high sensitivity combined to experimental simplicity. Under this context, synthetic and nature-based nanomaterials are interesting candidates to be applied as active layer in colorimetric sensors owing to their remarkable properties. Cellulosic nanostructures, for instance, can be employed for designing cellulose-based hybrid systems for sensors and biosensors, once this material is capable to host optically active materials, helping to prevent undesirable agglomerations and offering a nanoscaled scaffold for particles deposition (DU et al., 2017; GOLMOHAMMADI et al., 2017; GUO et al., 2017; KOSHY et al., 2017; POURREZA et al., 2015).

Additionally, cellulose is the most abundant compound in Earth, and cellulosic nanostructures can be similarly obtained from varied sources (EICHHORN, 2011; KLEMM et al., 2018).

Novel hybrid platforms combining polysaccharides, *e.g.* cellulosic nanostructures, with distinct materials, including metallic nanoparticles (MORALES-NARVÁEZ et al., 2015; TEODORO et al., 2018; YAN et al., 2016), luminescent chromophores (ABITBOL et al., 2013; DEVARAYAN and KIM, 2015; DONG and ROMAN, 2007), rare-earth ions (MORALES-NARVÁEZ et al., 2015; ZHAO et al., 2014), quantum dot nanoparticles (ABITBOL et al., 2017; CHEN et al., 2016; GUO et al., 2017), and conjugated polymers (VAN DEN BERG et al., 2007), have recently been reported. Specifically, the combination of metal nanoparticles and cellulosic nanostructures can yield a hybrid system (DONG et al., 2013; POURREZA et al., 2015) with unique electronic and optical properties, owing the localized surface plasmon resonance (SPR) effect of metal nanoparticles. SPR effect occurs due to the interaction of metallic nanoparticles with light, where photons from incident electromagnetic radiation cause the displacement of conduction free electrons of metallic nanoparticles, accordingly with wave oscillation (LIANG et al., 2012; BIGDELI et al., 2017). Due optical activity, AgNPs in solution normally present a yellow color by naked eye and exhibit a strong absorption band around 400 nm, detectable by UV-Vis absorption spectroscopy (KRUTYAKOV et al., 2008). The good synergism between these materials originates from the attachment of metal nanoparticles onto the cellulose surface due to electrostatic interactions between metallic cations in solution and regions of higher electron density of cellulose molecules, as hydroxyl and sulphate groups (JONOOBI et al., 2015; ROMAN and WINTER, 2004; TEODORO et al., 2017). Controlled experimental conditions allow silver cations to be reduced to metallic silver, which are then stabilized by negatively charged cellulosic groups, maintaining their sizes at the nanoscale.

In this context, here we report on the development of a novel optical colorimetric sensor for detecting hydrogen peroxide in an easy way using a low cost approach combining a polysaccharide and metallic nanoparticles. Specifically, the nanosensor was based on a hybrid system composed of cellulose nanowhiskers (CNW) and AgNPs (CNW:Ag), which were prepared by *in situ* chemical reduction using very diluted sodium borohydride solution. The reaction strategy employed guaranteed the dispersion of AgNPs and allowed exploring the high surface area of CNW. Moreover, the use of colloidal suspension excludes additional steps required to produce gels or films, which enables the colorimetric hybrid system to be directly employed as a H_2O_2 sensor after completion of this fast and simple green-synthesis employing cellulose.

2. **Materiais and Methods**

2.1. *Reagents*

White Cotton (Apolo - Brazil) was commercially obtained, while sulphuric acid, hydrogen peroxide, copper sulphate, zinc sulphate, iron sulphate, uric acid (UA) and glucose were purchased from Synth Chemical (Brazil). Dialysis membrane (D9402), silver nitrate, sodium borohydride and uric acid were purchased from Sigma-Aldrich.

2.2. *CNW:Ag synthesis*

The synthesis of CNW:Ag consisted in two steps: i) CNW extraction from cotton fibers and ii) application of CNW as stabilizing agent in AgNPs synthesis (TEODORO et al., 2018). CNW extraction was made via top-down method based in acid hydrolysis procedure, in which cotton fibers are mixed with 60.0 wt% H_2SO_4 aqueous solution, (1 g of fibers/20 mL of acid solution). The reaction was performed under constant heating and stirring, at 45 °C during 75 min. 500 mL of cold distilled water was added in order to stop chemical reaction, and the CNW was washed by centrifugation, at 10,000 rpm during 10

min, in order to remove impurities and acid excess. The precipitated was re-suspended in Milli-Q water and dialyzed against Milli-Q water until neutral pH was reached. Then, neutral CNW aqueous suspension was ultrasonicated during 5 min using 20% amplitude.

In a round-bottom flask connected to a reflux system, 20 mL of aqueous CNW suspension (50 mg. mL^{-1}) was mixed to 200 mL of $AgNO_3$ aqueous solution (1.0×10^{-3} mol. L^{-1}). Once reached the boiling point, 2 mL of immediately prepared sodium borohydride (1.0×10^{-3} mol. L^{-1}) was slowly dripped to reaction medium, under vigorous stirring. The reaction was performed during 40 min and stored in a glass flask protected from light.

2.3. CNW:Ag characterization

The morphologies of CNW and CNW:Ag were investigated by Field Emission Scanning Electron Microscopy (FESEM), using a PHILLIPS-XL30 FEG-SEM microscope. Diluted suspensions (0.5 $mg.mL^{-1}$) of CNW and CNW:Ag were stained with 100 µL of uranyl acetate (1.5 wt%). 1.5 µL of each stained suspension was dripped on a hot silicon board, and left to dry in a desiccator at room temperature. The presence of silver nanoparticles was evaluated by UV-Vis absorption spectroscopy, using an UV-16000 spectrometer Shimadzu spectrometer, software UV Probe 2.31, in which samples were placed in a 1 cm optical path quartz cell and ultrapure water (Millipore system) was used as blank.

The formation of silver nanoparticles in CNW:Ag was evaluated by UV-Vis absorption spectroscopy, monitoring the band at 400-425 nm, using a Shimadzu spectrometer (UV-16000 - software UV Probe 2.31), in which samples were placed in a 1 cm optical path quartz cell and ultrapure water (Millipore system) was used as blank.

The crystalline profile of CNW and its integrity after CNW:Ag synthesis was evaluated by X-ray diffraction (XRD) in the range of 5 - 80° and resolution

of 1°.min^{-1}. Crystallinity index (Ci) was calculated using Buschle-Diller-Zeronian equation (Eq. 1) (BUSCHLE- DILLER; ZERONIAN, 1992), considering the intensity at I_{200} (peak at 2θ= 22.6°) and the minimum intensity at I_{am} (2θ = 18°). I_{200} represents mainly crystalline components, while I_{am} represents the amorphous component.

$$Ci\ (\%) = [1 - (I_{am} / I_{200})] \times 100$$

Eq. 1

The amount of silver in CNW:Ag could be estimated by thermogravimetric analysis (TGA), using a Thermal analyzers TGA Q-500 TA instruments. Samples (10.0 ± 1.0 mg) were heated from room temperature until 600 °C, using a heating rate of 10 °C.min^{-1} and oxidizing atmosphere (synthetic air – 60 ml.min^{-1}).

2.4. Hydrogen peroxide detection experiments

Experiments to detect H_2O_2 were performed directly using the CNW:Ag aqueous suspension. Peroxide solutions were prepared in PBS buffer (pH 7.4), varying analyte concentrations in the range from 0.01 up to 600 µM. For this purpose, 1 mL of peroxide solution was added to 4 mL of CNW:Ag solution. The incubation time was optimized, in the range 10 – 60 min, monitoring the 410 nm band. From these data two linear calibration curves were obtained within the ranges of 0.01 – 30 µM and 60 – 600 µM. In order to evaluate the sensor selectivity and application to real samples analysis, interferents test (using cations and organic compounds) and with real samples (tap water, river water and commercial milk) were employed. Solutions tests containing interferents and real sample were also prepared in PBS buffer and the same proportion and incubation time was applied.

3. Results and Discussion

3.1. CNW:Ag characterization

Fig. 1 displays FESEM images of representative region of CNW and CNW:Ag samples. Typical rod-like structures were found to CNW, as consequence of efficient acid hydrolysis of cotton fibers, as shown in Fig. 1 (a). Fig. 1 (b) shows the structure of CNW:Ag, in which CNW long needles are decorated with spherical silver nanoparticles. Silver nanoparticles average diameter was determined as 15 ± 5 nm in agreement of previous work (TEODORO et al., 2018). The attachment of AgNPs onto cellulose occurs as a consequence of the interaction during the synthesis of silver ions and negatively charged groups (hydroxyl and sulphate) present on the CNW surface.

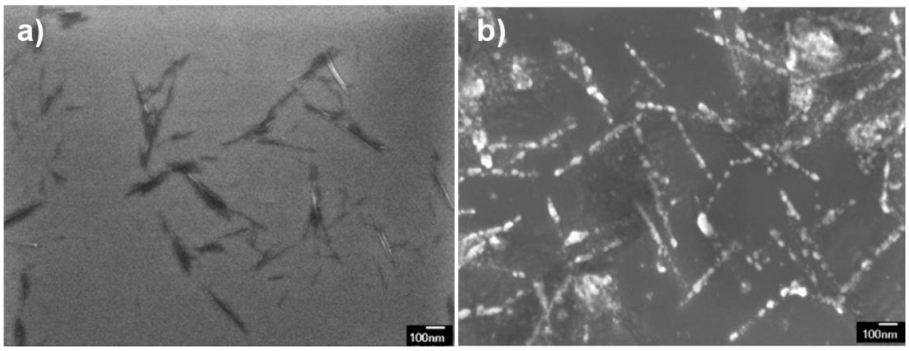

Fig. 1 – FESEM images of CNW (a) and CNW:Ag (b). (Reprinted with permission from TEODORO et al. (2019a). Copyright (2019) Elsevier)

The chemical reduction of silver ions to silver nanoparticles in CNW:Ag was confirmed by presence of a well-defined absorption band at 410 nm, as displayed in Fig. 2 (a). This is a typical AgNPs localized SPR band, as consequence of the movement of surface electrons from metallic silver nanostructures interacting with electromagnetic radiation (KRUTYAKOV et al., 2008).

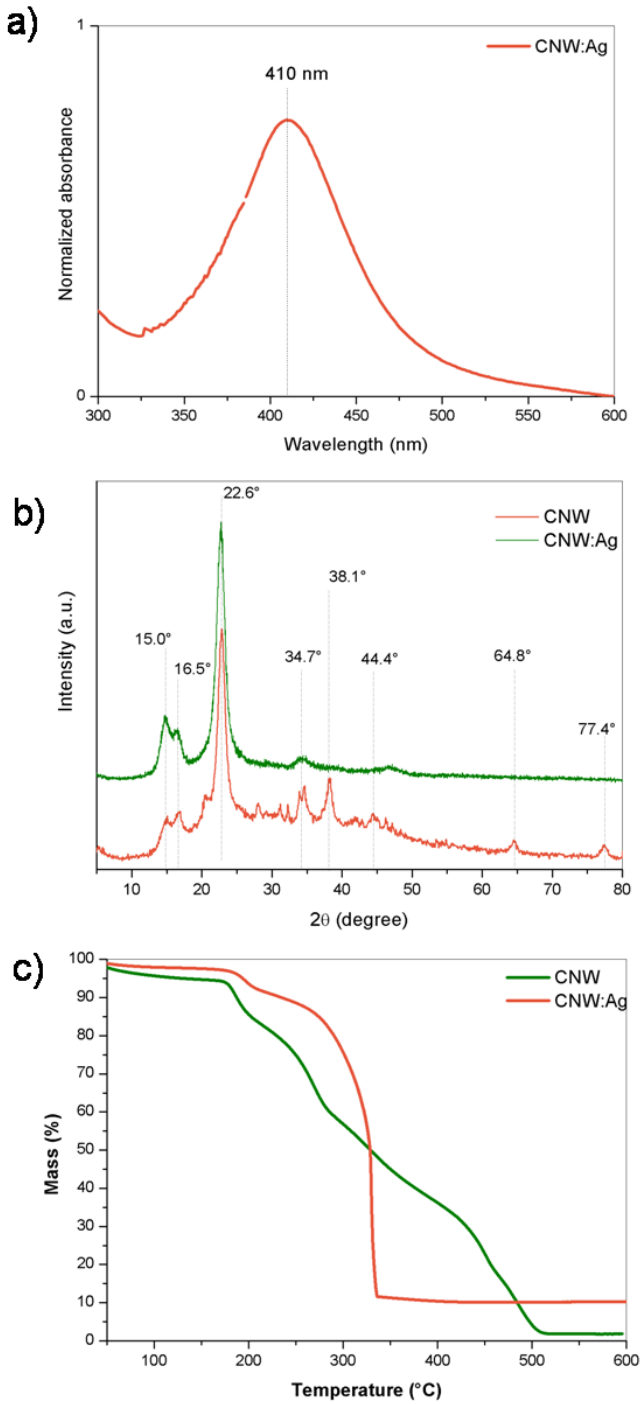

Fig. 2 – CNW:Ag characterization. (a) UV-Vis absorption spectrum, (b) XRD patterns, (c) TGA. (Reprinted with permission from TEODORO et al. (2019a). Copyright (2019) Elsevier)

XRD patterns of CNW and CNW:Ag are shown in Fig. 2 (b). It is possible to confirm the typical profile of natural cellulose as cellulose I polymorphism. Such crystalline structure exhibits triclinic Iα and monoclinic

structures Iβ, reflecting in three main crystalline peaks at 2θ = 15°, 17°, 22.7° regarded to diffraction caused by $(11\bar{0})$, (110) and (200) lattice planes, respectively (TEODORO et al., 2017). Narrow and well-defined peaks indicate an efficient removal of non-cellulosic compounds and amorphous regions of cellulose (JONOOBI et al., 2015). The same pattern found to CNW:Ag indicates that synthesis did not affect the original crystalline profile. High cellulose Ci values calculated to both samples, as described in Tab. 1, are typical for structures as *cellulose whiskers*, which are extracted from crystalline portion of cellulosic polymer. Peaks at 2θ = 38.1°, 44.4°, 64.8° and 77.4° are specific of (111), (200), (220), (311) crystallographic planes of face centered cubic structure of metallic silver nanoparticles (NARAYANAN; HAN, 2017; XU et al., 2016), confirming the presence of silver nanoparticles in CNW:Ag system.

Tab. 1 – Crystallinty index (*Ci*), initial temperature of degradation (T*onset*) and percentage of residual ashes at 600 °C of CNW and CNW:Ag

Sample	**Ci (%)**	**T_{onset} (°C)**	**Ashes at 600 °C (%)**
CNW	90.6	176	1.81
CNW:Ag	93.5	183	10.2

The amount of silver in CNW:Ag was estimated by TGA analysis (Fig. 2 (c)), considering that, under oxidative conditions, CNW thermal chemical degradation results in low residue content at 600 °C (MARTINS et al., 2011). Values obtained by thermograms analysis are summarized in Tab. 1. Cellulose compounds exhibit low to moderate thermo degradation profile, depending of structure, size and surface chemical composition (JONOOBI et al., 2015). Controlled heating under oxidizing atmosphere normally leads to water evaporation, carbohydrate molecules scission, free radicals formation, formation of carbonyl, carboxyl and hydroperoxide groups, followed by CO and CO_2

evolution, until charred residue (MARTINS et al., 2011; SHEN et al., 2013; YANG et al., 2007). A substantial increase nearly 8.4% of residue content was verified and must be due silver incorporation, indicating the presence of inorganic compounds.

Initial thermal degradation temperature (T_{onset}) of both samples was found around 150 - 200 °C, nonetheless, an evident change in CNW and CNW:Ag thermogram profiles can be observed. CNW displayed conventional profile of cellulose nanostructures obtained by hydrolysis with sulphuric acid, marked by several events. Each event represents the degradation of crystals with different size and sulphonation degrees (CORREA A. et al., 2014). In contrast, CNW:Ag profile reveals that the presence of silver nanoparticles onto CNW surface helped to protect them against an earlier thermal degradation, once silver compounds are more thermally and chemically stable (LI et al., 2011). The higher residual mass at 600 °C corresponds to presence of silver compounds (POURREZA et al., 2015).

3.2. *Colorimetric detection of hydrogen peroxide*

Different concentrations of hydrogen peroxide solutions (0.01 μM to 600 μM) were examined in order to determine the sensitivity of the colorimetric assay. The absorbance at 410 nm was used to evaluate the color of the system and determination of hydrogen peroxide. In other words, yellow color and high absorbance values at 410 nm indicate the presence of dispersed CNW/Ag, while low absorbance value indicates a degraded form of CNW/Ag (colorless). According to the UV–Vis absorption spectra of solutions (Fig 3 (a)), the increase of H_2O_2 concentration led to an absorbance decrease at 410 nm, reaching the minimum value for a 600 μM concentration, which indicates gradually degradation of the AgNPs. Therefore, by increasing the hydrogen peroxide concentration, the color of the as-prepared AgNPs gradually changed

from yellow to colorless (as displayed in Fig 3 (b)), suggesting the H_2O_2 concentration-dependent degradation of AgNPs.

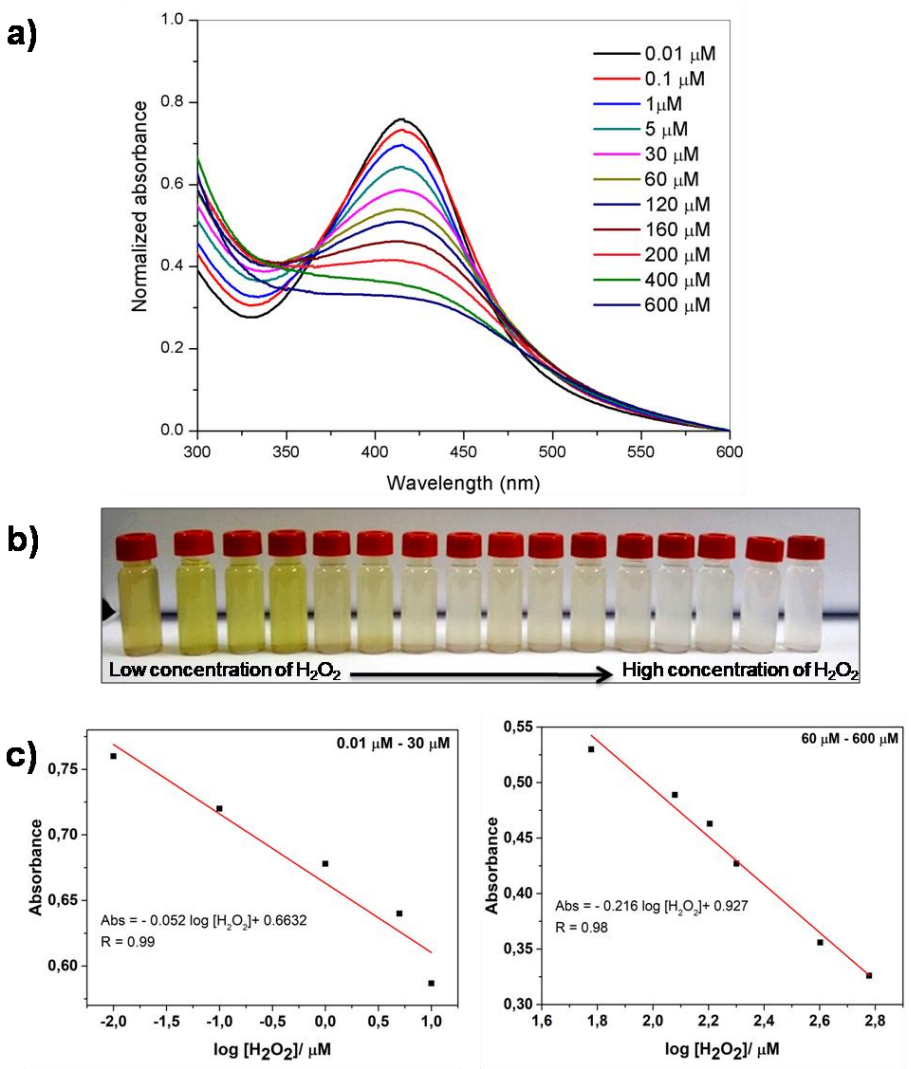

Fig. 3 - Colorimetric sensing of H_2O_2 using CNW/AgNPs (a) UV–vis absorption spectra in the presence of different concentration of the H_2O_2 (0.01 μM – 600 μM) (b) Photographs of solutions exposed to different H_2O_2 concentrations (c) Linear response of the colorimetric assay against increasing H_2O_2 concentrations. (Reprinted with permission from TEODORO et al. (2019a). Copyright (2019) Elsevier)

The determination of the detection limit (D.L.) was based on the standard deviation of the response and the curve slope, according to D.L. = 3.3 σ/S [1], in which σ corresponds to standard deviation of absorbance at 410 nm (measurements of five replicates), and S is the slope of the calibration curve (Fig 3 (c)). Hence the lowest detectable concentration (D.L.) of H_2O_2 using our colorimetric assay were 0.014 μM and 112 μM for the concentration ranges 0.01 μM - 30 μM and 60 - 600 μM, respectively. A comparison of sensor performance regarding our proposed H_2O_2 sensor and previous results is displayed in Tab 2. Our results indicate that the easy-synthesized cellulose nanowhiskers/silver nanoparticles sensor is sufficiently appropriate for colorimetric detection of H_2O_2.

Tab. 2 - Comparison of analytical performance of different modified electrodes for measurements of H_2O_2.

Method	Detection Limit (D.L.)	Linear Range	References
Colorimetric based on decomposition of Ag nanoparticles	1.60 μM	10–80 μM	(NITINAIVINIJ et al., 2014)
LSPR of silver nanoparticles with three different morphologies	0.37 nM (Triangular)	1 nM–1μM	(ZHANG; LI, 2016)
	5 μM (Spherical)	10–40 μM	
	110 μM (Cubic)	200–500 μM	

LSRP of green synthesize AgCl-NPs	8.6 nM	1–120 μM	(FARROKHNIA et al., 2017)
Luminescent sensor for H_2O_2 based on the AgNP - mediated quenching of an luminescent Ir(III) complex (Ir-1)	0.3 μM	0- 17 μM	(LIU et al., 2017)
LSPR characteristic of Ag nanoparticles	0.50 μM	50 μM – 5 mM	(AMIRJANI et al., 2016)
Colorimetric detection of H_2O_2 based in redox reaction involving H_2O_2 and AgNPs	0.014 μM 112 μM	0.01 μM - 30 μM 60 - 600 μM	This work

3.3. Discussion of mechanism of detection

Fig. 4 (a) illustrates the whole process of sensor building and mechanism of detection. Silver in cationic form is adsorbed onto the hydroxyl and sulphate groups present in CNW surface (i-ii). At this point, the solution is colorless. The addition of a small amount of reducing agent induces the formation of silver metallic nanoparticles onto CNW surface (iii). The presence of well-dispersed AgNP makes the suspension yellow colored. After these simple steps, the sensor is ready to use.

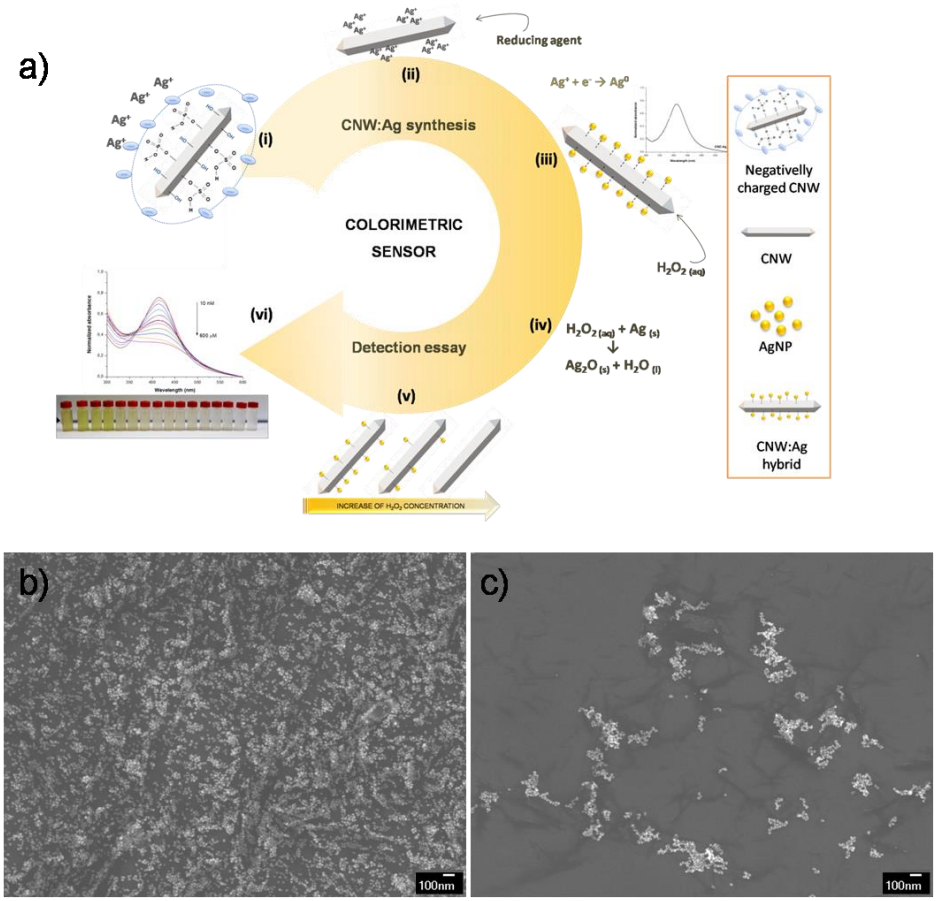

Fig. 4 - (a) Schematic representation of sensor building using CNW:Ag hybrid system and mechanism of H_2O_2 detection. FESEM images of CNW:Ag system (b) before and (c) after addition of 200 µM of H_2O_2, which shows a decrease in the size and amount of AgNP. (Reprinted with permission from TEODORO et al. (2019a). Copyright (2019) Elsevier)

Upon the addition of a strong oxidizing analyte as H_2O_2 the reverse process occurs, leading to oxidation of AgNP and consequent formation silver oxide (Ag_2O) (iv), whereas peroxide is decomposed in water and oxygen (FARROKHNIA et al., 2017). The oxirreduction occurs as described by followed chemical equation:

$$H_2O_{2\,(l)} + 2\,Ag_{\,(s)} \rightarrow Ag_2O_{\,(s)} + H_2O_{\,(l)} \qquad \text{Eq. 2}$$

As a consequence, the solution tends to become uncolored again, and the decreasing of its absorption is proportional to the analyte concentration (vi). The bleaching occurs as consequence of decreasing of AgNP size (NAIK et al., 2018) and formation of Ag_2O (which does not show absorbance in this region of the UV absorption spectra).

FESEM images of CNW:Ag hybrid system before and after addition of 200 μM of H_2O_2 are displayed in Figure 4 (b) and (c) respectively, where the latter reveals the decrease of the size and amount of AgNP, suggesting the corrosion of these structures by H_2O_2 action.

3.4. Interference studies

In order to investigate the selectivity of the proposed colorimetric assay for H_2O_2, some cations (Cu^{2+}, Zn^{2+}, Zn^{2+}, Fe^{2+}), organic interferences (Glucose), and blank sample have been tested. Fig. 5 shows the color changes of AgNPs against the competing metal/anions and H_2O_2 (30 μM). This figure indicates that the color change (from yellow to colorless) only occurs in the presence of H_2O_2, which is caused by an intense decrease of the absorption band intensity at 410 nm, corresponding to the degradation of AgNP. The other substances (cation and organic compounds) have not shown any influence on the hybrid suspension, confirming the efficiency of CNW/Ag hybrid system as a sensing platform for H_2O_2 colorimetric detection.

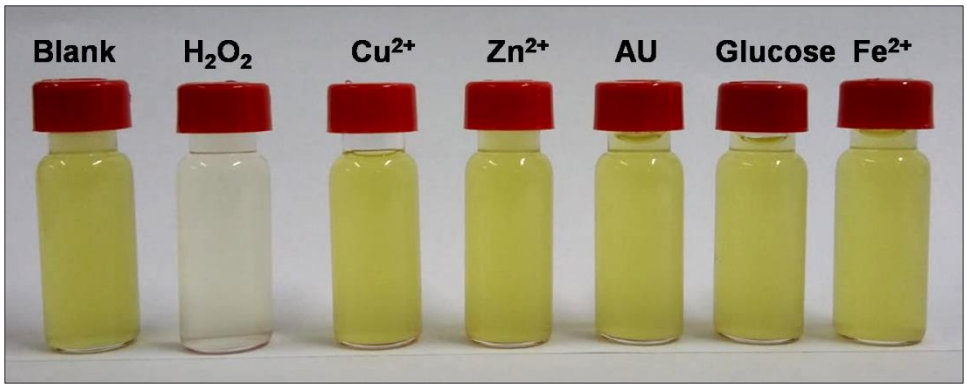

Fig. 5 - Selectivity investigation of the colorimetric sensor for H_2O_2. In the presence of distinct interferents (Cu^{2+}, Zn^{2+}, Fe^{2+}, uric acid (UA), Glucose), only the sample containing H_2O_2 (30 μM) became colorless. (Reprinted with permission from TEODORO et al. (2019a). Copyright (2019) Elsevier)

3.3. Analysis of H_2O_2 in commercial drinking water, river water and milk samples

In order to evaluate the applicability of the proposed colorimetric assay in real environmental analysis, detection of H_2O_2 was carried out using commercial drinking water, river water samples and milk samples using the standard addition method (CHAIYO et al., 2016). The river water samples were collected from the Monjolinho River (located in São Carlos - São Paulo/ Brazil) and filtered using a paper filter (J Prolab JP42). Analyzes were performed by adding 120 μM of the H_2O_2 and % recovery was calculated, as displayed in Tab 3. The obtained recoveries were in the range of 85-98% (Tab. 3), indicating that the developed assay can be used for the accurate determination of H_2O_2 in real samples analysis.

Tab. 3 - Recovery for the detection of H_2O_2 in commercial drinking water, river water and milk samples.

Sample (H_2O_2 - 120 μM)	**% Recovery**
River water	93
Tap water	85
Milk	98

4. Conclusions

A simple, affordable and reproducible route for the synthesis of silver nanoparticles (AgNPs) using cellulose nanowhiskers (CNW) was developed to produce a hybrid material (CNW/Ag) applied as a sensing platform for the colorimetric detection of H_2O_2. The results showed that the developed H_2O_2 sensor displayed low detection limits of 0.014 µM (concentration range of 0.01 µM - 30 µM) and 112 µM (concentration range of 60 - 600 µM). Furthermore, the sensing platform showed a good sensitivity and selective for detecting H_2O_2 in real samples and in the presence of other interfering substances. Thus, the developed sensor can be considered a potential approach for monitoring H_2O_2 with high sensitivity and selectivity. Moreover, the affordable approach does not require an additional step to produce gels or films, which enables the application of the hybrid colorimetric sensor immediately after completion of this fast and green synthesis.

Acknowledgments

The authors thank the financial support from Fundação de Amparo à Pesquisa do Estado de São Paulo (FAPESP) (grant numbers: 2014/21184-5, 2017/12174-4 and 2018/09414-6), Conselho Nacional de Desenvolvimento Científico e Tecnológico (CNPq), MCTI-SisNano (CNPq/402.287/2013-4), Coordenação de Aperfeiçoamento de Pessoal de Nível Superior - Brasil (CAPES) - Código de Financiamento 001 and Rede Agronano (EMBRAPA) from Brazil.

5. References

AASHRITHA, S. Synthesis of Silver Nanoparticles By Chemical Reduction Method and Their Antifungal Activity. **International Research Journal of Pharmacy**, v. 4, n. 10, p. 111–113, 2013.

ABE, K.; YANO, H. Cellulose nanofiber-based hydrogels with high mechanical strength. **Cellulose**, v. 19, n. 6, p. 1907–1912, 2012.

ABITBOL, T. et al. Fluorescent labeling and characterization of cellulose nanocrystals with varying charge contents. **Biomacromolecules**, v. 14, n. 9, p. 3278–3284, 2013.

ABITBOL, T. et al. Hybrid fluorescent nanoparticles from quantum dots coupled to cellulose nanocrystals. **Cellulose**, v. 24, n. 3, p. 1287–1293, 2017.

ADMINISTRATION, F. AND D. **Bad Bug Book, Foodborne Pathogenic Microorganisms and Natural Toxins. Second Edition.** [s.l: s.n.].

AFKHAMI, A. et al. Simultaneous trace-levels determination of Hg(II) and Pb(II) ions in various samples using a modified carbon paste electrode based on multi-walled carbon nanotubes and a new synthesized Schiff base. **Analytica Chimica Acta**, v. 746, p. 98–106, 2012.

AGNIHOTRI, S.; MUKHERJI, S.; MUKHERJI, S. Size-controlled silver nanoparticles synthesized over the range 5-100 nm using the same protocol and their antibacterial efficacy. **RSC Advances**, v. 4, n. 8, p. 3974–3983, 2014.

ALEMDAR, A.; SAIN, M. Isolation and characterization of nanofibers from agricultural residues - Wheat straw and soy hulls. **Bioresource Technology**, v. 99, n. 6, p. 1664–1671, 2008.

ALKMIM-FILHO, J. F. et al. Heavy metals investigation in bovine tissues in Brazil. **Food Science and Technology**, v. 34, n. 1, p. 110–115, 2014.

ALLEN, M. J.; TUNG, V. C.; KANER, R. B. Honeycomb carbon -- A study of graphene. **American Chemical Society**, v. 110, p. 132–145, 2009.

AMIRJANI, A. et al. Label-free surface plasmon resonance detection of hydrogen peroxide; A bio-inspired approach. **Sensors and Actuators, B: Chemical**, v. 227, p. 373–382, 2016.

ANDRE, R. S. et al. Improving the electrochemical properties of polyamide 6/polyaniline electrospun nanofibers by surface modification with ZnO nanoparticles. **RSC Adv.**, v. 5, n. 90, p. 73875–73881, 2015.

ARCOT, L. R. et al. Paper-based plasmon-enhanced protein sensing by controlled nucleation of silver nanoparticles on cellulose. **Cellulose**, v. 22, n. 6, p. 4027–4034, 2015.

ARINO, C. et al. Voltammetric determination of metal ions beyond mercury electrodes. A review. **Analytica Chimica Acta**, v. 990, p. 11–53, 2017.

ASADPOUR-ZEYNALI, K.; AMINI, R. A novel voltammetric sensor for mercury(II) based on mercaptocarboxylic acid intercalated layered double hydroxide nanoparticles modified electrode. **Sensors and Actuators, B: Chemical**, v. 246, p. 961–968, 2017.

ATKINS, P. **Princípios de Química - Atkins&Jones.pdf**. 5th ed ed. [s.l.] Bookman, 2012.

BALA, A.; GÓRSKI, Ł. Determination of mercury cation using electrode modified with phosphorothioate oligonucleotide. **Sensors and Actuators, B: Chemical**, v. 230, p. 731–735, 2016.

BARUD, H. S. et al. Antimicrobial Bacterial Cellulose-Silver Nanoparticles Composite Membranes. **Journal of Nanomaterials**, v. 2011, p. 1–8, 2011.

BECARO, A. A. et al. Toxicity of PVA-stabilized silver nanoparticles to algae and microcrustaceans. **Environmental Nanotechnology, Monitoring and Management**, v. 3, p. 22–29, 2014.

BECARO, A. A. et al. Postharvest Quality of Fresh-Cut Carrots Packaged in Plastic Films Containing Silver Nanoparticles. **Food Bioprocess Technology**, v. 9, n. 4, p. 637–649, 2016.

BERNDT, S. et al. Antimicrobial porous hybrids consisting of bacterial nanocellulose and silver nanoparticles. **Cellulose**, v. 20, n. 2, p. 771–783, 2013.

BIGDELI, A. et al. Nanoparticle-based optical sensor arrays. **Nanoscale**, v. 9, n. 43, p. 16546–16563, 2017.

BILIUTA, G.; COSERI, S. Cellulose: A ubiquitous platform for ecofriendly metal nanoparticles preparation. **Coordination Chemistry Reviews**, v. 383, p. 155–173, 2019.

BUSCHLE- DILLER, G.; ZERONIAN, S. H. Enhancing the reactivity and strength of cotton fibers. **Journal of Applied Polymer Science**, v. 45, n. 6, p. 967–979, 1992.

CAMPOS, A. et al. Production of Cellulose Nanowhiskers from Oil Palm Mesocarp Fibers by Acid Hydrolysis and Microfluidization. **Journal of Nanoscience and Nanotechnology**, v. 17, n. 7, p. 4970–4976, 2017.

CANO, A. et al. Development and characterization of active fi lms based on starch-PVA , containing silver nanoparticles. **Food Packaging and Shelf Life**, v. 10, p. 16–24, 2016.

CHAIYO, S. et al. Electrochemical sensors for the simultaneous determination of zinc, cadmium and lead using a Nafion/ionic liquid/graphene composite modified screen-printed carbon electrode. **Analytica Chimica Acta**, v. 918, p. 26–34, 2016.

CHAUHAN, P.; SHARMA, S. Nanomaterials for Sensing Applications. **Journal of Nanomedicine Research**, v. 3, n. 5, p. 1–8, 2016.

CHEN, C. et al. Electrospun Polymer Nanofibers Decorated with Noble Metal Nanoparticles for Chemical Sensing. **Nanoscale Research Letters**, v. 12, 2017.

CHEN, L. et al. CdS quantum dot-functionalized cellulose nanocrystal films for anti-counterfeiting applications. **Nanoscale**, v. 8, n. 27, p. 13288–13296, 2016.

CHEN, Y. et al. Smart cellulose/graphene composites fabricated by: In situ chemical reduction of graphene oxide for multiple sensing applications. **Journal of Materials Chemistry A**, v. 6, n. 17, p. 7777–7785, 2013.

CHENG, H. et al. Biomedical application and controlled drug release of electrospun fibrous materials. **Materials Science and Engineering C**, v. 90, n. 2017, p. 750–763, 2018.

CHINNAPPAN, A. et al. An overview of electrospun nanofibers and their application in energy storage, sensors and wearable/flexible electronics. **Journal of Materials Chemistry C**, v. 5, n. 48, p. 12657–12673, 2017.

CORREA, A. C. et al. Cellulose nanofibers from curaua fibers. **Cellulose**, v. 17, n. 6, p. 1183–1192, 2010.

CORREA, D. S. et al. Nanostructured Conjugated Polymers in Chemical Sensors: Synthesis , Properties and Applications. **Journal of Nanoscience and Nanotechnology**, v. 14, p. 1–19, 2014b.

DAIKUZONO, C. M. et al. Information Visualization and Feature Selection Methods Applied to Detect Gliadin in Gluten-Containing Foodstu ff with a Microfluidic Electronic Tongue. **ACS Applied Materials and Interfaces**, v. 9, p. 19646–19652, 2017.

DESILVA, K. K. H. et al. Chemical reduction of graphene oxide using green reductants. **Carbon**, v. 119, p. 190–199, 2017.

DEVARAYAN, K.; KIM, B.-S. Reversible and universal pH sensing cellulose nanofibers for health monitor. **Sensors and Actuators, B: Chemical**, v. 209, p. 281–286, 2015.

DI NATALE, C. et al. Multicomponent analysis on polluted waters by means of an electronic tongue. **Sensors and Actuators, B: Chemical**, v. 44, n. 1–3, p. 423–428, 1997.

DI ROSA, A. R. et al. Fusion of electronic nose, electronic tongue and computer vision for animal source food authentication and quality

assessment – A review. **Journal of Food Engineering**, v. 210, p. 62–75, 2017.

DING, B. et al. Electrospun nanomaterials for ultrasensitive sensors. **Materials Today**, v. 13, n. 11, p. 16–27, 2010.

DIRECÇÃO, C. DE. ICH Topic Q2 (R1) Validation of Analytical Procedures : Text and Methodology. **International Conference on Harmonization**, 2005.

DONG, H. et al. Cellulose nanocrystals as a reinforcing material for electrospun poly(methyl methacrylate) fibers: Formation, properties and nanomechanical characterization. **Carbohydrate Polymers**, v. 87, n. 4, p. 2488–2495, 2012.

DONG, H. et al. Hydrogel, aerogel and film of cellulose nanofibrils functionalized with silver nanoparticles. **Carbohydrate Polymers**, v. 95, n. 2, p. 760–767, 2013.

DONG, S.; ROMAN, M. Fluorescently labeled cellulose nanocrystals for bioimaging applications. **Journal of the American Chemical Society**, v. 129, n. 45, p. 13810–13811, 2007.

DROGAT, N. et al. Antimicrobial silver nanoparticles generated on cellulose nanocrystals. **Journal of Nanoparticle Research**, v. 13, n. 4, p. 1557–1562, 2011.

DU, X. et al. Nanocellulose-based conductive materials and their emerging applications in energy devices - A review. **Nano Energy**, v. 35, p. 299–320, 2017.

DUFRESNE, A. Cellulose nanomaterial reinforced polymer nanocomposites. **Current Opinion in Colloid and Interface Science**, v. 29, p. 1–8, 2017.

DURAN, N. et al. Potential Use of Silver Nanoparticles on Pathogenic Bacteria, their Toxicity and Possible Mechanisms of Action. **Journal Of The Brazilian Chemical Society**, v. 21, n. 6, p. 949–959, 2010.

EDWARDS, J. V. et al. Nanocellulose-Based Biosensors : Design ,

Preparation , and Activity of Peptide-Linked Cotton Cellulose Nanocrystals Having Fluorimetric and Colorimetric Elastase Detection Sensitivity. **Engineering**, v. 2013, n. September, p. 20–28, 2013.

EICHHORN, S. J. Cellulose nanowhiskers: promising materials for advanced applications. **Soft Matter**, v. 7, n. 2, p. 303, 2011.

FACURE, M. H. M. et al. Detection of trace levels of organophosphate pesticides using an electronic tongue based on graphene hybrid nanocomposites. **Talanta**, v. 167, n. November 2016, p. 59–66, 2017a.

FACURE, M. H. M. et al. Detection of trace levels of organophosphate pesticides using an electronic tongue based on graphene hybrid nanocomposites. **Talanta**, v. 167, p. 59–66, 2017b.

FANTONI, R. F. Como a poliamida substituiu a seda: uma história da descoberta da poliamida 66. **Polímeros**, v. 22, n. 1, p. 1–6, 2012.

FARROKHNIA, M. et al. Colorimetric sensor assay for detection of hydrogen peroxide using green synthesis of silver chloride nanoparticles: Experimental and theoretical evidence. **Sensors and Actuators, B: Chemical**, v. 246, p. 979–987, 2017.

GELADI, P. Notes on the history and nature of partial least squares (PLS) modelling. **Journal of Chemometrics**, v. 2, n. 4, p. 231–246, 1988.

GOH, Y. F.; SHAKIR, I.; HUSSAIN, R. Electrospun fibers for tissue engineering, drug delivery, and wound dressing. **Journal of Materials Science**, v. 48, n. 8, p. 3027–3054, 2013.

GOLMOHAMMADI, H. et al. Nanocellulose in Sensing and Biosensing. **Chemistry of Materials**, v. 29, n. 13, p. 5426–5446, 2017.

GOULART, L. A. et al. Synergic effect of silver nanoparticles and carbon nanotubes on the simultaneous voltammetric determination of hydroquinone, catechol, bisphenol A and phenol. **Microchimica Acta**, v. 185, n. 1, p. 12, 2018.

GUERRINI, L. M. et al. Electrospinning and characterization of

polyamide 66 nanofibers with different molecular weights. **Materials Research**, v. 12, n. 2, p. 181–190, 2009.

GUO, J. et al. Photoluminescent Hybrids of Cellulose Nanocrystals and Carbon Quantum Dots as Cytocompatible Probes for in Vitro Bioimaging. **Biomacromolecules**, v. 18, n. 7, p. 2045–2055, 2017.

HAJIPOUR, M. J. et al. Antibacterial properties of nanoparticles. **Trends in Biotechnology**, v. 30, n. 10, p. 499–511, 2012.

HASSABO, A. G. et al. Impregnation of silver nanoparticles into polysaccharide substrates and their properties. **Carbohydrate Polymers**, v. 122, p. 343–350, 2015.

HEINRICH, J.; WEISKOPF, D. State of the Art of Parallel Coordinates. **Eurographics Conference on Visualization (EuroVis)**, p. 95–116, 2013.

HERMAN, A.; HERMAN, A. P. Nanoparticles as Antimicrobial Agents : Their Toxicity and Mechanisms of Action. **Journal of Nanoscience and Nanotechnology**, v. 14, n. 1, p. 946–957, 2014.

HSU, C. L.; CHANG, K. S.; KUO, J. C. Determination of hydrogen peroxide residues in aseptically packaged beverages using an amperometric sensor based on a palladium electrode. **Food Control**, v. 19, n. 3, p. 223–230, 2008.

HUANG, S. et al. Preparation and properties of electrospun poly (vinyl pyrrolidone)/cellulose nanocrystal/silver nanoparticle composite fibers. **Materials**, v. 9, n. 7, 2016.

HUBBE, M. A. et al. Cellulosic Nanocomposites: a Review. **BioResources**, v. 3, n. 3, p. 929–980, 2008.

INSELBERG, A.; DIMSDALE, B. Parallel coordinates: a tool for visualizing multi-dimensional geometry. In: **Proceedings of the First IEEE Conference on Visualization: Visualization `90**. San Francisco, CA, USA, USA: IEEE, 1990. p. 361–378.

IVNITSKI, D. et al. Biosensors for detection of pathogenic bacteria. **Biosensor & Bioelectronics**, v. 14, p. 599–624, 1999.

JAISWAL, M.; KOUL, V.; DINDA, A. K. *In vitro* and *in vivo* investigational studies of a nanocomposite-hydrogel-based dressing with a silver-coated chitosan wafer for full-thickness skin wounds. **Journal of Applied Polymer Science**, v. 43472, p. n/a-n/a, 2016.

JEDRZEJUK, A. et al. Some factors affecting longevity of cut lilacs. **Postharvest Biology and Technology**, v. 111, p. 247–255, 2016.

JOLLIFFE, I. T. Principal Component Analysis and Factor Analysis. In: **Principal Component Analysis**. New York, NY: Springer New York, 1986. p. 115–128.

JONOOBI, M. et al. Different preparation methods and properties of nanostructured cellulose from various natural resources and residues: a review. **Cellulose**, v. 22, n. 2, p. 935–969, 2015.

JOSE, A.; RAY, J. G. Toxic heavy metals in human blood in relation to certain food and environmental samples in Kerala, South India. **Environmental Science and Pollution Research**, v. 25, n. 8, p. 7946–7953, 2018.

JUNIOR, M. A. M. et al. Preparation of silver and gold nanoparticles: a simple method to introduce nanotechnology into teaching laboratories. **Química Nova**, v. 35, n. 9, p. 1872–1878, 2012.

JUSTINO, C. I. L.; DUARTE, A. C.; ROCHA-SANTOS, T. A. P. Recent progress in biosensors for environmental monitoring: A review. **Sensors (Switzerland)**, v. 17, n. 12, 2017.

KAFY, A. et al. Cellulose/graphene nanocomposite as multifunctional electronic and solvent sensor material. **Materials Letters**, v. 159, p. 20–23, 2015.

KAFY, A. et al. Cellulose nanocrystal/graphene oxide composite film as humidity sensor. **Sensors and Actuators, A: Physical**, v. 247, p. 221–

226, 2016.

KAMISAN, A. I. et al. Synthesis of Graphene via Green Reduction of Graphene Oxide with Simple Sugars. **Advanced Materials Research**, v. 1107, p. 542–546, 2015.

KARIMI, A. et al. Rapid and sensitive detection of hydrogen peroxide in milk by Enzyme-free electrochemiluminescence sensor based on a polypyrrole-cerium oxide nanocomposite. **Sensors and Actuators, B: Chemical**, v. 271, n. May, p. 90–96, 2018.

KARKRA, R. et al. Classification of heavy metal ions present in multi-frequency multi-electrode potable water data using evolutionary algorithm. **Applied Water Science**, v. 7, n. 7, p. 3679–3689, 2017.

KHAN, B. A. et al. Processing and properties of antibacterial silver nanoparticle-loaded hemp hurd / poly (lactic acid) biocomposites. **Composites Part B**, v. 100, p. 10–18, 2016.

KHOSHBIN, Z. et al. Simultaneous detection and determination of mercury (II) and lead (II) ions through the achievement of novel functional nucleic acid-based biosensors. **Biosensors and Bioelectronics**, v. 116, n. March, p. 130–147, 2018.

KIMLING, J. et al. Turkevich Method for Gold Nanoparticle Synthesis Revisited. v. 110, p. 15700–15707, 2006.

KLEMM, D. et al. Nanocellulose as a natural source for groundbreaking applications in materials science: Today's state. **Materials Today**, 2018.

KOGA, H. et al. Topochemical synthesis and catalysis of metal nanoparticles exposed on crystalline cellulose nanofibers. **Chemical communications (Cambridge, England)**, v. 46, n. 45, p. 8567–8569, 2010.

KOLAROVA, K. et al. Preparation and characterization of silver nanoparticles in methyl cellulose matrix and their antibacterial activity and their antibacterial activity. **Japanese Journal of Applied Physics**, v. 56, n. 6S1, p.

06GG09-1-06GG09-4, 2017.

KOSHY, O. et al. A Flexible, Disposable Hydrogen Peroxide Sensor on Graphene Nanoplatelet-Coated Cellulose. **Current Analytical Chemistry**, v. 13, n. 6, p. 480–487, 2017.

KRUTYAKOV, Y. A. et al. Synthesis and properties of silver nanoparticles: advances and prospects. **Russian Chemical Reviews**, v. 77, n. 3, p. 233–257, 2008.

LEE, J. H. et al. Fabrication of flexible, transparent silver nanowire electrodes for amperometric detection of hydrogen peroxide. **Sensors and Actuators B: Chemical**, v. 224, p. 789–797, mar. 2016.

LEGIN, A. et al. Tasting of beverages using an electronic tongue. **Sensors and Actuators, B: Chemical**, v. 44, n. 1–3, p. 291–296, 1997.

LEÓN-SILVA, S.; FERNÁNDEZ-LUQUEÑO, F.; LÓPEZ-VALDEZ, F. Silver Nanoparticles (AgNP) in the Environment : a Review of Potential Risks on Human and Environmental Health. **Water, Air, & Soil Pollution**, v. 227, 2016.

LI, B. et al. Green reduction of graphene oxide by sugarcane bagasse extract and its application for the removal of cadmium in aqueous solution. **Journal of Cleaner Production**, v. 189, p. 128–134, jul. 2018a.

LI, H. et al. Nano-silver treatments reduced bacterial colonization and bio fi lm formation at the stem-ends of cut gladiolus ‘ Eerde ’ spikes. **Postharvest Biology and Technology**, v. 123, p. 102–111, 2017.

LI, L. et al. Simultaneous stripping determination of cadmium and lead ions based on the N-doped carbon quantum dots-graphene oxide hybrid. **Sensors and Actuators, B: Chemical**, v. 255, p. 1762–1770, 2018b.

LI, M. et al. Nanostructured sensors for detection of heavy metals: A review. **ACS Sustainable Chemistry and Engineering**, v. 1, n. 7, p. 713–723, 2013.

LI, S. M. et al. Cellulose-silver nanocomposites: Microwave-

assisted synthesis, characterization, their thermal stability, and antimicrobial property. **Carbohydrate Polymers**, v. 86, n. 2, p. 441–447, 2011.

LIANG, A. et al. The surface-plasmon-resonance effect of nanogold/silver and its analytical applications. **TrAC - Trends in Analytical Chemistry**, v. 37, p. 32–47, 2012.

LIN, W. C.; LI, Z.; BURNS, M. A. A Drinking Water Sensor for Lead and Other Heavy Metals. **Analytical Chemistry**, v. 89, n. 17, p. 8748–8756, 2017.

LIU, H. et al. Preparation of silver nanoparticles on cellulose nanocrystals and the application in electrochemical detection of DNA hybridization. **Cellulose**, v. 18, n. 1, p. 67–74, 2011.

LIU, H. et al. Colorimetric and ultrasensitive detection of H2O2based on Au/Co3O4-CeOxnanocomposites with enhanced peroxidase-like performance. **Sensors and Actuators, B: Chemical**, v. 271, p. 336–345, 2018.

LIU, Y. et al. Progress on sensors based on nanomaterials for rapid detection of heavy metal ions. **Science China Chemistry**, v. 60, n. 3, p. 329–337, 2017.

LU, Y. et al. A review of the identification and detection of heavy metal ions in the environment by voltammetry. **Talanta**, v. 178, p. 324–338, 2018.

LVOVA, L. et al. Electronic tongue for microcystin screening in waters. **Biosensors and Bioelectronics**, v. 80, p. 154–160, 2016.

MAHMOUDIAN, M. R.; BASIRUN, W. J.; ALIAS, Y. A sensitive electrochemical Hg2+ ions sensor based on polypyrrole coated nanospherical platinum. **RSC Advances**, v. 6, n. 43, p. 36459–36466, 2016.

MANEERUNG, T.; TOKURA, S.; RUJIRAVANIT, R. Impregnation of silver nanoparticles into bacterial cellulose for antimicrobial wound dressing. **Carbohydrate Polymers**, v. 72, n. 1, p. 43–51, 2008.

MARQUES, I. et al. Detection of traces of triclosan in water.

Applied Surface Science, v. 421, p. 142–147, 2017.

MARTINS, M. A. et al. Extraction and characterization of cellulose whiskers from commercial cotton fibers. **Journal of Materials Science**, v. 46, n. 24, p. 7858–7864, 2011.

MARZOUK, W. et al. Ag-nanocomposite based on carboxymethylcellulose for humidity detection : Green synthesis and sensing performances. **Journal of Applied Polymer Science**, v. 133, n. 28, p. 1–9, 2016.

MATSUYAMA, K. et al. Antibacterial and antifungal properties of Ag nanoparticle-loaded cellulose nanofiber aerogels prepared by supercritical CO2 drying. **Journal of Supercritical Fluids**, v. 143, p. 1–7, 2019.

MAUTNER, A. et al. Nitrate removal from water using a nanopaper ion-exchanger. **Environ. Sci.: Water Res. Technol.**, v. 2, n. 1, p. 117–124, 2016.

MERCANTE, L. A. et al. Electrospun polyamide 6/poly(allylamine hydrochloride) nanofibers functionalized with carbon nanotubes for electrochemical detection of dopamine. **ACS Applied Materials and Interfaces**, v. 7, n. 8, p. 4784–4790, 2015.

MERCANTE, L. A. et al. Electrospinning-based (bio)sensors for food and agricultural applications: A review. **Trends in Analytical Chemistry**, v. 91, p. 91–103, 2017a.

MERCANTE, L. A. et al. One-pot preparation of PEDOT:PSS-reduced graphene decorated with Au nanoparticles for enzymatic electrochemical sensing of H2O2. **Applied Surface Science**, v. 407, p. 162–170, 2017b.

MIGLIORINI, F. L. et al. Voltammetric cadmium (II) sensor based on a fluorine doped tin oxide electrode modified with polyamide 6 / chitosan electrospun nanofibers and gold nanoparticles. p. 1077–1084, 2017a.

MIGLIORINI, F. L. et al. Voltammetric cadmium(II) sensor based

on a fluorine doped tin oxide electrode modified with polyamide 6/chitosan electrospun nanofibers and gold nanoparticles. **Microchimica Acta**, v. 184, n. 4, p. 1077–1084, 2017b.

MINGHIM, R.; PAULOVICH, F. V; LOPES, A. A. Content-based text mapping using multi-dimensional projections for exploration of document collections. **Proc. SPIE**, v. 6060, p. 60600S, 2006.

MOHAN, V. B. et al. Graphene-based materials and their composites: A review on production, applications and product limitations. **Composites Part B: Engineering**, v. 142, p. 200–220, 2018.

MOON, R. J. et al. **Cellulose nanomaterials review: structure, properties and nanocomposites**. [s.l: s.n.]. v. 40

MORALES-NARVÁEZ, E. et al. Nanopaper as an Optical Sensing Platform. **ACS Nano**, v. 9, n. 7, p. 7296–7305, 2015.

MORONES, J. R. et al. The bactericidal effect of silver nanoparticles. **Nanotechnology 16**, v. 16, n. 10, p. 2346–2353, 2005.

NAG, A.; MITRA, A.; MUKHOPADHYAY, S. C. Graphene and its sensor-based applications: A review. **Sensors and Actuators, A: Physical**, v. 270, p. 177–194, 2018.

NAIK, A. N. et al. Nafion membrane incorporated with silver nanoparticles as optical test strip for dissolved hydrogen peroxide: Preparation, deployment and the mechanism of action. **Sensors and Actuators, B: Chemical**, v. 255, p. 605–615, 2018.

NARAYANAN, K. B.; HAN, S. S. Colorimetric detection of manganese(II) ions using alginate-stabilized silver nanoparticles. **Research on Chemical Intermediates**, v. 43, n. 10, p. 5665–5674, 2017.

NCCLS. **Methods for Dilution Antimicrobial Susceptibility Tests for Bacteria That Grow Aerobically; Approved Standard—Sixth Edition. NCCLS document M7-A6**. Pennsylvania 19087-1898: [s.n.]. v. 23

NCCLS. **Performance Standards for Antimicrobial Disk**

Susceptibility Tests; Approved Standard. Eighth Edi ed. Pennsylvania 19087-1898 USA: [s.n.].

NIKIFOROV, A. et al. Non-thermal plasma technology for the development of antimicrobial surfaces : a review. **Journal of Physics D: Applied Physics**, v. 49, n. 20, p. 204002, 2016.

NITINAIVINIJ, K. et al. Colorimetric determination of hydrogen peroxide by morphological decomposition of silver nanoprisms coupled with chromaticity analysis. **Analytical Methods**, v. 6, n. 24, p. 9816–9824, 2014.

OLIVEIRA, J. E. et al. Modification of electrospun nylon nanofibers using layer-by-layer films for application in flow injection electronic tongue: Detection of paraoxon pesticide in corn crop. **Sensors and Actuators, B: Chemical**, v. 171–172, p. 249–255, 2012.

ORANI, A. M.; MANDJUKOV, P.; VASSILEVA, E. Determination of selected trace elements in marine biota samples with the application of fast temperature programs and solid sampling continuous source high resolution atomic absorption spectroscopy: method validation. **International Journal of Environmental Analytical Chemistry**, v. 97, n. 8, p. 710–729, 2017.

PADALKAR, S. et al. Natural biopolymers: Novel templates for the synthesis of nanostructures. **Langmuir**, v. 26, n. 11, p. 8497–8502, 2010.

PAL, S.; TAK, Y. K.; SONG, J. M. Does the antibacterial activity of silver nanoparticles depend on the shape of the nanoparticle? A study of the gram-negative bacterium Escherichia coli. **Journal of Biological Chemistry**, v. 73, n. 6, p. 1712–1720, 2007.

PAULOVICH, F. V et al. Information visualization techniques for sensing and biosensing. **Analyst**, v. 136, n. 7, p. 1344, 2011.

PAVINATTO, A. et al. Layer-by-Layer assembled films of chitosan and multi-walled carbon nanotubes for the electrochemical detection of 17 α -ethinylestradiol. **Journal of Electroanalytical Chemistry**, v. 755, p. 215–

220, 2015.

PENG, B. et al. Current progress in aptasensors for heavy metal ions based on photoelectrochemical method: A review. **Current Analytical Chemistry**, v. 14, n. 1, p. 4–12, 2018.

PENG, H. et al. Simultaneous reduction and surface functionalization of graphene oxide by natural cellulose with the assistance of the ionic liquid. **Journal of Physical Chemistry C**, v. 116, n. 30, p. 16294–16299, 2012.

PÉREZ-RÀFOLS, C. et al. A screen-printed voltammetric electronic tongue for the analysis of complex mixtures of metal ions. **Sensors and Actuators, B: Chemical**, v. 250, p. 393–401, 2017.

PODRAZKA, M. et al. Electronic tongue-A tool for all tastes? **Biosensors**, v. 8, n. 1, p. 1–24, 2017.

POURREZA, N. et al. Green in-situ synthesized silver nanoparticles embedded in bacterial cellulose nanopaper as a bionanocomposite plasmonic sensor. **Biosensors and Bioelectronics**, v. 74, p. 353–359, 2015.

PROMPHET, N. et al. An electrochemical sensor based on graphene/polyaniline/polystyrene nanoporous fibers modified electrode for simultaneous determination of lead and cadmium. **Sensors and Actuators, B: Chemical**, v. 207, p. 526–534, 2015.

RAGAVAN, K. V. et al. Chitosan as a peroxidase mimic: Paper based sensor for the detection of hydrogen peroxide. **Sensors and Actuators B: Chemical**, v. 272, p. 8–13, 2018.

RAI, M.; YADAV, A.; GADE, A. Silver nanoparticles as a new generation of antimicrobials. **Biotechnology Advances**, v. 27, n. 1, p. 76–83, 2009.

RAJESHKUMAR, S.; BHARATH, L. V. Mechanism of plant-mediated synthesis of silver nanoparticles – A review on biomolecules involved, characterisation and antibacterial activity. **Chemico-Biological Interactions**, v.

273, p. 219–227, 2017.

REICH, S. et al. Polymer nanofibre composite nonwovens with metal-like electrical conductivity. **npj Flexible Electronics**, v. 2, n. 1, p. 3–8, 2018.

RENEKER, D. H.; YARIN, A. L. Electrospinning jets and polymer nanofibers. **Polymer**, v. 49, n. 10, p. 2387–2425, 2008.

RIUL-JR, A. et al. Recents advances in electronic tongues. **Analyst**, v. 135, p. 2481–2495, 2010.

ROMAN, M.; WINTER, W. T. Effect of sulfate groups from sulfuric acid hydrolysis on the thermal degradation behaviour of bacterial cellulose. **Biomacromolecules**, n. 5, p. 1671–1677, 2004.

ROTTER, G.; ISHIDA, H. FTIR separation of nylon- 6 chain conformations: Clarification of the mesomorphous and γ- crystalline phases. **Journal of Polymer Science Part B: Polymer Physics**, v. 30, n. 5, p. 489–495, 1992.

ROUSSEEUW, P. J. Silhouettes: A graphical aid to the interpretation and validation of cluster analysis. **Journal of Computational and Applied Mathematics**, v. 20, p. 53–65, 1987.

ROY, D. et al. Cellulose modification by polymer grafting: a review. **Chemical Society reviews**, v. 38, n. 7, p. 2046–64, 2009.

SAHOO, P. K. et al. Solvothermal synthesis of reduced graphene oxide/Au nanocomposite-modified electrode for the determination of inorganic mercury and electrochemical oxidation of toxic phenolic compounds. **Electrochimica Acta**, v. 180, p. 1023–1032, 2015.

SCAGION, V. P. et al. An electronic tongue based on conducting electrospun nanofibers for detecting tetracycline in milk samples. **RSC Advances**, v. 6, p. 103740–103746, 2016.

SEIL, J. T.; WEBSTER, T. J. Antimicrobial applications of nanotechnology: Methods and literature. **International Journal of**

Nanomedicine, v. 7, p. 2767–2781, 2012.

SENTHAMIZHAN, A.; CELEBIOGLU, A.; UYAR, T. Flexible and highly stable electrospun nanofibrous membrane incorporating gold nanoclusters as an efficient probe for visual colorimetric detection of Hg(ii). **Journal of Materials Chemistry A**, v. 2, n. 32, p. 12717–12723, 2014.

SERRANO, N.; GONZÁLEZ-CALABUIG, A.; DEL VALLE, M. Crown ether-modified electrodes for the simultaneous stripping voltammetric determination of Cd(II), Pb(II) and Cu(II). **Talanta**, v. 138, n. Ii, p. 130–137, 2015.

SHEN, D. et al. The Overview of Thermal Decomposition of Cellulose in Lignocellulosic Biomass. In: KADLA, J. (Ed.). . **Cellulose - Biomass conversion**. [s.l.] IntechOpen, 2013.

SHIN, Y. et al. Facile stabilization of gold-silver alloy nanoparticles on cellulose nanocrystal. **Journal of Physical Chemistry C**, v. 112, n. 13, p. 4844–4848, 2008.

SILVA, A. B.; BRETAS, R. E. S. Preparation and characterization of PA6/PAni-TSA nanofibers. **Synthetic Metals**, v. 162, n. 17–18, p. 1537–1545, 2012.

SINGH, R. et al. STD sensor based on Biosensors and Bioelectronic nucleic acid functionalized nanostructured polyaniline. **Biosensors and Bioelectronics**, v. 24, p. 2232–2238, 2009.

SIQUEIRA, G. et al. Mechanical properties of natural rubber nanocomposites reinforced with cellulosic nanoparticles obtained from combined mechanical shearing, and enzymatic and acid hydrolysis of sisal fibers. **Cellulose**, v. 18, n. 1, p. 57–65, 2011.

SIQUEIRA, M. C. et al. Evaluation of Antimicrobial Activity of Silver Nanoparticles for Carboxymethylcellulose Film Applications in Food Packaging. **Journal of Nanoscience and Nanotechnology**, v. 14, p. 5512–5517, 2014.

SPAGNOL, C. et al. Cellulose nanowhiskers decorated with silver nanoparticles as an additive to antibacterial polymers membranes fabricated by electrospinning. **Journal of Colloid and Interface Science**, v. 531, p. 705–715, 2018.

SPERLING, L. H. **INTRODUCTION TO PHYSICAL POLYMER**. 4th ed ed. Bethlehem, Pennsylvania: John Wiley & Sons, 2006.

SRIKAR, S. K. et al. Green Synthesis of Silver Nanoparticles : A Review. **Green and Sustainable Chemistry**, v. 6, n. 1, p. 34–56, 2016.

STOBINSKI, L. et al. Graphene oxide and reduced graphene oxide studied by the XRD, TEM and electron spectroscopy methods. **Journal of Electron Spectroscopy and Related Phenomena**, v. 195, p. 145–154, 2014.

SUBBIAH, T. et al. Electrospinning of nanofibers. **Journal of Applied Polymer Science**, v. 96, n. 2, p. 557–569, 2005.

SUN, M. et al. Simultaneous detection of Pb2+, Cu2+and Hg2+by differential pulse voltammetry at an indium tin oxide glass electrode modified by hydroxyapatite. **Electrochimica Acta**, v. 283, p. 1223–1230, 2018.

SURESHKUMAR, M.; SISWANTO, D. Y.; LEE, C. Magnetic antimicrobial nanocomposite based on bacterial cellulose and silver nanoparticles. **Journal of Materials Chemistry**, v. 20, n. 33, p. 6948–6955, 2010.

SURYABHASKARAM, D.; CHERUKU, R.; GOVINDARAJ, G. Sugar Assisted Graphene : A Green Synthesis Approach. **International Journal of ChemTech research**, v. 6, n. 6, p. 3291–3293, 2014.

TCHOUNWOU, P. B. et al. Heavy Metals Toxicity and the Environment. **Molecular, Clinical and Environmental Toxicology**, v. 101, p. 133–164, 2012.

TEIXEIRA, E. DE M. et al. Sugarcane bagasse whiskers: Extraction and characterizations. **Industrial Crops and Products**, v. 33, n. 1, p. 63–66, 2011.

TEIXEIRA, E. M. et al. Cellulose nanofibers from white and naturally colored cotton fibers. **Cellulose**, v. 17, n. 3, p. 595–606, 2010.

TEODORO, K. B. R. et al. Whiskers de fibra de sisal obtidos sob diferentes condições de hidrólise ácida: efeito do tempo e da temperatura de extração. **Polímeros**, v. 21, n. 4, p. 280–285, 2011.

TEODORO, K. B. R. et al. Surface Functionalization of Cellulose Whiskers for Nonpolar Composites Applications. In: THAKUR, V. K.; THAKUR, M. K.; KESSLER, M. R. (Eds.). . **Handbook of Composites from Renewable Materials - Volume 4: Functionalization**. [s.l.] Scrivener Publishing LLC, 2017. p. 199–223.

TEODORO, K. B. R. et al. Cellulose Whiskers Influence the Morphology and Antibacterial Properties of Silver Nanoparticles Composites. **Journal of Nanoscience and Nanotechnology**, v. 18, n. 7, p. 1–8, 2018.

TEODORO, K. B. R. et al. Detection of hydrogen peroxide (H_2O_2) using a colorimetric sensor based on cellulose nanowhiskers and silver nanoparticles. **Carbohydrate Polymers**, v. 212, n. February, p. 235–241, 2019a.

TERRA, I. A. A. et al. Optically active electrospun nanofibers for heavy metals sensing. p. 1–17, 2017.

TERRA, I. A. A.; MERCANTE, L. A. Fluorescent and Colorimetric Electrospun Nanofibers for Heavy-Metal Sensing. **Biosensors**, v. 7, n. 4, 2017.

TINGAUT, P.; ZIMMERMANN, T.; SÈBE, G. Cellulose nanocrystals and microfibrillated cellulose as building blocks for the design of hierarchical functional materials. **Journal of Materials Chemistry**, v. 22, n. 38, p. 20105, 2012.

TOKO, K. Taste sensor with global selectivity. **Materials Science and Engineering C**, v. 4, n. 2, p. 69–82, 1996.

TRUSOVAS, R. et al. Recent Advances in Laser Utilization in the

Chemical Modification of Graphene Oxide and Its Applications. **Advanced Optical Materials**, v. 4, n. 1, p. 37–65, 2016.

TSAI, T. et al. Antibacterial cellulose paper made with silver-coated gold nanoparticles. **Scientific Reports**, v. 7, p. 1–10, 2017.

VAN DEN BERG, O. et al. Nanocomposites based on cellulose whiskers and (semi)conducting conjugated polymers. **Journal of Materials Chemistry**, v. 17, n. 26, p. 2746, 2007.

WANG, J.; WINDBERGS, M. Functional electrospun fibers for the treatment of human skin wounds. **European Journal of Pharmaceutics and Biopharmaceutics**, v. 119, p. 283–299, 2017.

WANG, Q.; MOSER, J.-E.; GRÄTZEL, M. Electrochemical Impedance Spectroscopic Analysis of Dye-Sensitized Solar Cells. **The Journal of Physical Chemistry B**, v. 109, n. 31, p. 14945–14953, 2005.

WEI, J. et al. Stripping voltammetric determination of mercury(II) based on SWCNT-PhSH modified gold electrode. **Sensors and Actuators, B: Chemical**, v. 190, p. 968–974, 2014.

WEI, Y. et al. SnO2/reduced graphene oxide nanocomposite for the simultaneous electrochemical detection of cadmium(II), lead(II), copper(II), and mercury(II): An interesting favorable mutual interference. **Journal of Physical Chemistry C**, v. 116, n. 1, p. 1034–1041, 2012.

WILSON, D.; ALEGRET, S.; DELVALLE, M. Simultaneous Titration of Ternary Mixtures of Pb(II), Cd(II) and Cu(II) with Potentiometric Electronic Tongue Detection. **Electroanalysis**, v. 27, n. 2, p. 336–342, 2015.

XU, F. et al. Fabrication of cellulose fine fiber based membranes embedded with silver nanoparticles via Forcespinning. **Journal of Polymer Engineering**, v. 36, n. 3, p. 269–278, 2016.

YAN, Y. et al. Dual-emissive nanohybrid of carbon dots and gold nanoclusters for sensitive determination of mercuric. **Nano Research**, v. 9, n. 7, p. 2088–2096, 2016.

YANG, H. et al. Characteristics of hemicellulose, cellulose and lignin pyrolysis. **Fuel**, v. 86, n. 12–13, p. 1781–1788, 2007.

YANG, S. et al. Ultrasensitive surface-enhanced Raman scattering detection in common fluids. **Proceedings of the National Academy of Sciences**, v. 113, n. 2, p. 268–273, 2016.

YANG, Y. et al. Synthesis of highly fluorescent gold nanoclusters and their use in sensitive analysis of metal ions. **Analyst**, v. 142, n. 23, p. 4486–4493, 2017.

YARIN, A. L. Coaxial electrospinning and emulsion electrospinning of core-shell fibers. **Polymers for Advanced Technologies**, v. 22, n. 3, p. 310–317, 2011.

ZEYTUNCU, B.; MORCALI, M. H. Fabrication and Characterization of Antibacterial Polyurethane Acrylate-based Materials. **Materials Research**, v. 18, n. 4, p. 867–872, 2015.

ZHANG, C. et al. Preparation of cellulose/graphene composite and its applications for triazine pesticides adsorption from water. **ACS Sustainable Chemistry and Engineering**, v. 3, n. 3, p. 396–405, 2015.

ZHANG, L.; LI, L. Colorimetric detection of hydrogen peroxide using silver nanoparticles with three different morphologies. **Analytical Methods**, v. 8, n. 37, p. 6691–6695, 2016.

ZHAO, J. et al. Luminescent and transparent nanopaper based on rare-earth up-converting nanoparticle grafted nanofibrillated cellulose derived from garlic skin. **ACS Applied Materials and Interfaces**, v. 6, n. 17, p. 14945–14951, 2014.

ZHU, C. et al. Reducing sugar: New functional molecules for the green synthesis of graphene nanosheets. **ACS Nano**, v. 4, n. 4, p. 2429–2437, 2010.

ZHU, R. et al. Fabrication and characterization of Nylon 6/cellulose nanofibrils melt-spun nanocomposite filaments. **Composites Part A: Applied**

Science and Manufacturing, v. 97, p. 111–119, 2017.

ZULKIFLI, F. H. et al. A facile synthesis method of hydroxyethyl cellulose-silver nanoparticle scaffolds for skin tissue engineering applications. **Materials Science and Engineering C**, v. 79, p. 151–160, 2017.

ZULKIFLI, S. N.; RAHIM, H. A.; LAU, W. Detection of contaminants in water supply: A review on state-of-the-art monitoring technologies and their applications. **Sensors & Actuators: B. Chemical**, v. 255, p. 2657–2689, 2018.

ZUO, Y. et al. Simple and green synthesis of piperazine-grafted reduced graphene oxide and its application for the detection of Hg(II). **Nanotechnology**, v. 29, n. 16, 2018.

APPENDIX B

Publication rights and permissions

B1 - Journal of Nanoscience and Nanotechnology – American Society Publishiers rights and permissions

Kelcilene B. R. Teodoro, Rafaela C. Sanfelice, Luiz H. C. Mattoso, Daniel S. Correa, **Cellulose whiskers influence the morphology and antibacterial properties of silver nanoparticles composites**, Journal of Nanoscience and Nanotechnology, **18**, 4876-4883, 2018.

Gmail Kelcilene Teodoro <kbr.teodoro@gmail.com>

Request permission for thesis

Dr. H. S. Nalwa <nalwa@mindspring.com> 27 de fevereiro de 2019 20:52
Para: Kelcilene Teodoro <kbr.teodoro@gmail.com>
Cc: Daniel Souza Correa <daniel.correa@embrapa.br>

Since this is your own research article in JNN so you are free to re-use whole article or figures in your PhD thesis. Just cite reference that is all.

From: Kelcilene Teodoro [mailto:kbr.teodoro@gmail.com]
Sent: Wednesday, February 27, 2019 2:39 PM
To: jnn@aspbs.com
Cc: Daniel Souza Correa
Subject: Request permission for thesis

Dear Dr. Hari Singh Nalwa,

My name is Kelcilene Teodoro, I am author of the paper " Cellulose whiskers influence the morphology and antibacterial properties of silver nanoparticles composites" (DOI: https://doi.org/10.1166/jnn.2018.15285) published in Journal of Nanoscience and Nanotechnology.

The reason of my contact aims to gently request the permission to use this paper in my thesis as part of the prerequisite for obtaining the PhD title.

The requested permissions for the other works were granted at no charge. However, the Copyright Clearance Center requires US$$7683.50 for JNN permission. Considering that we do not have available this fund, I would like request you the permission to publish this paper in my thesis.

Thank you for considering this request.

Kind regards,

Kelcilene B R Teodoro / Dr Daniel S Correa

--

MSc. Kelcilene B. R. Teodoro

Doutoranda em Química

PPGQ-UFSCar e Embrapa Instrumentação

B2 - Carbohydrate Polymers – Elsevier rights and permissions

Kelcilene B. R. Teodoro, Flávio M. Shimizu, Vanessa P. Scagion, Daniel S. Correa, **Ternary nanocomposites based on cellulose nanocrystals, silver nanoparticles and electrospun nanofibers: use in a electronic tongue for heavy metal detection**, Sensors and Actuators B: Chemical, **290**, 387-395, 2019.

B3 - Carbohydrate Polymers – Elsevier rights and permissions

Kelcilene B. R. Teodoro, Fernanda L. Migliorini, Murilo H. Facure, Daniel S. Correa, **Conductive electrospun nanofibers containing cellulose nanowhiskers and reduced graphene oxide for the electrochemical detection of mercury(II)**, Carbohydrate Polymers, **207**, 747-754, 2019.

Copyright Clearance Center RightsLink®

Home | Account Info | Help

Title: Conductive electrospun nanofibers containing cellulose nanowhiskers and reduced graphene oxide for the electrochemical detection of mercury(II)

Author: Kelcilene B.R. Teodoro,Fernanda L. Migliorini,Murilo H.M. Facure,Daniel S. Correa

Publication: Carbohydrate Polymers

Publisher: Elsevier

Date: 1 March 2019

Logged in as:
Kelcilene Teodoro
LOGOUT

Please note that, as the author of this Elsevier article, you retain the right to include it in a thesis or dissertation, provided it is not published commercially. Permission is not required, but please ensure that you reference the journal as the original source. For more information on this and on your other retained rights, please visit: https://www.elsevier.com/about/our-business/policies/copyright#Author-rights

BACK | CLOSE WINDOW

B4 - Carbohydrate Polymers – Elsevier rights and permissions

K. B. R. Teodoro, F. L. Migliorini, W. A. Christinelli, D. S. Correa, **Detection of hydrogen peroxide (H_2O_2) using a colorimetric sensor based on cellulose nanowhiskers and silver nanoparticles**. Carbohydrate Polymers, **212**, 235-241, 2019.

B5 – RCS Advances – The Royal Society of Chemistry rights and permissions

Permission to use the Figure 1.3, which was extracted from the article “Size-controlled silver nanoparticles synthesized over the range 5–100 nm using the same protocol and their antibacterial efficacy” (AGNIHOTRI et al. 2014).

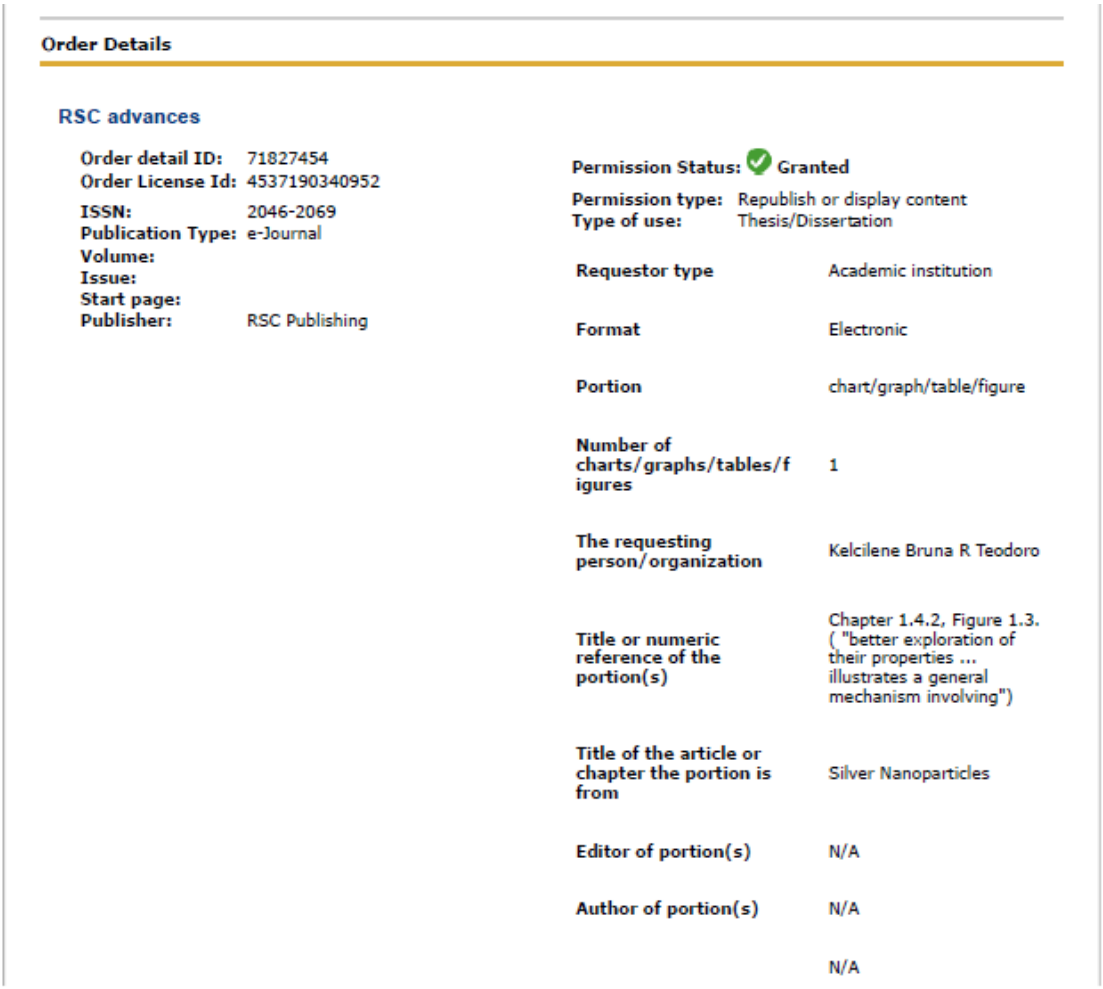

Order Details

RSC advances

Order detail ID:	71827454
Order License Id:	4537190340952
ISSN:	2046-2069
Publication Type:	e-Journal
Volume:	
Issue:	
Start page:	
Publisher:	RSC Publishing

Permission Status: Granted

Permission type: Republish or display content
Type of use: Thesis/Dissertation

Requestor type	Academic institution
Format	Electronic
Portion	chart/graph/table/figure
Number of charts/graphs/tables/figures	1
The requesting person/organization	Kelcilene Bruna R Teodoro
Title or numeric reference of the portion(s)	Chapter 1.4.2, Figure 1.3. ("better exploration of their properties ... illustrates a general mechanism involving")
Title of the article or chapter the portion is from	Silver Nanoparticles
Editor of portion(s)	N/A
Author of portion(s)	N/A
	N/A

Volume of serial or monograph	
Issue, if republishing an article from a serial	N/A
Page range of portion	7
Publication date of portion	2019
Rights for	Main product
Duration of use	Current edition and up to 5 years
Creation of copies for the disabled	no
With minor editing privileges	no
For distribution to	Worldwide
In the following language(s)	Original language of publication
With incidental promotional use	no
Lifetime unit quantity of new product	Up to 499
Title	Ternary nanocomposites based on cellulose nanocrystals, conductive materials and electrospun fibers applied in sensors for detecting metals in water
Institution name	UFSCar
Expected presentation date	Mar 2019

Note: This item will be invoiced or charged separately through CCC's **RightsLink** service. More info **$ 0.00**